HEAT TRANSFER IN RECTANGULAR CHANNELS (AR=2:1) OF THE GAS TURBINE BLADE AT HIGH ROTATION NUMBERS

A Dissertation

by

JIANG LEI

Submitted to the Office of Graduate Studies of
Texas A&M University
in partial fulfillment of the requirements for the degree of

DOCTOR OF PHILOSOPHY

August 2011

Major Subject: Mechanical Engineering

Heat Transfer in Rectangular Channels (AR=2:1) of the Gas Turbine Blade at High Rotation Numbers

Copyright August 2011 Jiang Lei

HEAT TRANSFER IN RECTANGULAR CHANNELS (AR=2:1) OF THE GAS TURBINE BLADE AT HIGH ROTATION NUMBERS

A Dissertation

by

JIANG LEI

Submitted to the Office of Graduate Studies of
Texas A&M University
in partial fulfillment of the requirements for the degree of

DOCTOR OF PHILOSOPHY

Approved by:

Chair of Committee,	Je-Chin Han
Committee Members,	Sai Lau
	Hamn-Ching Chen
	David Staack
Head of Department,	Dennis O'Neal

August 2011

Major Subject: Mechanical Engineering

ABSTRACT

Heat Transfer in Rectangular Channels (AR=2:1) of the Gas Turbine Blade at High Rotation Numbers. (August 2011)

Jiang Lei, B.S., Xi'an Jiaotong University;

M.S., Xi'an Jiaotong University

Chair of Advisory Committee: Dr. Je-Chin Han

Gas turbine blade/vane cooling is obtained by circulating the high pressure air from compressor to the internal cooling passage of the blade/vane. Heat transfer and cooling effect in the rotating blade is highly affected by rotation. The typical rotation number for the aircraft engine is in the range of 0~0.25 and for the land based power generation turbine in the range of 0~05. Currently, the heat transfer data at high rotation numbers are limited. Besides, the investigation of heat transfer phenomena in the turn region, especially near hub portion is rare. This dissertation is to study the heat transfer in rectangular channels with turns in the tip or the hub portion respectively at high rotation numbers close to the engine condition.

The dissertation experimentally investigates the heat transfer phenomena in a two-pass rectangular channel (AR=W/H=2:1) with a 180^o sharp turn in the tip portion. The flow in the first passage is radial outward and after the turn in the second passage, the flow direction is radial inward. The hydraulic diameter (D_h) of the channel is 16.9 mm. Parallel square ribs with an attack angle (α) of 45^o are used on leading and trailing

surfaces to enhance the heat transfer. The rib height-to-hydraulic diameter ratio (e/D_h) is 0.094. For the baseline smooth case and the case with rib pitch-to-height ratio (P/e) 10, channel orientation angles (β) of 90^o and 135^o were tried to model the cooling passage in the mid and rear portion of the blade respectively. Two other P/e ratios of 5 and 7.5 were studied at $\beta=135^o$ to investigate their effect on heat transfer. The data are presented under high rotation numbers and buoyancy parameters by varying the Reynolds number (Re=10,000~40,000) and rotation speed (rpm=0~400). Corresponding rotation number and buoyancy parameter are ranged as 0~0.45 and 0~0.8 respectively.

The dissertation also studies the heat transfer in a two-pass channel (AR=2:1) connected by a 180^o U bend in the hub portion. The flow in the first passage is radial inward and after the U bend, the flow in the second passage is radial outward. The cross-section dimension of this channel is the same as the previous one. To increase heat transfer, staggered square ribs ($e/D_h=0.094$) are pasted on leading and trailing walls with an attack angle (α) of 45^o and pitch-to-height ratio (P/e) of 8. A turning vane in the shape of half circle (R=18.5 mm, t=1.6 mm) is used in the turn region to guide the flow for both smooth and ribbed cases. Channel orientation angles (β) of 90^o and 135^o were taken for both smooth and ribbed cases. The heat transfer data were taken at high rotation numbers close to previous test section.

DEDICATION

This dissertation is dedicated to my loving parents for their unconditional support and endless love.

ACKNOWLEDGEMENTS

I am very grateful to Dr. Je-Chin Han for the opportunity to study in his lab and for the knowledge I received in both his courses and my research. I appreciate the help and concern given by Dr. Sai Lau while I was a teaching assistant. I also want to express my gratitude to Dr. Hamn-Ching Chen for his selfless guidance and help in CFD research and courses. Thanks also to Dr. David Staack for his help when I served in his course as his teaching assistant.

Also, I would like to thank my girl friend, who gives me consolation and encouragement when I feel afraid, lonely and helpless. I also want to express my gratitude to all my friends.

NOMENCLATURE

A_{htr}	heater surface area
A_p	copper plate projection area
A_c	turning vane cross section area
AR	aspect ratio
Bo_x	local buoyancy parameter
c_p	specific heat at constant pressure
D_h	hydraulic diameter
e	rib height
H	channel height
h	regionally averaged heat transfer coefficient
i	designate a given region in the channel
I	current
k	thermal conductivity of air
m	mass flow rate
Nu	regionally averaged Nussult number
Nu_o	Nusselt number for a fully-developed flow in a stationary smooth pipe
Nu_s	stationary regionally averaged Nusselt number
P	rib pitch
Pr	Prandtl number of air

Q_n	net heat transfer rate
Q_l	external heat loss rate
R_x	local radius of rotation
$\overline{R}$	mean radius of rotation
R	radius of the turning vane
r_i	radius of the inner wall in the turn portion
r_o	radius of the hub wall in the turn portion
Re	Reynolds number
Ro	rotation number, $\Omega D_h / U_b$
S	height of the turning vane
t	thickness of the turning vane
$T_{w,x}$	regionally averaged wall temperature
$T_{b,x}$	local coolant temperature
$T_{f,x}$	local film temperature
U_b	velocity in streamwise direction
V	voltage
W	channel width
α	rib attack angle
β	channel orientation angle
μ	dynamic viscosity of coolant
$\rho_{b,x}$	local air density based on local bulk temperature
$\rho_{w,x}$	local air density based on local wall temperature

$\Delta\rho/\rho_{b,x}$	local bulk-to-wall density ratio ($\Delta\rho=\rho_{b,x}-\rho_{w,x}$)
$(\Delta\rho/\rho)_{in}$	inlet density ratio
Ω	rotation speed

.

TABLE OF CONTENTS

Page

LIST OF FIGURES

Page

Page

Page

LIST OF TABLES

1. INTRODUCTION

1.1 Gas Turbine Blade Internal Cooling

The continuous demand for greater thrust or efficiency requires the designer to increase the turbine inlet temperature. Cooling technology provides the protection to the blade from excessive thermal stresses and possible premature failure of the material brought by the hot gas. As one of the major component, internal cooling techniques have been developed for decades. Most important features of gas turbine internal cooling are presented in Gas Turbine Heat Transfer and Cooling Technology [1]. Relatively cool air from the high pressure stage of the compressor is ducted to the turbine blade and various ways are used to cool the blade down as shown in **Figure 1**. Internal cooling techniques of gas turbine includes: jet impingement, rib-turbulated cooling, pin-fin cooling and jet ejection. Those techniques are applied to different portions of blade based on the local heating condition and geometry. Channels of different aspect ratios inside the turbine blade are shown in **Figure 2**. The internal cooling channels are affected by several factors, such as: channel aspect ratio, rib turbulator configuration, channel orientation, rotation and flow parameters. The cooling channels composed of single-pass (with radial outward flow) and multi-pass (with both radial outward and inward flow) are fabricated inside the turbine blade and the coolant is circulating in the passages to remove the heat conducted from outside.

This dissertation follows the style of Journal of Heat Transfer.

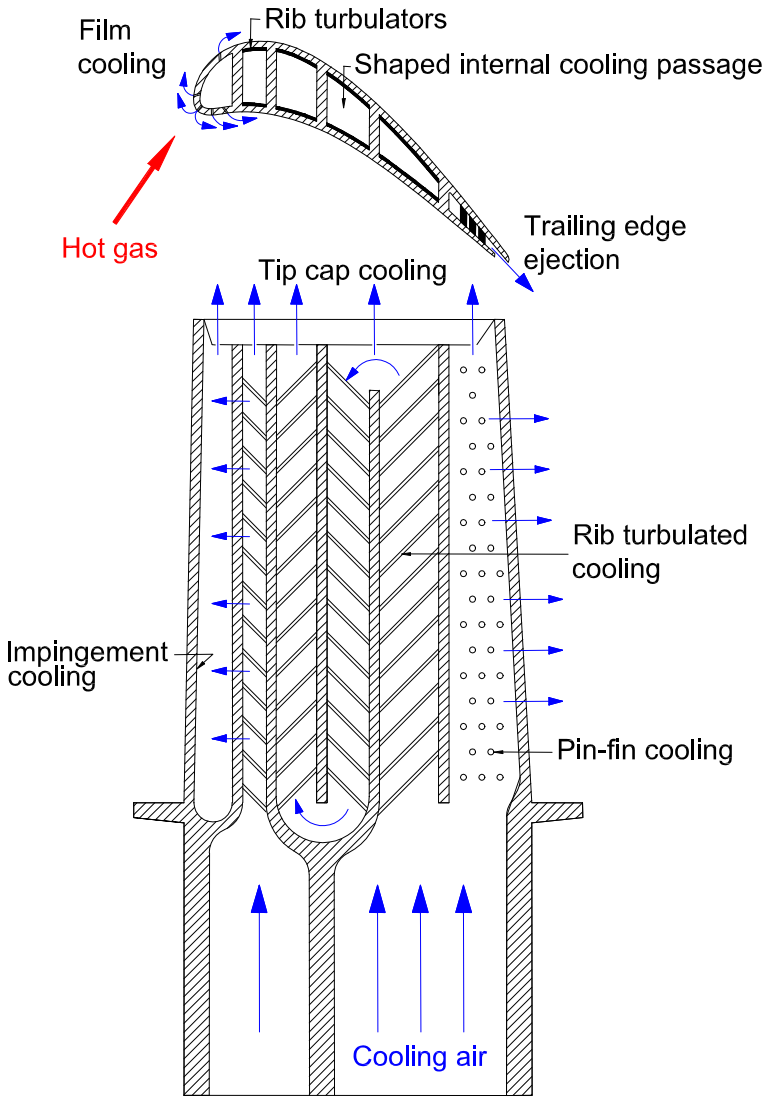

Fig. 1 Turbine blade cooling techniques

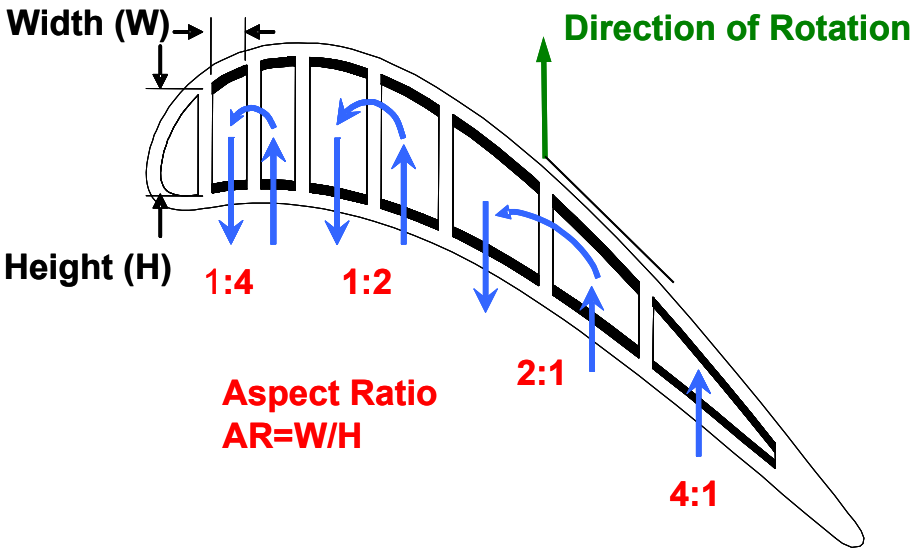

Fig. 2 Turbine blade cooling channels with different aspect ratios

1.2 Internal Cooling in Two Pass Rectangular Channels

In real turbines, the blade rotates at very high speed and rotating test facilities are built to simulate the flow and heat transfer in the blade internal cooling passage. The effect of rotation is referred as rotation number (Ro), described as the ratio of the Coriolis force to flow inertia force. Wagner et al. [2, 3] provided sets of data in a smooth square channel with both radial outward and inward flow in a serpentine multi-passage rotating square channel. In their experiments, rotation number ranged from 0.0 to 0.48. They concluded that the local heat transfer coefficients in the first passage were found to decrease up to 60 percent on the leading surface and increase 250 percent on the trailing surface from the non-rotation levels. Han et al. [4] studied the influence of uneven wall temperature in a two-pass smooth square channel. The results suggested that the effect of uneven wall temperatures in the second-pass radial inward flow is greater than that in the first-pass radial outward flow. Huh [5] studied the rotation effect on heat transfer in a two-pass smooth rectangular channel (AR=2:1) with developing flow in radial outward direction in the first pass. The rotation number in this experiment ranged from 0.0 to 0.45. Results showed that heat transfer was highly increased in the sharp 180^{o} turn portion. Dutta et al. [6] carried out simulation using a two-equation turbulence model with new term for Coriolis and rotation-induced buoyancy to predict the heat transfer on the leading and trailing surface of a rotating square channel with radial outward flow. Flow separation was observed and explained on the leading wall to enhance heat transfer. Liu et al. [7] experimentally investigated the rotational effect on heat transfer in a smooth two-pass rectangular channel (AR=1:4) with re-directed sharp bend entrance.

The rotation number ranges from 0 to 0.67 and the buoyancy parameter ranges from 0 to 2.0 by varying the inlet density ratio from 0.11 to 0.16. It is concluded that in the first pass, the rotational effect is reduced by the entrance condition and in the second pass, both leading and trailing surfaces experience heat transfer enhancement over stationary case. It is also observed that on the tip wall Nusselt ratio (Nu/Nu_s) goes up to 2.4 at the highest rotation number. Zhou et al. [8] studied the heat transfer and pressure drop in a rotating 4:1 aspect ratio smooth channel at two orientation angles of 90^o and 45^o. Reynolds number covers 10,000 to 150,000 and rotation number ranges 0 to 0.6. Three density ratios of 1.0, 1.5, and 2.0 were applied. In the first passage with radially outward flow, it is observed that heat transfer experiences an increase and then degradation on LE surface, which is different from the square smooth channel. Increased density ratio promotes heat transfer on all walls. Orientation angle is important because tilted channel has heat transfer reduced on the destabilized surface and has it enhanced on the stabilized surface.

Taslim et al. [9] performed an experiment studying the effect of rotation on heat transfer using liquid crystal technique in criss-cross ribbed channel with P/e=10 and e/D_h=0.133, 0.250, and 0.333. The rotational number varied from 0.0 to 0.3. Wagner et al. [10] extended his work from smooth to ribbed-roughed channels. The rib turbulators were distributed on two opposite sides of the passage normal to the flow direction with P/e=10 and e/D_h=0.1. The overall heat transfer coefficient in the passage was almost doubled compared with the smooth case and local heat transfer coefficients varied from 0.65 to 4.5 times to smooth case. Zhou et al. [11] reported heat transfer measurement of

a rotating two-pass 4:1 aspect ratio channel with ribs skewed 45^o to the flow. The Reynolds number ranged from 10,000 to 70,000 while rotation number ranged from 0.0 to 0.7. It was observed that both the effect of rotation and the effect of density ratio in the 4:1 channel are smaller than those in the ribbed square channel.

Rectangular channels with different aspect ratios are widely used in laboratories to model the real internal cooling passages inside the turbine blade. A number of previous studies have shown that the aspect ratio of the channel plays an important role in the heat transfer and flow field. In many studies, data were taken and discussed in stationary condition to understand the effect of aspect ratio on heat transfer with different rib profiles. Han [12] studied the effect of aspect ratio on heat transfer for five different channels (AR=1:4, 1:2, 1:1, 2:1, and 4:1) at two different rib pitch to height ratios (P/e=10 and 20). A correlation based on heat transfer and friction coefficient was developed for ribbed channels covering aspect ratio, rib spacing, rib height, and Reynolds number. It was also concluded that local heat transfer in the small aspect-ratio channel is higher than the large aspect-ratio channel. Han and Park [13] investigated the combined effects of rib flow-angle and channel aspect ratio in channels (AR=1:1, 2:1, and 4:1) with rib flow-angles varied from 30^o, 45^o, 60^o, and 90^o. A correlation between heat transfer and friction coefficient was obtained to account for rib flow-angle, rib spacing, channel aspect-ratio, rib height and Reynolds number. Park et al. [14] studied the combined effects of channel aspect ratio (AR=1:4, 1:2, 1:1, 2:1, and 4:1), rib flow-angle (α=30^o, 45^o, 60^o, and 90^o) and Reynolds number on heat transfer and pressure drop. The results suggest that the narrow channels (AR=1:4 and 1:2) give better heat transfer

performance than wide ones (AR=2:1 and 4:1). $60^o/45^o$ angled ribs are recommended for square channel, $45^o/60^o$ angled ribs for narrow channels and $30^o/45^o$ angled ribs for wide channels.

In rotating condition, the effect of the aspect ratio was studied by both experiment and computer simulation. Fu et al. [15, 16] performed experiments in an unpressurized test section for five different ribbed channels (AR=1:4, 1:2, 1:1, 2:1, and 4:1). The highest rotation number obtained was around 0.3 at Reynolds number of 5,000, which is too low compared to the real turbine blade cooling. Su et al. [17] reported his CFD results on rotating channels with AR=1:1, 1:2, and 1:4. The rotation number ranged from 0.0 to 0.28. Their results showed that for large Reynolds numbers, the effect of rotation decreases with a decrease in aspect ratio.

The rib spacing in the internal cooling passage began from stationary channels and was proved by many researchers to be very important to heat transfer and pressure drop. Too large spacing can result in reduction of the heat transfer enhancement brought by ribs. Too small spacing can induce large pressure drop. Han et al. [18] studied the effect of rib shape, attack angle (α) and rib pitch-to-height ratio (P/e) on heat transfer and friction coefficient in a narrow ribbed channel (AR=12:1). As P/e ratio varies from 5 to 7.5, 10, 15, and 20, both friction factor and Stanton number increase at first and then decrease with the maximum value occur at P/e=10. Taslim and Spring [19] applied liquid crystal technique to investigate the effects of rib profile and rib pitch-to-height ratio (P/e) in a rectangular 2:1 channel. Their results showed that the for given rib profile and blockage ratio (e/D_h), an optimum rib pitch-to-height ratio (P/e) existed.

For the rotating channels, the heat transfer and pressure drop are also prominently influenced by the rib spacing. Liu et al. [20] studied the effect of angled rib spacing (P/e=3, 5, 7.5, and 10) in a rotating channel with AR=1:2. The rotation number in their experiment ranged from 0.0 to 0.2. The results showed that for this 1:2 channel, the P/e=3 case had the best heat transfer performance while the P/e=5 case presented the largest pressure drop. It was also noted that the effect of rotation was increased as angled rib spacing decreased. Huh et al. [21] studied the effect of angled rib spacing (P/e=2.5, 5, and 10) in a rotating channel with AR=1:4. The rotation number in their study varied from 0.0 to 0.65. The results showed that the P/e=2.5 case had the highest heat transfer enhancement. It was also noted sharp-bend entrance had a significant effect on first pass heat transfer enhancement and rib spacing and rotation effects were reduced in second pass.

In real turbines, the leading/trailing wall of the channel is not always perpendicular to the direction of rotation because of the blade shape and the channel location. To keep the uniformity, channel orientation here for the single-pass or multi-pass cooling channel is defined based on the passage with radial outward flow as the direction pointing from the passage center to the outer wall center seen from the blade tip to hub. The channel orientation angle (β) is calculated from the channel orientation to the rotation direction in counter-clock-wise. The effect of channel orientation on heat transfer of a two-pass smooth square channel can be obtained analogically from the study by Park and Lau [22] using naphthalene sublimation. The channel orientation angles (β) studied are 90^o and 135^o. The rotation number ranged up to 0.24 for a constant

Reynolds number of 5,500. The result shows that the orientation significantly affects the local mass transfer in the first passage. However, it does not lower the average of mass transfer on the leading wall and increases it on the trailing wall. Parsons et al. [23] performed experiments to study the effect of channel orientation (β=90^o and 135^o) and wall heating condition in a two-pass square channel with 60^o and 90^o ribs on leading and trailing surfaces. The largest rotation number of 0.35 was obtained at the lowest Reynolds number of 2,500. Results showed that heat transfer coefficients in the 135^o orientation case decreased for the first pass trailing and second pass leading surfaces and increase for the first pass leading and second pass trailing surfaces compared to the perpendicular case. Johnson et al. [24] conducted experiments in smooth and ribbed multi-pass square channels, where the passages were at a channel orientation angle of 90^o, 135^o and 215^o. The rotation number ranged from 0 to 0.48. It was concluded that for the smooth surface, in the first pass on the leading wall, the heat transfer of 135^o orientation case was almost twice of 90^o case. However, for the afterward passes and ribbed cases, the difference between orientation angles is less. In addition, for the 135^o orientation case, the effects of Coriolis and buoyancy forces on heat transfer in the rotating channel were reduced compared to 90^o orientation case. Dutta and Han [25] studied heat transfer in a two-pass square channel with an orientation angle of 90^o, 135^o and 180^o. Data of both smooth and rough surfaces equipped with half-V ribs were provided. It was shown that Nusselt number ratios vary with the channel orientation angle. Azad et al. [26] performed heat transfer experiments in a rotating two-pass rectangular ribbed channel with AR=2:1 and P/e=10 for channel orientations 90^o and

135^{o} respectively. The rotation number ranged from 0 to 0.21. The results showed that 90^{o} orientation channel produced higher heat transfer over 135^{o} orientation. Al-Hadhrami et al. [27] obtained heat transfer data for a two-pass rectangular channel with AR=2:1 for two channel orientations 90^{o} and 135^{o} using smooth and 45^{o} V-shaped ribbed surfaces. The rotation number varied from 0.0 to 0.21. They concluded that 90^{o} orientation channel produced higher rotation effect on heat transfer over 135^{o} orientation.

The geometry of the turn region makes the flow complicated by separation, recirculation and turn-induced secondary flows. As a result, heat transfer behavior is largely affected and the research in this topic remains popular for many years. Metzger and Sahm [28] investigated the heat transfer within and around a 180^{o} sharp turn in a smooth channel with rectangular cross-section. The height and width of the channel and the turn clearance were non-dimensional to study different configurations at different Reynolds number. Results showed that the maximum regionally averaged heat transfer coefficients are two to three times of the fully-developed values. Han et al. [29] obtained a detailed mass transfer distribution around a 180^{o} sharp turn in a two-pass square channel for both smooth and ribbed top surfaces using naphthalene sublimation technique. Results showed that the Sherwood number on all surfaces around the turn in the roughed channel is higher than that in the smooth channel. For both the smooth and ribbed channels, the Sherwood number after the turn is higher than that before the turn. Schabacker et al. [30] studied the flow characteristics of a two-pass square channel with roughed top walls using PIV techniques. The 3D mean velocity field and turbulence quantities of the flow were obtained under high spatial resolution. It was observed that in

the 180^o sharp turn region the flow field is more complicated by the interaction of the rib-induced and turn-induced secondary flows. After the bend, ribs quickly dominate and recover the flow from the turn effect. Son et al. [31] carried out experiments using PIV to study the correlation between high Reynolds number turbulent flow and wall heat transfer in a two-pass square channel roughed by orthogonal ribs. Detailed profile of averaged velocity and turbulent energy for both mainstream and secondary flow was provided. The result suggests that the characteristics of secondary flow are closely correlated with the wall heat transfer enhancements for both smooth and ribbed wall. Lucci et al. [32] provided the simulation data of flow filed and heat transfer of channel composed of an upstream square passage and a downstream rectangular passage (AR=2:1). The two passages are connected by a 180^o U bend. Three different turbulence models were implemented.

In addition to that, in the rotating condition, the combined effect of rotation and turn increases the complexity of the flow and heat transfer in the turn region and afterward passages. Cheah et al. [33] measured the velocity field in a rotating two-pass smooth channel by LDA. The result showed that flow separation occurs at downstream of the 180^o U-bend and positive rotation increases the re-attachment length while negative rotation decreases the re-attachment length. It is also concluded that the streamwise turbulence intensity at downstream of the bend is much more affected by rotation compared to that at upstream of the bend. Hwang and Lai [34] performed a numerical study of laminar flow and thermal field in a rotating smooth two-pass channel with a 180^o sharp turn in hub portion. Their result reveals that rotation effect is more

obvious for the radial inward flow than for the outward flow. It is also shown that the rotation-induced buoyancy enhances the peripherally averaged heat transfer in the radial inward passage while its effect can be negligible in the radial outward passage. Flow separation is observed on the leading surface of the radial outward passage when rotation buoyancy is strong enough. Liou and Chen [35] measured the flow field and heat transfer in a rotating rectangular channel with a 180^o sharp turn. LDV was used to obtain the flow visualization data to interpret the heat transfer distribution. It is concluded that the turn-induced secondary flow and turbulence enhancement associated with the unsteadiness of the separation bubble are responsible for the significant heat transfer increase in the first part of second passage. Liou et al. [36] presented their measurements of the turbulent flow field in a smooth two-pass channel under rotating and non-rotating conditions. In the turn region, the data reveal that symmetric Dean vortices for non-rotating case are gradually dominated by a single vortex most of which impinges directly on the leading-outer corner. It is observed that a high level of turbulent kinetic energy is closely related to dominant vortex inside the turn.

In the turn portion and downstream passage of the cooling channel, pressure loss occurs from the complicated turn-induced secondary flow and mainstream separation and recirculation. In the updated design of turbine internal cooling channels, guide vanes are used to weaken those prominent flow features. Luo and Razinsky [37] presented a numerical study of the turbulent flow through a 180^o sharp turn and U-bend respectively, with or without the guide vane. The vane is shaped as a half circle (of diameter D) with straight extensions of 1.5D on both ends. For the sharp turn case, by installing the guide

vane, the separation zone on the inner wall right after the turn is substantially reduced while the secondary flow kinetic energy (SKE) is also recued by 38%. It is also observed that the pressure gradient between the outer and the inner wall is largely reduced by 22%, which is attributable to the reduction in SKE. For the U-bend case, the guide vane greatly reduces the separation from the divider tip to downstream, as well as the secondary vortices strength and pressure gradient between outer and inner wall. Besides, a comparison between sharp turn and U-bend gives the conclusion that the rounding of outer wall helps the vane achieve a larger reduction of pressure loss and flow separation. Zehnder et al. [38] performed experiment to measure the effect of the guide vane on heat transfer and pressure loss in a rib-roughed rectangular two-pass channel connected by a 180^{o} sharp turn. CFD simulation was also used to prove the result. The guide vane was shaped as a quarter circle. Three vane configurations were tested, such as: vane near the inner wall, vane near the outer wall, and the combination of those two. Experimental results showed that for pressure loss, both the inner vane structure and dual-vane structure obtained a decrease of pressure drop as much as 25% while outer vane structure experienced an increase. For heat transfer, all the structures did not present a prominent decrease in the turn region while they showed a substantial drop in the region right after the turn, where the dual-vane structure had the largest decrease as much as 20%. For the flow behavior, the separation bubble on the inner surface was suppressed by the inner vane in two of the vane configurations. Chen et al. [39] studied the heat transfer and pressure drop in a rib-roughed square two-pass channel connected by a 180^{o} U-bend. Both measurement and simulation were performed to prove and compare. A

similar shape of guide vane to research done by Luo and Razinsky [37] (half-circle with extensions at two ends) was applied to the turn portion with or without ribs. The result shows that after installing the vane in the turn portion without ribs, the loss coefficient of the turn was reduced by 66% and the friction factor of the whole channel was reduced by 38% while heat transfer in the downstream passage was reduced by 35%.

1.3 Objectives

The heat transfer in the blade tip portion is influenced largely by rotation, thus the investigation of blade cooling on tip turn portion is very important. Currently, very limited information is available in open literature on the heat transfer characteristics in the tip turn portion connecting the two pass 2:1 aspect ratio rectangular channel. Besides, the rotating experiments conducted in previous research on the two pass 2:1 aspect ratio rectangular channel were focusing on the rotation number around 0.1. In real engine condition, the rotation number is 2~3 times larger than 0.1 for air engine and 5~6 times for land-based turbine. Thus, extending the experimental rotation number and buoyancy parameter to realistic ranges is vital for the turbine designer when they apply these non-dimensional parameters to real engine condition to get actual values. Angled ribs with attack angle (α) of 45^{o} will be glued on leading and trailing surfaces. Three rib pitch-to-height ratios (P/e) will be tested. In addition, the effect of channel orientations will be studied for both smooth and ribbed surface. The test matrix is shown in **Table 1**. The objectives of the study on the two pass rectangular channel (AR=2:1) with a tip turn are:

1. Study the heat transfer profile in the two pass 2:1 aspect ratio channel including tip turn portion under stationary and rotating conditions.
2. Provide information of heat transfer on trailing, leading, outer, inner and tip walls under high rotation number (Ro=0~0.45) and buoyancy parameter (Bo_x=0~0.8) conditions to understand the effects of rotation number and buoyancy parameter.
3. Develop correlations of heat transfer on all surfaces of this two pass 2:1 channel at high rotation number and buoyancy parameter.
4. Study the effect of channel orientation ($\beta=90^o$ and 135^o) on heat transfer in the rectangular channel with smooth or rib-roughed leading and trailing surfaces (P/e=10).
5. Investigate the effect of rib pitch-to-height ratios (P/e=5, 7.5 and 10) on heat transfer in the rectangular channel under stationary and rotating conditions

The heat transfer in the blade hub portion is also very important and greatly influenced by rotation. However, very limited information in open literature can be obtained on heat transfer in the hub turn portion of a rotating channel. In addition, turning vanes are applied in the turn portion to guide the flow. Thus, to study the heat transfer in the hub turn portion of the channel with or without the guide vane is necessary. Besides, angled ribs ($\alpha=45^o$) are used on leading and trailing surfaces in the stagger pattern for the rib pitch-to-height ratio (P/e) of 8. Two channel orientation angles (β) of 90^o and 135^o are used for every case to study the orientation effect on heat transfer.

The test matrix can be seen in **Table 1**. The objectives of the research on the two pass rectangular channel (AR=2:1) with a hub turn are listed:

1. Study the heat transfer profile in the channel especially the hub turn portion in non-rotating and rotating conditions.
2. Provide information of heat transfer on trailing, leading, side and inner walls especially in the hub turn region under high rotation number (Ro=0~0.45) and buoyancy parameter (Bo_x=0~0.8) conditions.
4. Study the effect of staggered ribs (e/D_h=0.094, P/e=8) on heat transfer in both non-rotating and rotating conditions.
5. Investigate the effect of turning vane on heat transfer in the two-pass channel with both smooth and rib-roughed surfaces in stationary and rotating conditions.
6. Study the effect of channel orientation on heat transfer in this rotating channel for both smooth and ribbed surfaces with or without the turning vane.

Table 1 Test matrix for rectangular channels (AR=2:1) with a tip turn and a hub turn

Geometry	Configuration	Rotation Speeds	Orient. Angle	Density Ratio	Re	Ro	Bo
Two-pass 2:1 channel Tip Turn	Smooth	400 rpm | 0 rpm	90° | 135°	0.11	10k | 40k	0.45 | 0	0.8 | 0
	P/e=5						
	P/e=7.5						
	P/e=10						
Two-pass 2:1 channel Hub Turn	Smooth	400 rpm | 0 rpm	90° | 135°	0.11	10k | 40k	0.45 | 0	0.8 | 0
	Smooth + Vane						
	Ribbed (P/e=8)						
	Ribbed + Vane						

2. EXPERIMENT SETUP

2.1 Rotating Facility

The rotating facility used to conduct the experiments for the current study is shown in **Figure 3**. A steel table is used as the support structure. A 25 hp electric motor is used to drive the shaft which spins the arm. Counterweights are used to balance the arm so that minimal vibrations are experienced during rotation. Air from a compressor enters an ASME square-edge orifice meter (not shown) where the mass flow rate is measured. Air enters the rotating assembly at the bottom of the shaft via a rotary union and then passes through the hub and goes into the bore of the arm. A rubber hose is used to direct the flow from the arm to the pressure vessel in which the test section is placed. After the air flows through the test section, it exits the pressure vessel. The hot exhaust air is then directed by another rubber hose to the bore of the arm. A ½-inch copper tube, which passes through the bore of the slip ring, is used to direct the air from the rotating arm bore to the top rotary union. Steel pipe is connected to the top rotary union and a valve is used to adjust the back pressure of the system.

2.2 Two Pass Rectangular Channel (AR=2:1) with a Tip Turn

The geometry of the two-pass channel with a 180^{o} sharp turn in the blade tip portion is shown in **Figure 4**. As shown, the air enters the test section through a 9.525 mm circular inlet hose and then expands to the rectangular cross-section of the test section passage. Width (W) of the flow channel is defined as the distance between the

outer and inner surfaces and height (H) of the channel is the distance between the leading and trailing surfaces as seen in **Figure 4 (b) and (c)** respectively. The channel in this study had a height of 12.70 mm and a width of 25.40 mm, resulting in a hydraulic diameter (D_h) of 16.93 mm and an aspect ratio of AR=(W/H)=2:1. It is shown that two screens were placed prior to the unheated region of the test section, to help spread the flow at the entrance. The wire diameter of the screen is 0.015 mm. A nylon substrate, with a low thermal conductivity, is used to support the copper plates and heaters. Between adjacent copper plates is a strip of insulation material which prevents conduction and create a smooth surface between them. The flowing air is heated using prefabricated rubber-silicone heaters that are placed beneath the copper plates as seen in **Figure 4 (c)**. A total of 8 heaters are used for the outer, inner, leading and trailing walls. An additional heater is used for the tip region. Thermally conductive paste is used between the heaters and the copper plates in order to reduce contact resistance.

Figure 4 also shows that the test channel consists of two passes. The flow in the first passage is radial outward, and after the 180º turn with a square outer wall, the flow in the second pass is radial inward. There are a total of twelve regions in the test section in streamwise direction as shown in **Figure 4 (a)**. Each passage consists of six regions, except for inner walls, which have 5 regions as shown and labeled in **Figure 4 (c)**. The overall length of each passage is 203.0 mm. The heated channel length of each passage is 157.0 mm and the unheated entrance length is 46.0 mm. One thermocouple is placed at the inlet and exit respectively to measure the air temperature as it enters or leaves the test section.

The thickness of all copper plates is 3.175 mm. The copper plates on the leading and trailing walls are square in shape and measure 23.81 mm x 23.81 mm except for those in the turn regions (#6 & #7 on both leading and trailing surfaces) which measure 28.58 mm x 28.58 mm and fillet 6.35 mm at the inner corner. The outer and inner wall copper plates are rectangular and measure 23.81 mm x 12.70 mm. The tip copper plates are rectangular with dimensions of 29.37 mm x 12.70 mm. Blind holes, with a diameter of 1.59 mm, are drilled 1.59 mm deep on the backside of each copper plate. Thermocouples are placed inside of the blind holes of the copper plates and are affixed to the copper plates using highly conductive epoxy. Temperature measurements were made on all of the leading, trailing, outer, inner and tip cap copper plates. Thus, a total of 48 temperature measurements were made from copper plates. As shown in **Figure 4 (c)**, the channel orientation angles (β) based on the definition provided before are 90^o and 135^o as to approximate the rotation of a cooling passage in different portions of a real turbine blade.

Ribs with a square cross-section are placed on the leading and trailing walls of the first and the second passages. The rib height (e) is 1.59 mm and three ratios of the rib pitch (P) to the rib height (e) integrated in this paper are P/e=5, 7.5 and 10 respectively. The ribs are placed at an attack angle (α) of 45^o to the mainstream flow and the ribs on leading and trailing walls are parallel to each other. The configurations of the rib P/e ratios and attack angle (α) are shown in **Figure 5**.

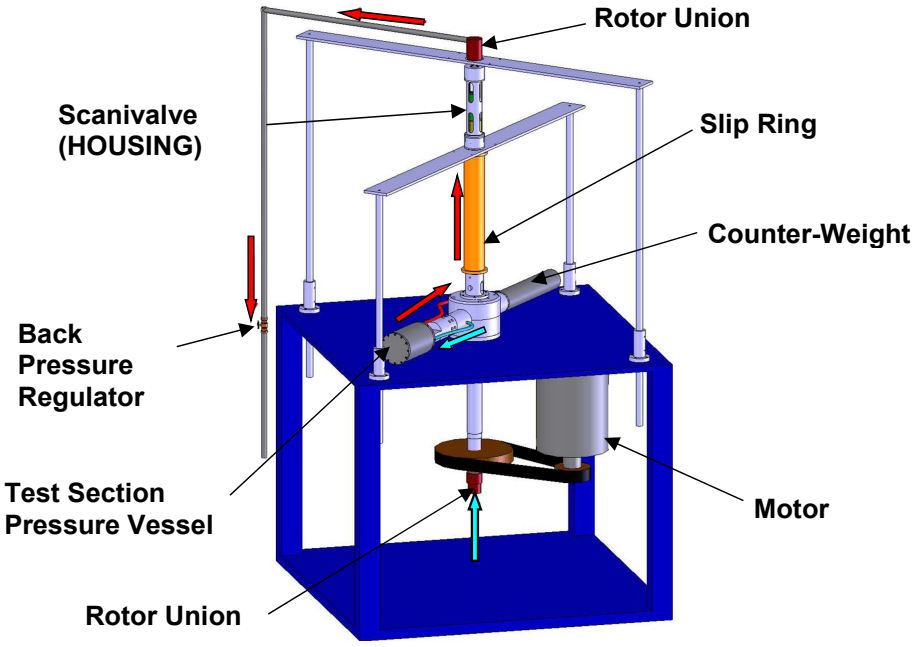

Fig. 3 Rotating facility used to perform the heat transfer experiment

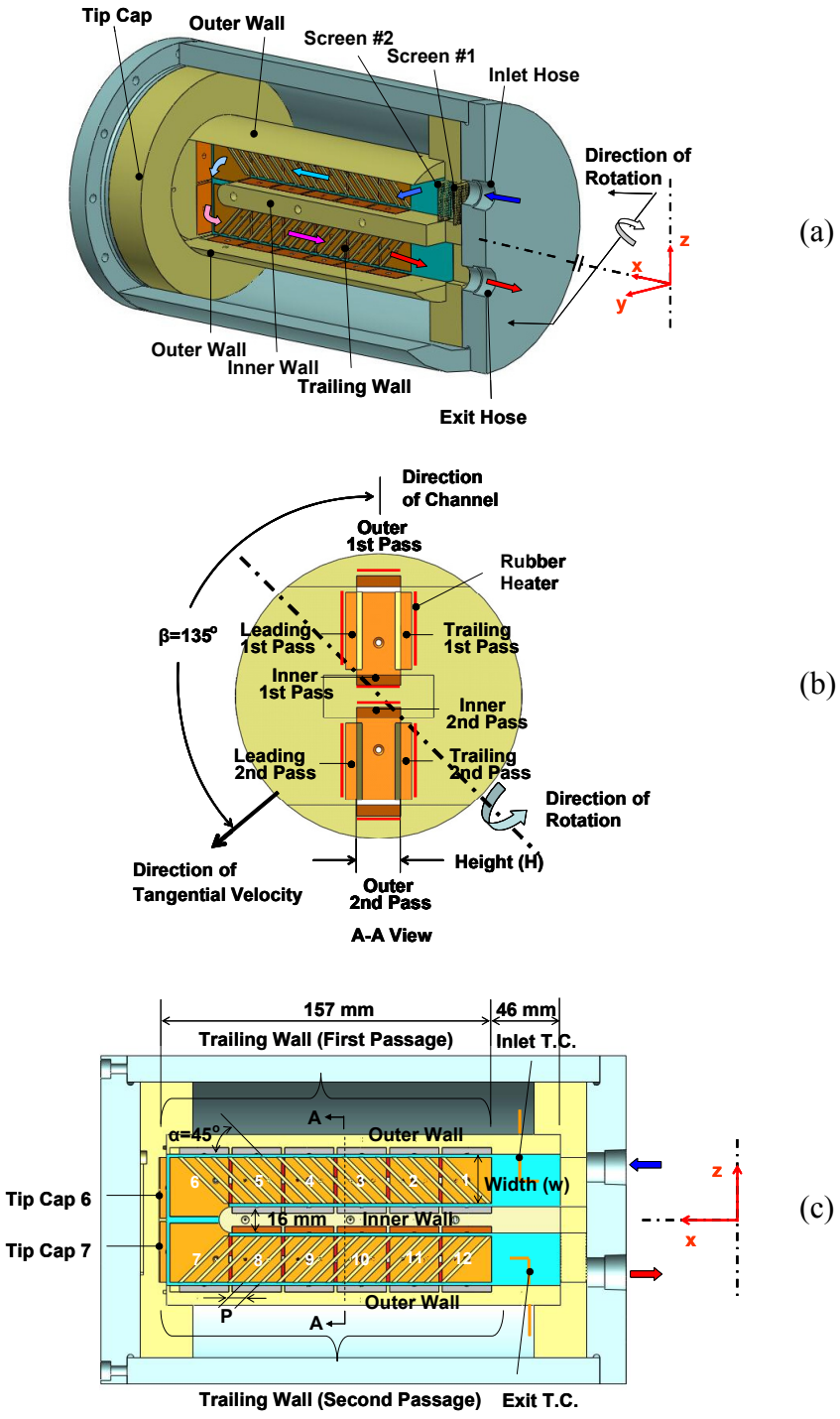

Fig. 4 Sketch of the AR=2:1 channel with a tip turn: (*a*) 3-D view (*b*) top view showing names of walls and corresponding heaters (*c*) section view showing copper plate numbering

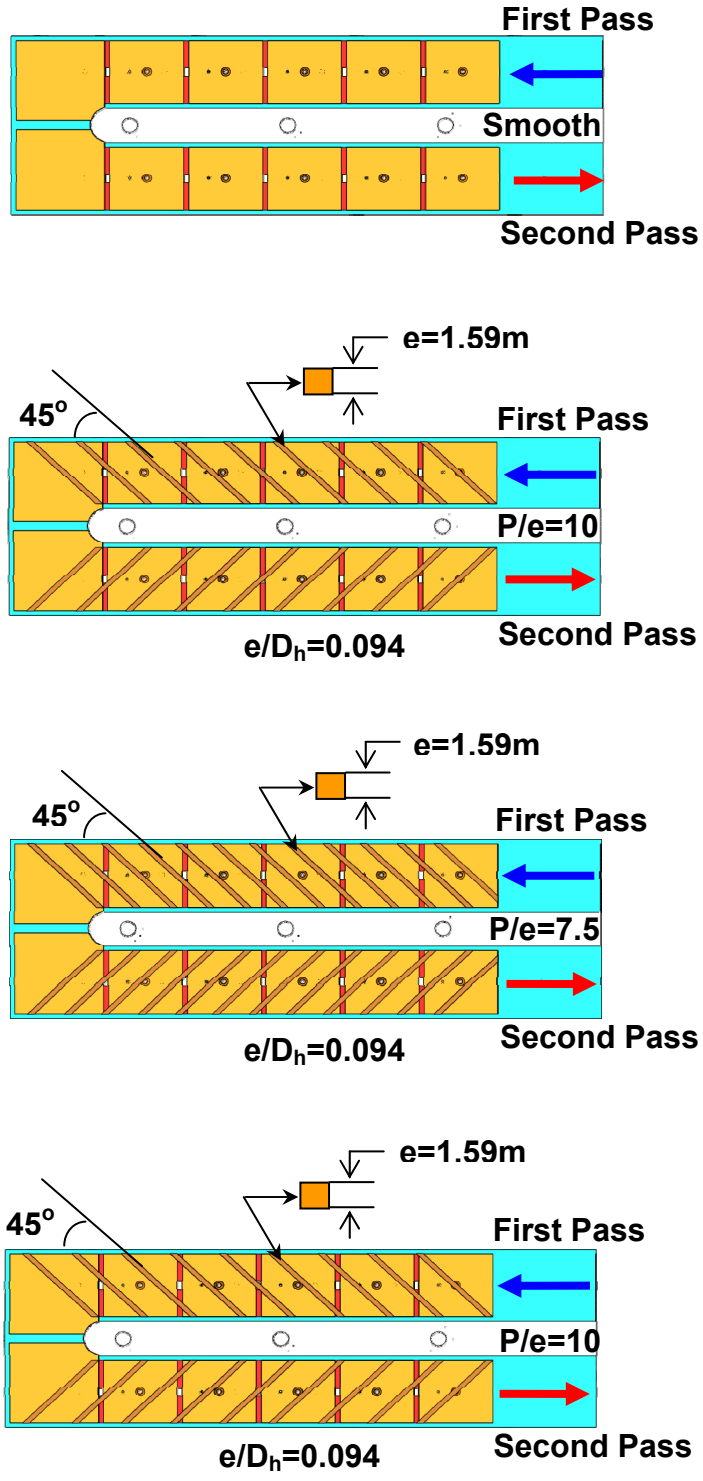

Fig. 5 Surface condition of the AR=2:1 channel with a tip turn

2.3 Two Pass Rectangular Channel (AR=2:1) with a Hub Turn

The geometry of the two pass channel connected by a 180^o U bend in the blade hub portion is shown in **Figure 6**. The air loop of the rotating facility outside the pressure vessel is the same as described for the previous test section. The air supply and exhaust pattern inside the pressure vessel is different. As shown in **Figure 6**, inside the pressure vessel, rubber hoses of 9.525 mm in diameter are used to connect the test section with the pressure vessel air inlet/exit. On the aluminum plate of pressure vessel, hose fittings are threaded in the inlet and exit holes directly. At the inlet and exit of the test section, two aluminum connection parts are used to joint the test section with the hose fittings. Air enters the pressure vessel through rubber hose and then expands into the passage with square cross-section before the turn. After the 180^o sharp turn, air goes into the first passage of rectangular cross-section. The two-pass experimental channel with heated surfaces starts from here and ends right after the second passage before the other 180^o sharp turn. Width (W) and height (H) of the channel are defined and shown in **Figure 6 (b) and (c)** respectively. The channel in this study has a height of 12.70 mm and a width of 25.40 mm, same as the rectangular channel with a tip turn and consequently the same aspect ratio of 2. The substrate made of SLS PA nylon, with thermal conductivity of 0.7 W/(m K), is used to support the copper plates and heaters. Between adjacent copper plates is a strip of insulation material which prevents conduction and create a smooth surface between them. The flowing air is heated using prefabricated Kapton heaters that are placed beneath the copper plates as seen in **Figure 6 (c)**. In both first and second passages respectively, 4 heaters are used for side, inner,

leading and trailing walls. In the hub turn region, 3 heaters are applied on side, leading and trailing surfaces. Thermally conductive paste is used between the heaters and the copper plates in order to reduce contact resistance.

Figure 6 reveals that the heated test channel is composed of two passages and a 180^o U bend. Before the 180^o U bend in the first passage, the flow is radial inward, and after the 180^o U bend in the second passage, the flow is radial outward. In both first and second passages, there are 4 heated walls circumferentially as leading, trailing, side and inner walls. In the 180^o U bend portion, 3 heated walls are named as leading, trailing and hub (side) wall. Note, only in this 180^o U bend portion, side wall can be called as hub wall also. There are a total of fourteen regions in the test section in streamwise direction as shown in **Figure 6 (a)**. As shown and labeled in **Figure 6 (c)**, the first and the second passages consist of five regions respectively, except for side walls, which have 4 regions. In the hub turn portion, there are four regions on side, leading and trailing walls. The overall length of first/second passage is 127.0 mm and the unheated entrance length is 62.0 mm. In the turn portion the divider radius equals 7.32 mm (r_i =0.3W) and side wall radius equals 31 mm (r_o=1.3W). Two thermocouples are placed at the inlet and exit respectively to measure the air temperature as it enters or leaves the test section.

The thickness of all copper plates is 3.175 mm. In the first and the second passages, the copper plates on the leading and trailing walls are square in shape and measure 23.81 mm x 23.81 mm and the side and inner wall copper plates are rectangular and measure 23.81 mm x 12.70 mm, both of which are the same as those used in the tip turn test section. For the turn region, on trailing and leading walls, the copper plates are

identically fan-shaped and on the side wall, they are identically arc-shaped. Blind holes, with a diameter of 1.59 mm, are drilled 1.59 mm deep on the backside of each copper plate. Thermocouples are placed inside of the blind holes of the copper plates and are affixed to the copper plates using highly conductive epoxy. Temperature measurements were made on all of the leading, trailing, side and inner copper plates. Thus, a total of 50 temperature measurements were made from copper plates. Similarly, the channel orientation angles (β) based on the definition are 90^o and 135^o as to approximate the rotation of a cooling passage in different portions of a real turbine blade.

Ribs with a square cross-section are placed on the leading and trailing walls of the first/second passage and the turn region. The rib height (e) is 1.59 mm and the rib pitch (P) to the rib height (e) ratio in this test is P/e=8. The ribs are placed at an attack angle (α) of 45^o to the mainstream flow on leading and trailing walls in a staggered pattern. Turning guide vane in the shape of half circle with radius R ($R \approx D_h$), height S (S=H) and thickness t (t=e) is installed for some cases. Both ends of the vane are rounded to prevent flow separation. The configurations of ribs and the vane are shown in **Figure 7**.

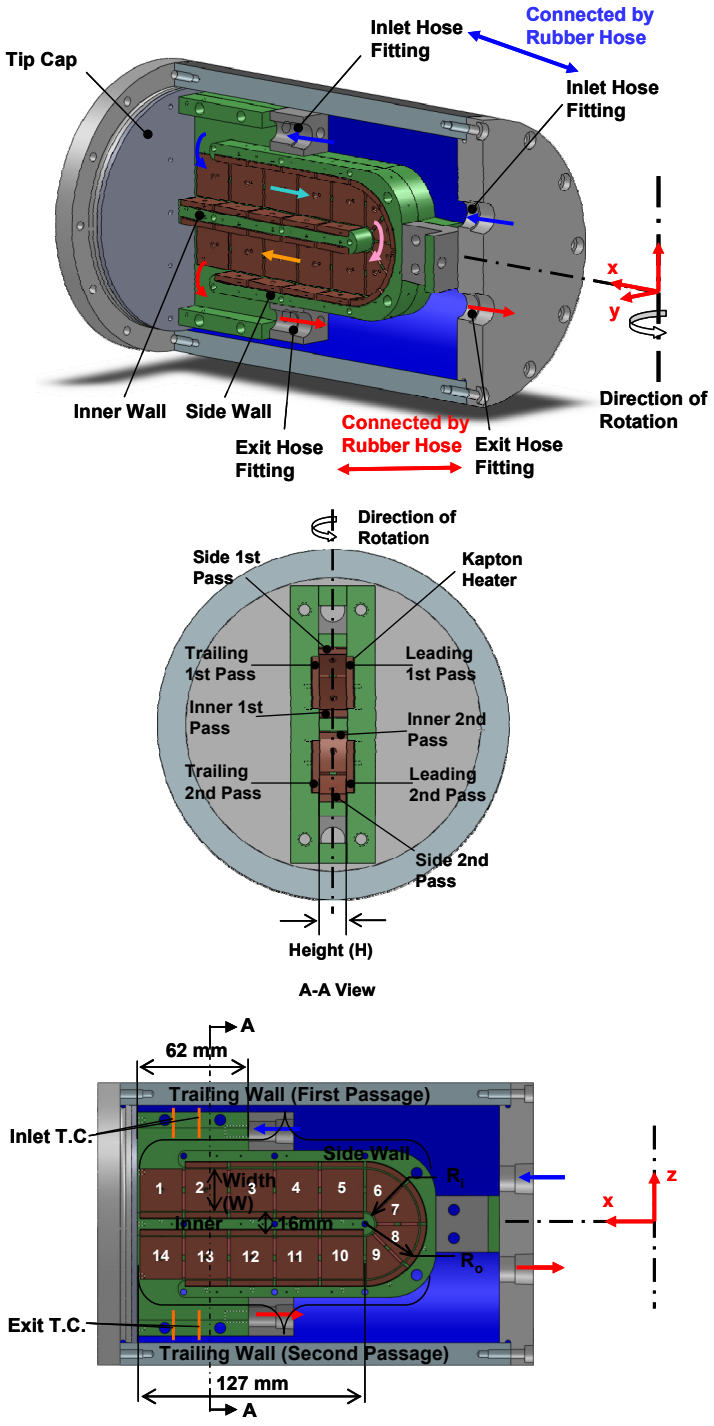

Fig. 6 Sketch of the AR=2:1 channel with a hub turn: (*a*) 3-D view (*b*) top view showing names of walls and corresponding heaters (*c*) section view copper plate numbering

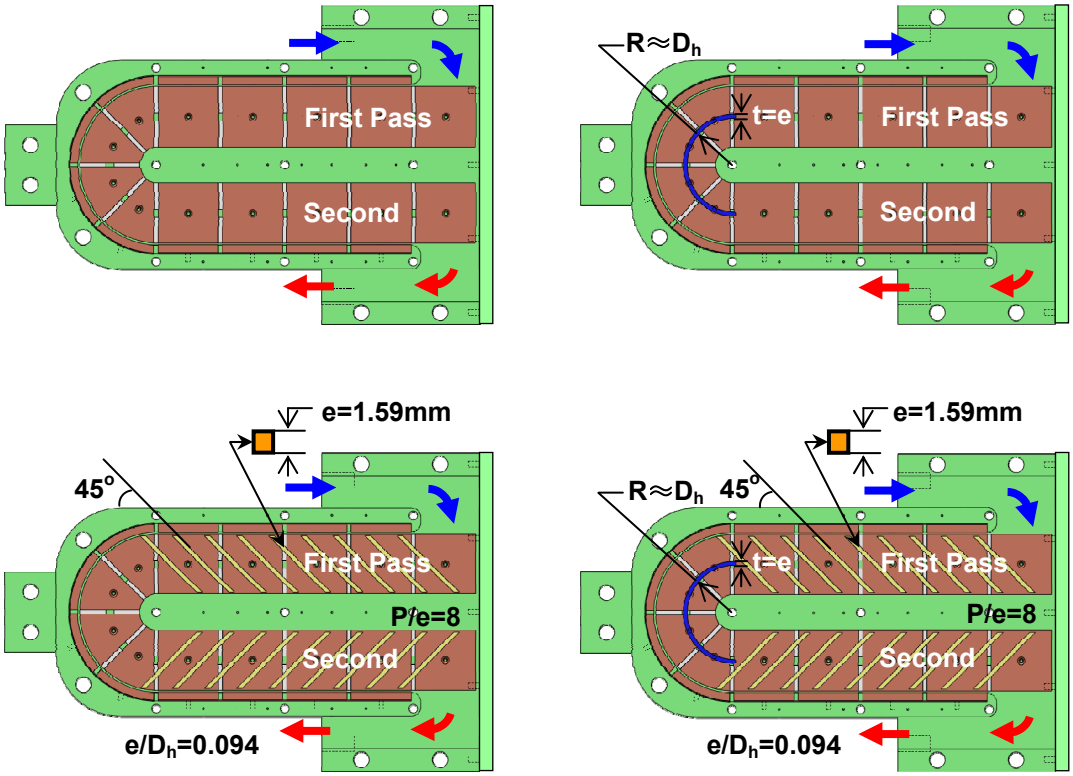

Fig. 7 Surface condition of the AR=2:1 channel with a hub turn

3. DATA REDUCTION

3.1 Heat Transfer Measurement

This study investigates the regionally averaged heat transfer coefficient (h) at various locations within a rotating duct. A uniform wall temperature of 65°C, in the circumferential direction, is maintained at regions 4 and 10 throughout all the tests. In the current study, the regionally averaged heat transfer coefficient is calculated using the net heat transferred to the air from the heated copper plate (Q_n), the projected surface area of each copper plate (A_p), the local region wall temperature of the plate ($T_{w,x}$), and the local bulk mean temperature of the air flow in the channel ($T_{b,x}$). Therefore, the regionally averaged heat transfer coefficient is given as

$$h=(Q_n/A_p)/(T_{w,x}-T_{b,x}) \quad (1)$$

The net heat transfer rate is calculated as:

$$Q_n=(V^2/R)(A_p/A_{htr})-Q_l \quad (2)$$

The voltage (V) is measured with a multi-meter and the resistance (R) is measured with a multi-meter before the heater is installed. To obtain the heat input to a copper plate, the power input to each heater is multiplied by the ratio of the projected area (A_p) to the total heater area (A_{htr}) and a uniform heat flux by the heater is assumed. In order to determine the external heat losses (Q_l) escaping from the test section during the experiment, two heat loss calibration tests are performed for each rotational speed, including stationary. The first heat loss calibration test is performed at a lower wall temperature than the experiment wall temperature. Similarly, a second heat loss

calibration test is performed at a higher wall temperature than the experiment wall temperature. During the heat loss calibration tests, the wall temperature of each copper plate is maintained by supplying power to each heater with the variac transformers. A successful heat loss calibration test for each copper plate is achieved when the total power input to the test section reaches equilibrium with the environment (i.e. the wall temperature reaches a steady state condition). The heat loss which occurs during the experiment is then determined by interpolating between the two sets of heat loss data. It is noted that heat loss calibration tests were performed at all rotational speed conditions considered in the present study and the stationary case as well. In order to minimize natural convection effects during the heat loss calibration tests, an insulating material was placed inside of the flow channel.

The local regional wall temperature ($T_{w,x}$) is directly measured using the thermocouple installed in the blind hole on the backside of each copper plate. Because the plates are made of copper, which has a high thermal conductivity, the temperature of each plate is assumed uniform. One thermocouple at the inlet and another thermocouple at the outlet of the test section measure the inlet and outlet bulk temperatures, respectively. Therefore, the local bulk air temperature at any location in the test section can be calculated using linear interpolation. Another method to get the bulk temperature is by energy balance.

The Dittus-Boelter/McAdams correlation for heating ($T_{w,x} > T_{b,x}$) is used in this study to provide a basis of comparison. The Dittus-Boelter/McAdams correlation is used to calculate the Nusselt number (Nu_o) for fully developed turbulent flow through a

smooth stationary pipe. Therefore, the heat transfer enhancement (Nu/Nu_o ratio) is given as:

$$(Nu/Nu_o)=[(h\cdot D_h)/k][1/(0.023\cdot Re^{0.8}\cdot Pr^{0.4}] \quad (3)$$

where heat transfer coefficient (h) is calculated by Eq. (1). All air properties are taken based on the channel average bulk air temperature with a Prandtl number (Pr) for air of 0.71.

3.2 Uncertainty Analysis

An uncertainty analysis was performed based on the method described by Kline and McClintock [40]. For the tip turn test section, air properties were based on the mean bulk air temperature, which may introduce uncertainty for air properties such as density, conductivity, specific heat and viscosity. These uncertainties influence the accuracy of calculated Reynolds number, rotation number, buoyancy parameter and Nusselt number. For the hub turn test section, air properties were compensated locally at every region based on local bulk temperature and corresponding information provided by NIST. Some of the above parameters, such as: Reynolds number and rotation number were re-calculated regionally. The comparison between these values and the channel-averaged ones tells that the difference is less than 5%.

For the tip turn test section, the estimated uncertainty for the temperature instrumentation is 0.5°C. At lowest Reynolds number (Re=10,000), the maximum uncertainty of the Re is approximately 10% and the maximum uncertainty of the Nu is estimated as 12.5%. For the hub turn test section, the estimated uncertainty for the

measured temperature is 0.5°C. At lowest Reynolds number (Re=10,000), the maximum uncertainty for Nu is estimated as 10.5%.

4. RESULTS AND DISCUSSIONS

4.1 Two Pass Rectangular Channel (AR=2:1) with a Tip Turn

4.1.1 Flow Behavior

The heat transfer behavior is highly connected with the flow field and analysis of the flow behavior is helpful to understand the heat transfer phenomenon. The flow field parameter includes: mainstream velocity, secondary flow velocity, turbulence intensity, etc. They are correlated to each other and all of them are influential to the heat transfer result. For example, The flow behaviors of the mainstream in the 2:1 channel with a tip turn in stationary condition include, mainstream flow, entrance-induced separation, turn-induced separation and mainstream flow deflected by ribs as shown in **Figure 8**. When the mainstream flow enters the test section through the upstream hose, it separates immediately because of the sudden-expansion entrance. Then, the flow develops in the first passage and it enters the 180^{o} sharp turn portion. Due to the square shape of the outer (tip) wall corners, two separation vortices form there. Near the inner wall, mainstream starts to separate because of the curvature. A circulation zone is formed on the inner wall right after the turn in the second passage due to the separation and consequently, mainstream is squeezed toward the outer wall. Besides, Dean vortex is generated in the cross-section plane perpendicular to the mainstream flow direction and it pushes the mainstream core toward the outer (tip) surface as shown in **Figure 9**. In the second passage, the mainstream recovers to a more uniformed profile after it passes the circulation region. Finally, the flow exits the test section through exit hose and forms

another separation zone. According to research done by son et al. [31], in the smooth channel, before the sharp turn, turbulence kinetic energy level is low and it is elevated significantly in the turn region and after-turn passage. Near the boundary between recirculation flow and the mainstream in the second passage, due to the shear, the turbulence level is the highest in the whole channel.

The influence of ribs on local flow behavior is shown in **Figure 9**. When the mainstream flow near the roughed surface passes over the rib, it separates from the wall due to the rib. This separation results in low heat transfer just downstream of the rib, due to the hot cell trapped in the recirculation area. However, when the mainstream flow reattaches to the wall (between two ribs), the heat transfer level is largely elevated. Redevelopment of the boundary layer then begins from here. This pattern of separation, recirculation, reattachment and redevelopment continues throughout the channel along with the repeating ribs. In addition to general flow patterns due to ribs, they increase turbulent mixing which helps to increase the heat transfer on surfaces. In addition to the mainstream flow impingement, separation, recirculation and reattachment, it is deflected by the rib. In the first passage as an example, air flows along the angled ribs from the inner wall to side wall and goes back to the center portion of the channel, forming a pair of vortex. The conceptual view of the rib-induced vortex is shown in **Figure 9 (a) and (b)**.

The flow behavior and consequent heat transfer level is also influenced by rotation and rotation induced buoyancy forces. **Figure 10** shows the mainstream and the secondary flows induced by rotation and rotation-induced buoyancy forces. The Coriolis

force favors the trailing surface in the first passage with radial outward flow and favors the leading surface in the second passage with radial inward flow. However, due to the reversed directions of mainstream and buoyancy force, to some point, flow starts to reverse and separation is formed. Simultaneously, the Coriolis force induces a pair of vortices, favoring the trailing surface in the radial outward passages and leading surface in the radial inward passages for the orientation angle (β) of 90^o. In the tilted channel ($\beta=135^o$), as in **Figure 10 (b)**, the pair of vortices impinges on the trailing surface and the outer wall in the first passage with radial outward flow. They impinge on the leading surface and the outer wall in the second passage with radial inward flow. The combination of these complex flow behaviors may result in enhancement of the heat transfer, or they may have a negative impact on the heat transfer trend.

Rotation causes a difference in the heat transfer. The effect of rotation is evaluated by the rotation number (Ro), defined as the ratio of the Coriolis force to the inertial force as shown in Eq. (4).

$$Ro=(\Omega D_h)/U_b \tag{4}$$

The combined effect of rotation and coolant temperature gradient is evaluated by the local buoyancy parameter (Bo_x). For heated channels, the inertial force is in the same direction as the centrifugal force in the first pass with radially outward flow and in the opposite direction in the second pass with radially inward flow. The local buoyancy parameter is defined in Eq. (5).

$$Bo_x=(\Delta\rho/\rho_{b,x})(Ro)^2(R_x/D_h) \tag{5}$$

This local buoyancy parameter can be re-written by incorporating the measured wall and bulk air temperatures as shown in Eq. (6).

$$Bo_x=[(T_{w,x}-T_{b,x})/T_{f,x}](Ro)^2(R_x/D_h) \quad (6)$$

Local film temperature ($T_{f,x}$) is the average of the local wall and the local bulk temperatures as shown in Eq. (7).

$$T_{f,x}=(T_{w,x}+T_{b,x})/2 \quad (7)$$

The corresponding rotation number Ro and channel-averaged buoyancy parameter Bo at each tested Reynolds number and rotational speed are shown in **Figure 12**.

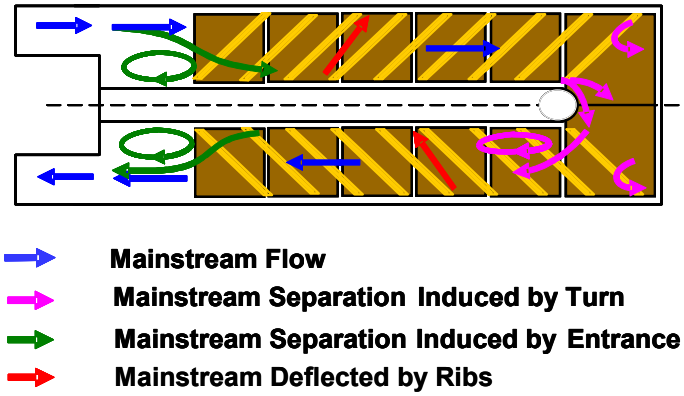

Fig. 8 Conceptual view of the mainstream flow behaviors in the 2:1 test section with a tip turn

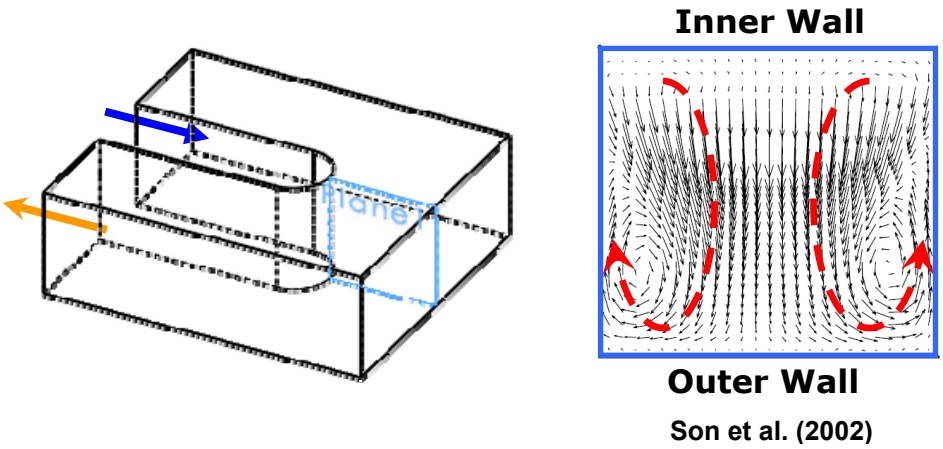

Son et al. (2002)

Fig. 9 Conceptual view of the secondary flow behaviors induced by turn

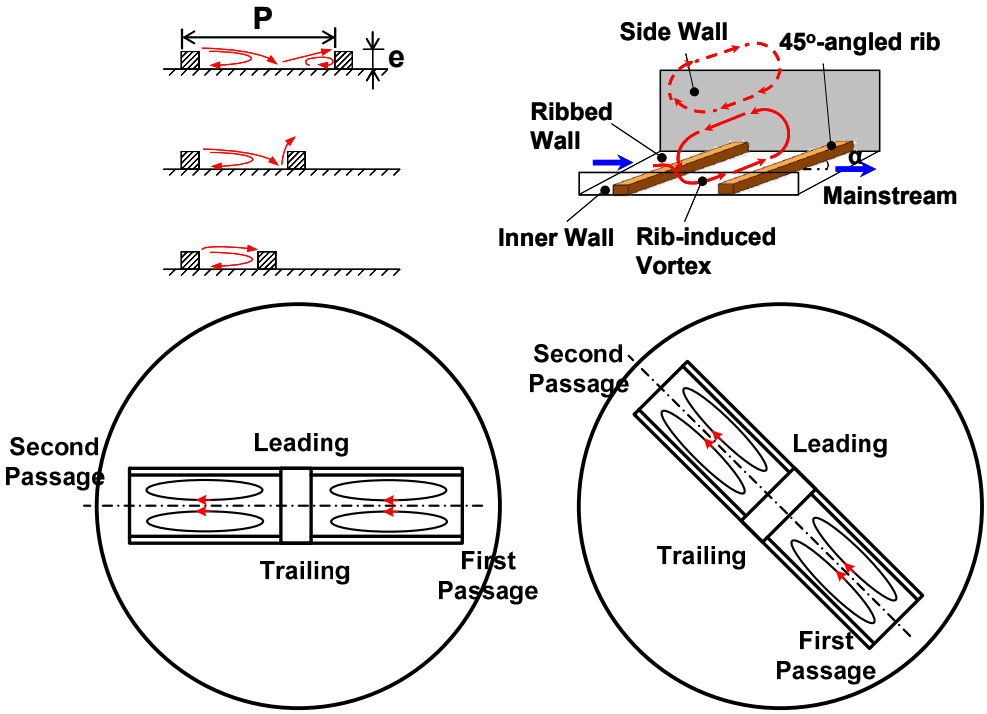

Fig. 10 Conceptual view of the mainstream and secondary flow behaviors induced by ribs

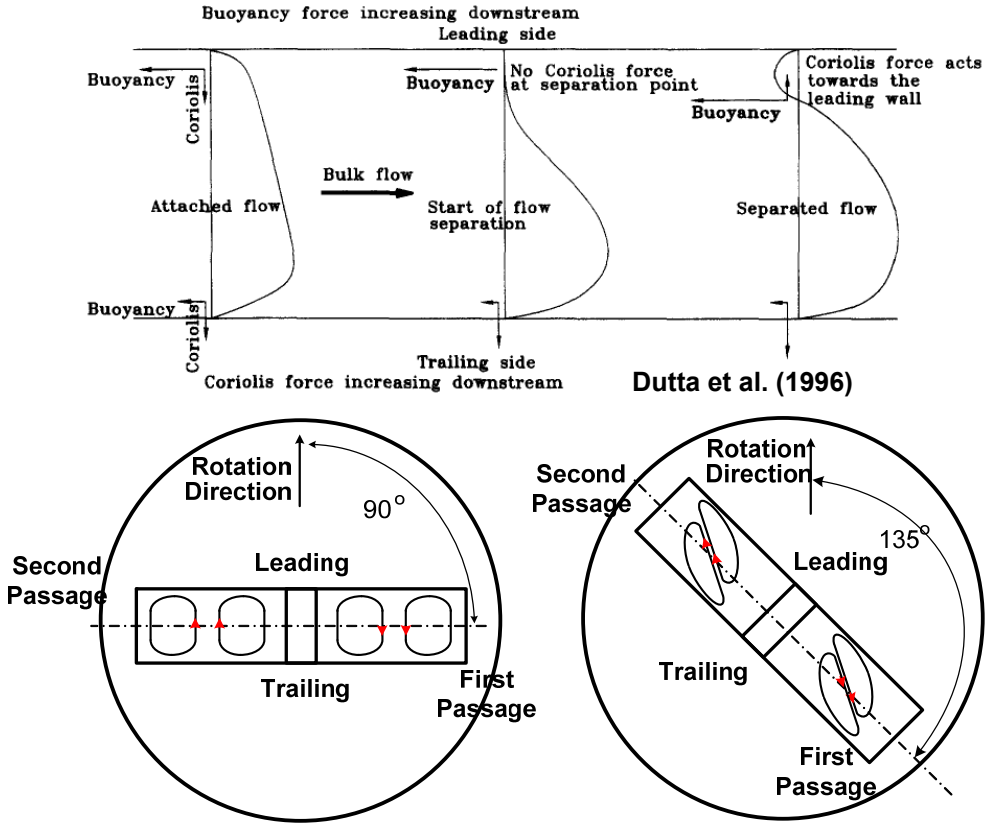

Fig. 11 Conceptual view of the mainstream and secondary flow behaviors induced by rotation

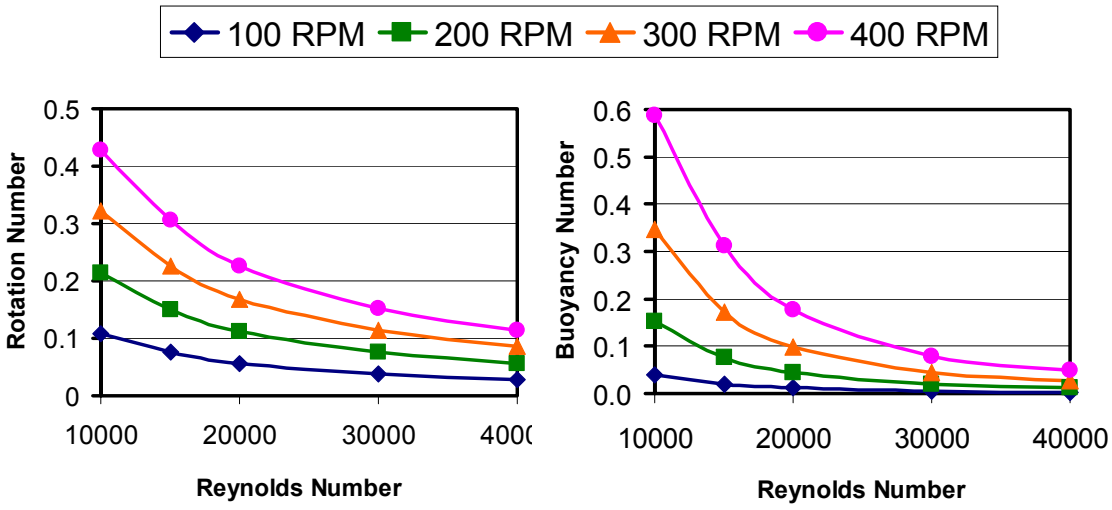

Fig. 12 Rotation number and buoyancy parameter at different Re and rotation speeds

4.1.2 Heat Transfer in Stationary Channel

When the channel is not rotating, the flow complexity is reduced because of the absence of the Coriolis and rotation-induced buoyancy forces. The rib effects previously stated as mainstream flow separation, recirculation and reattachment, turbulent mixing, and angled rib-induced secondary flow still exist.

The Nusselt ratio distributions of smooth and ribbed cases in the stationary channel at Re=20,000 and 40,000 are shown in **Figure 13**. For the smooth case, in the first passage, Nu_s/Nu_o ratio presents a characteristic trend of decreasing due to entrance effect on all walls. In the turn region (#6 & #7), heat transfer elevates prominently on trailing and leading walls because of turn-induced secondary flow and increased level of turbulent mixing. The substantial growth of heat transfer on outer wall is because of the curvature-induced Dean vortex, which impinges the mainstream core on outer surface. In the second passage, Nu_s/Nu_o ratio decreases on leading and trailing walls and it reduces at a higher rate on outer wall, however, on the inner wall, Nu_s/Nu_o ratio remains a constant low value due to flow separation bubble along the divider wall and increases near exit.

For the ribbed cases, on leading, trailing and inner walls, the Nu_s/Nu_o ratio experiences a decrease and increase in the first and the second passages, however, heat transfer drops substantially in the turn portion on leading and trailing walls. On the outer wall, the Nu_s/Nu_o ratio presents a similar trend as the smooth case in the first pass and obtains its maximum in the second pass. The decrease of heat transfer in the first/second passage on leading and trailing walls, similarly, is due to the entrance effect and the next

increase is attributed to the rib-deflected mainstream, rib-induced secondary vortex and rib-enhanced turbulent mixing. In the turn portion, heat transfer on leading and trailing surfaces is largely decreased because most area in copper plate #6 and #7 is absent of ribs as shown in **Figure 5**. The lower level of heat transfer on outer wall is due to the reduced size and strength of Dean vortex, which is eased by the angled rib-induced vortex from upstream. The relatively low heat transfer on the outer wall compared to inner in the first passage and opposite trend in the second passage is due to the angle of ribs, by which, relatively cold mainstream flow moves from the inner wall and impinges on outer as warm fluid in the first pass and vise versa. In the first or second passage, the effect of rib spacing (P/e) is obvious on leading and trailing surfaces as well as inner and outer walls, however, in the turn portion it is not significant. The Nu_s/Nu_o ratio increases as P/e ratio decreases in the passages due to the enhanced angled rib-induced secondary flows, but, in the turn portion, because of the partial coverage of ribs, the Nu_s/Nu_o ratio drops to the same low level for all P/e ratios. The effect of Reynolds number on Nusselt number ratio is observed between **Figure 13 (a) and (b)**. The Nu_s/Nu_o ratio on all surfaces in the channel decreases slightly with increasing Reynolds number. This can be explained as that the increase of Nu_s is not as much as the increase of Nu_o, which is determined by the Dittus-Boelter/McAdams correlation.

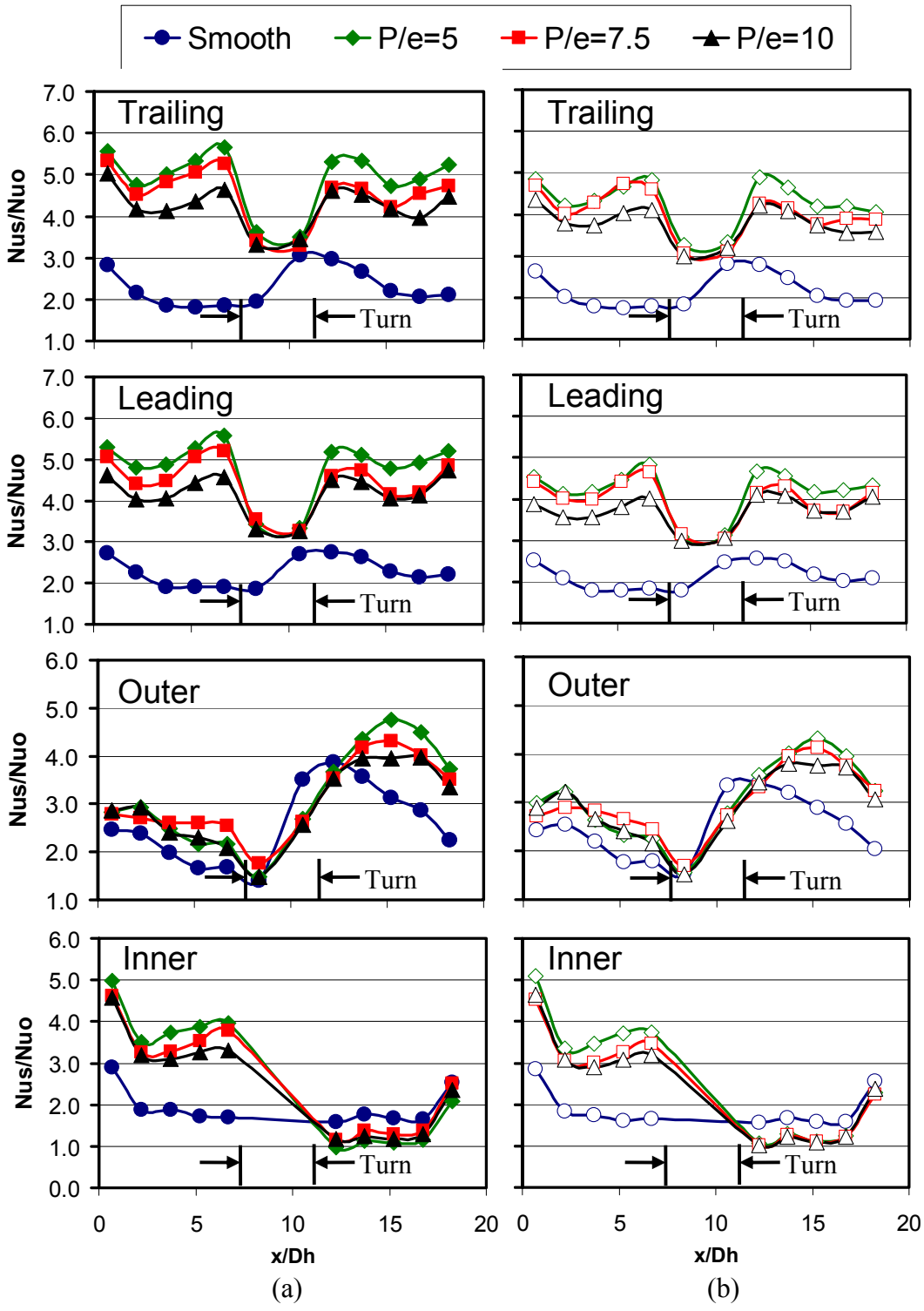

Fig. 13 Stationary streamwise Nu_s/Nu_o ratio at (*a*) Re=20k and (*b*) Re=40k

4.1.3 Heat Transfer in Rotating Channel

When channel is rotating, the fluid inside the channel is subjective to inertial force, rotation induced buoyancy force and Coriolis force. The inertial force is coincident with the mainstream flow direction, while the centrifugal force continuously acts in the radially outward sense. The Coriolis force acts perpendicular to the mainstream flow direction. As shown in **Figure 10**, with an channel orientation angle of 90^{o} and radially outward flow (first pass), the Coriolis force pushes the core fluid mass towards the trailing wall and results in a pair of cross-stream vortices that impinge directly on to the trailing surface. Furthermore, the Coriolis force on average causes the mass of coolant near the trailing wall to be greater than that near the leading wall. Due to mass continuity, the local axial velocity near the trailing wall is increased while the velocity near the leading wall decreases. In a heated channel, a temperature gradient throughout the coolant is developed under rotating conditions thereby resulting in a variation of fluid density. With a radial outward flow, the fluid mass near the trailing wall is of lower temperature since the coolant bulk flow velocity is skewed as previously mentioned. The density of the coolant will tend to be greater near the trailing wall. The centrifugal force acts strongly near the trailing wall since the fluid is heavier and accelerates the heavier fluid towards the tip of the channel. The result is a further increase in local axial velocity near the trailing wall and flow stabilization near the leading wall. Thus, the heat transfer will generally increase on the trailing wall and decrease on the leading wall.

After the 180^{o} sharp turn, flow direction alters from radial outward towards radial inward. With a radial inward flow, the direction of the Coriolis force changes. The rotation-induced vortices now impinge on the leading surface and the axial velocity profile is skewed towards the leading wall. This tends to increase heat transfer on the leading wall (relative to the stationary frame) and decrease heat transfer on the trailing wall. However, the centrifugal force and the inertial force of the fluid are counteracting in the second pass with a radially inward flow direction. Thus, comparing to the first passage with radial outward flow in which centrifugal force causes the velocity of the fluid to increase even further (above the Coriolis force effects) on the trailing surface, now the centrifugal force retards the local axial velocity near the leading wall in the second pass since the coolant density is higher near the leading wall. Overall, the axial velocity profile with radial inward flow is not as strongly skewed towards the leading wall. This results in less of a difference between the trailing and leading wall heat transfer coefficients with radially inward flow.

After placing the smooth channel at an angle of 135^{o} to the direction of rotation as shown in **Figure 11**, the Coriolis force induced vortices become asymmetric. The secondary flow due to rotation tends to travel from the inner-leading corner towards the outer-trailing corner in the first pass and from the inner-trailing corner towards the outer-leading corner in the second pass. Thus, the rotation induced vortices no longer directly impinge on the trailing surface in the first pass or the leading surface in the second pass. This behavior has been reported by Azad et al [26] and Al-Hadhrami et al [27] for 2:1 aspect ratio channels inclined at an angle of 135^{o}. The inclusion of ribs on the leading

and trailing surfaces of the cooling channel creates rib induced vortices as shown in **Figure 10**. In the current study the angled rib secondary flow is directed from the inner wall towards the outer wall in the first pass and from the outer wall towards the inner wall in the second pass. The interaction of the two secondary flows (Coriolis and rib induced vortices) can be constructive or destructive. This interaction will determine the heat transfer behavior in the rotating channel with ribs and at different angles of rotation.

Figure 14 shows the streamwise Nu/Nu_o ratio distribution at different speeds of rotation ranging from 0-400 rpm. Results from the smooth cases are presented (smooth $\beta=90^o$, smooth $\beta=135^o$) at a fixed Reynolds number of 20,000. The effect of the angle of rotation on heat transfer is clearly seen for the smooth channel. **Figure 14 (b) (d)** show the heat transfer distribution on leading surface of the smooth channel for $\beta=90^o$ and $\beta=135^o$. In the first pass, with the channel normal to the direction of rotation, increasing the rotational speed from 0 to 400 rpm reduces the Nu/Nu_o ratio by about 12% below the stationary case at x/D_h=5.2. This decrease is due to Coriolis force effects on the mainstream velocity distribution. The flow near the leading wall is decelerated which causes the heat transfer to decrease. However, when the channel is oriented at an angle of 135^o, rotation causes a beneficial increase in heat transfer slightly (compared to stationary) on the first pass smooth leading surface. This beneficial heat transfer increase is a result of the effect of the rotation angle. The angle of the channel alters the formation of the Coriolis force induced vortices, causing the secondary fluid motion to be from the outer-leading corner towards the inner-trailing corner. In the turn region, the Nu/Nu_o ratios increase greatly with rotation and a maximum value of 4.0 is reached at

x/D_h = 10.6 for the $\beta=90^o$ case. At the same location with the channel at $\beta=135^o$, the maximum value for Nu/Nu_o is reduced to 3.0. In the second passage, the effect of the angle of rotation on heat transfer of the leading surface is mostly seen far downstream. The turn induced secondary flow interacts with rotation induced vortices and thus, effects of β do not appear until turn secondary flow effects diminish further downstream.

The smooth results on trailing surface are presented in **Figure 14 (a) (c)**. Little difference is seen in heat transfer levels for the smooth first pass trailing surface at the two angles of rotation studied. Except for the entry region, note that orienting the channel at $\beta=135^o$ did not cause a decrease in heat transfer which might be expected since the Coriolis force induced vortices no longer directly impinge on the trailing surface at this angle. In the turn region, a maximum Nu/Nu_o ratio of 4.0 is reached at x/D_h =10.6 for the $\beta=90^o$ case. At the same location for the $\beta=135^o$ case, the maximum Nu/Nu_o ratio is 3.1. In the second pass, rotation causes the heat transfer on the trailing surface to decrease below the stationary case for both angles of rotation studied.

Figure 14 also shows that for the ribbed channel, the general trend is that the Nu/Nu_o decreases from the entrance but increases again due to angled rib-induced vortices and then decreases again when approaching the 180^o sharp turn since there are no ribs placed in the turn region. However, from **Figure 14 (f) (h)**, the effect of rotation on heat transfer is minimal on the leading surface in the first pass of the ribbed channel regardless of channel orientation. The heat transfer on the trailing surface in the first pass with ribs as shown in **Figure 14 (e) (g)** similarly shows a smaller dependence on rotation compared to the smooth channel. Overall heat transfer in the ribbed channel for both

cases ($\beta=90^o$, $\beta=135^o$) increase by approximately 5% over the stationary case, whereas in the smooth channel the increase due to rotation is more than 30%. This reduced effect of rotation (in the ribbed channel) is due to the interaction of rib induced vortices with rotation induced vortices. However, note that on the trailing surface, the maximum Nu/Nu_o ratio of 5.5 for the ribbed channel is greater than that of the smooth. In the second pass, the angled rib directs the mainstream flow near surface from the outer wall towards the inner wall. After it hits the inner wall, it returns back towards the outer wall through center portion of the channel, forming a pair of rib-induced secondary vortices. The heat transfer on the ribbed leading surface in the second pass shows a slight increase with rotation for both channels. The trailing surface heat transfer with ribs, for both channel orientations, decreases with rotation continuously with increasing rotational speed. However, the effect of rotation is less in the ribbed compared to the smooth. In the second pass, the flow field becomes quite complex with interactions between rotation induced vortices, rib induced vortices, and turn induced vortices.

The streamwise Nu/Nu_o ratio distribution for leading and trailing walls with smooth and different P/e ratios (P/e=5, 7.5, and 10) at Reynolds number of 20,000 are presented in **Figure 15**. For the smooth case, on the trailing surface, the Nu/Nu_o ratio increases with increasing rotation speed in the first pass and decreases in the second pass. However, on the leading surface, the Nu/Nu_o ratio is not as sensitive to rotation speed as that on the trailing surface in the whole channel. The heat transfer behavior of the trailing surface is mostly due to the Coriolis force which pushes mainstream toward trailing in the first pass and leading in the second pass. Rotational buoyancy also helps

the trailing surface in the first pass due to the additional near-wall turbulence. For the ribbed cases, on the trailing surfaces, the Nu/Nu_o ratio presents a streamwise distribution similar to the stationary case, except for the area near turn portion (copper plates #5, #6, #7, and #8), where heat transfer level increases 25% approximately. Obviously, the ribs reduce the effect of rotation in the first and second passage. The variation of the Nu/Nu_o ratio for different rotation speeds (100~400 rpm) is reduced in the whole channel. Comparatively, on the leading surface, except for the similar trend of streamwise distribution as trailing, Nu/Nu_o ratio decreases with higher rotation speed in the first pass and increases in the second pass, in which a larger effect of rotation is observed than the smooth case. The effect of P/e ratios on heat transfer in the rotating channel plays a role similar to that in the stationary channel on leading and trailing walls. The Nu/Nu_o ratio increases with decreasing P/e ratio in the whole channel except for the turning portion where Nu/Nu_o ratio keeps the same level.

The streamwise Nu/Nu_o ratio distribution on outer and inner walls is shown in **Figure 16**. For the smooth case, on the outer wall, the Nu/Nu_o ratio is increased with increasing rotation speed in both passages and in the first passage a larger effect of rotation is shown. An opposite trend is observed on the inner wall that Nu/Nu_o ratio is decreased slightly with increasing rotation speed in both passes. For the present passage orientation of 135^o shown in **Figure 10**, the change of heat transfer due to rotation on outer and inner surfaces is due to the secondary vortex induced by rotation at $\beta=135^o$, which impinges on the trailing and the outer wall in the first passage and impinges on the leading and the outer surface in the second passage. For the ribbed cases, on the

outer wall, the difference of Nu/Nu_o ratio between stationary and different rotation speeds is reduced in the first pass and greatly increased in the second pass comparing with the smooth case, which is attributed to the combined effect of rotation and the angled ribs. As shown in **Figures 10** and **11**, near outer wall of the first passage, vortices induced by ribs and rotation are in opposite directions and as a result, the effect of rotation is weakened by ribs on first pass outer wall. Contrarily, the effect of rotation is strengthened by ribs on the second pass outer wall. The effect of P/e ratios is to increase overall Nu/Nu_o level on most surfaces when reducing P/e. On the first pass outer wall and the second pass inner wall, Nu/Nu_o is not sensitive to P/e ratios. It is noted that the Nu/Nu_o ratios are relatively low on the second pass inner wall. This is possibly due to the separation bubble on the divider wall induced by the 180^o sharp turn.

The effect of rotation on heat transfer is greater in the smooth 2:1 channel compared to the ribbed. Similarly, the channel orientation effect is greater in the smooth channel, especially in the second passage. The smooth channel oriented at an angle of 135^o, shows a smaller difference in heat transfer levels between the leading and trailing surfaces compared to the 90^o smooth channel. For both channel orientations, rotation has more obvious effect on the trailing surface than the leading surface in both smooth and ribbed channels. The effect of rotation on heat transfer for different rib pitch-to-height ratios (P/e=5, 7.5, and 10) cases is almost the same. On trailing and inner surfaces, in rotating condition, little difference is observed between different rotating speeds. On leading and outer walls, the effect or rotation is obviously seen.

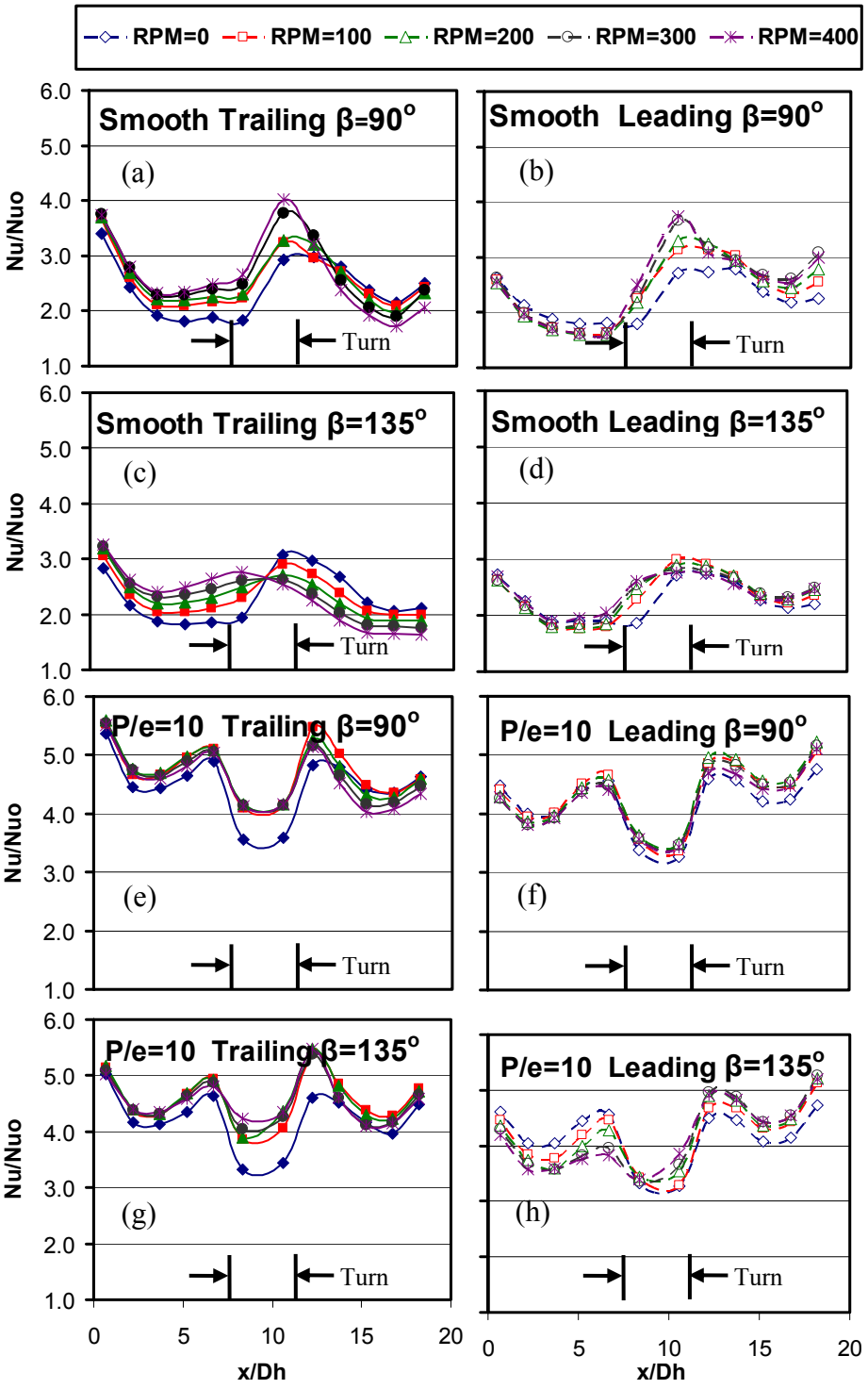

Fig. 14 Streamwise Nu/Nu_o ratio for Re=20k at β=90° and 135° for (*a*)~(*d*) smooth channel and (*e*)~(*h*) ribbed channel (P/e=10)

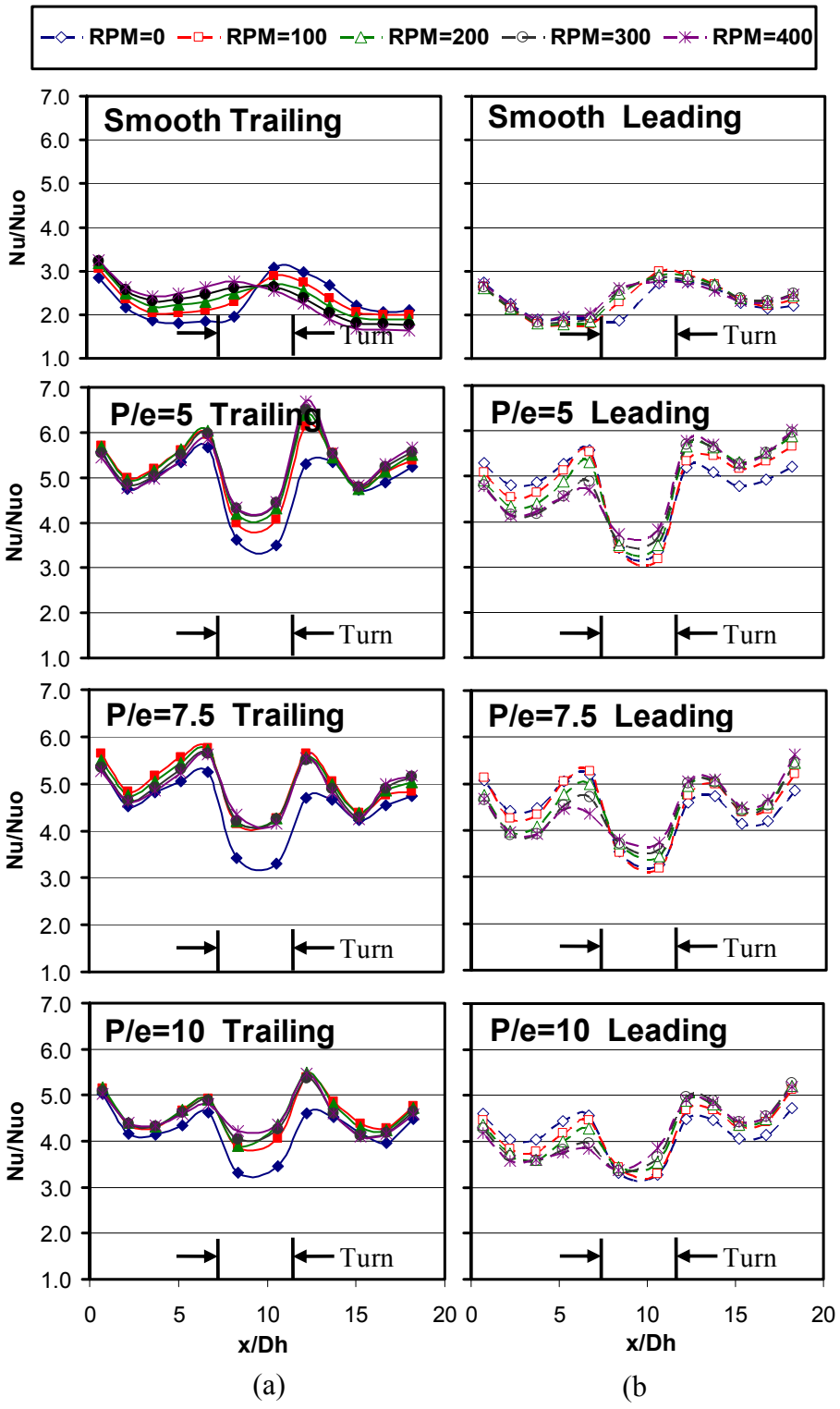

Fig. 15 Streamwise Nu/Nu_o ratio for Re=20K at β=135° on (*a*) trailing surface (*b*) leading surface for smooth and different P/e cases

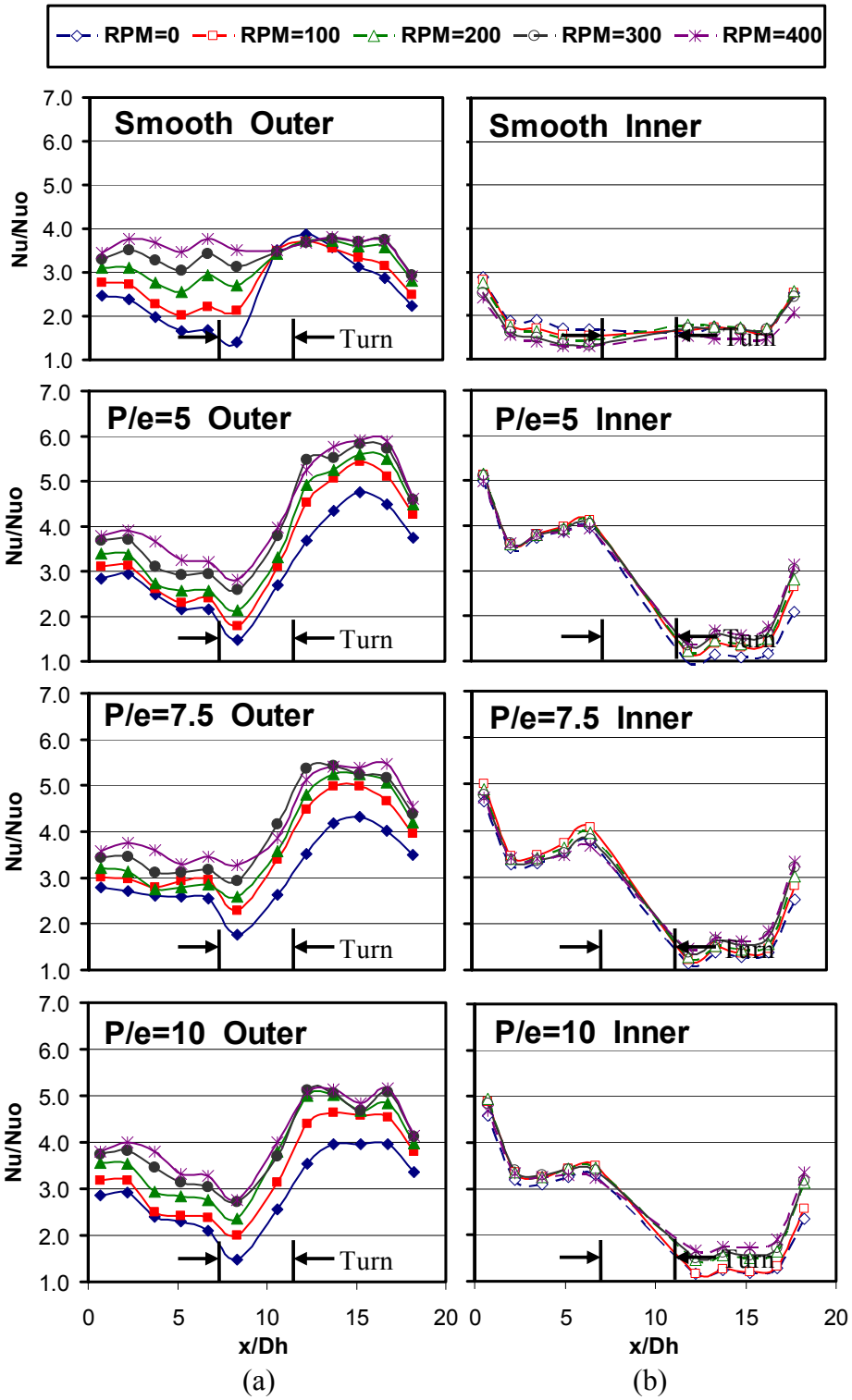

Fig. 16 Streamwise Nu/Nu_o ratio for Re=20K at β=135° on (*a*) outer wall (*b*) inner wall for smooth and different P/e cases

4.1.4 Rotation Number Effect

The rotation number (Ro) as defined in Eq. (4) is used to describe the ratio of the Coriolis force to the bulk inertial force and can be reached by various combinations of rotational speed and mainstream flow velocity. The rotation number in this study varies from 0 to 0.45. In this study, the effect of rotation on heat transfer (Nu/Nu_s) is presented as a function of the rotation number. The stationary Nusselt number (Nu_s) is chosen as the denominator so that the effects of rotation can be compared.

Correlations between regionally averaged Nu/Nu_s and Ro at region #4 and #10 are shown in **Figure 17**. Results for both smooth and ribbed channels are provided at both orientation angles of 90^o and 135^o. At the selected regions, the entrance and exit effects are expected to be at the minimum, respectively. Furthermore, the turn effect at these locations is expected to be at a minimum as well. Al-Qahtani et al [41] showed that after a distance of $5D_h$ downstream of the turn in the second passage, the Dean vortices have diminished in strength. Thus, the dominating effect is rotation induced vortices (for the smooth channel) and the combined effect of rib and rotation induced vortices for the ribbed channel.

In the first passage (at region #4) with radial outward flow, for the smooth channel, the increase of Ro causes heat transfer (Nu/Nu_s) on the trailing surface to increase by approximately 65-70% at both orientation angles. On leading surface for $\beta=90^o$ smooth case, Nu/Nu_s ratio drops as much as 20% due to the effect of Coriolis force. However, a beneficial increase of heat transfer on the leading surface is clearly seen for the $\beta=135^o$ smooth case. This increase is due to reversed flow cells on the

leading surface as previously described and reported by Wagner et al. [2] and Dutta et al. [6]. On outer and inner walls of the smooth channel at $\beta=90^o$, Nu/Nu_s experiences a substantial increase to 1.8 and a slight decrease to 0.9 respectively. When channel is tilted ($\beta=135^o$), because of the Coriolis effect on outer and inner as shown in **Figure 11**, the variation of heat transfer on outer and inner due to rotation largely increased. In the first passage (region #4) of the ribbed channel the effect of Ro is minimal on leading and trailing surfaces for the $\beta=90^o$ case. However for the $\beta=135^o$ case, a decrease in Nu/Nu_s is observed on the leading surface. Concerning outer and inner walls of the ribbed channel, at $\beta=90^o$, Nu/Nu_s on both of them is increasing due to rotation, which can be explained as the direct impingement on inner wall in the first passage by rib-induced vortex. When channel is tilted ($\beta=135^o$), Nu/Nu_s on outer does not change much from the perpendicular rotating, however, the inner surface shows a decreased trend because the Coriolis-induced vortex is in the opposite direction as the rib-induced one and in dominance near inner wall.

In the second passage (region #10) the flow is radial inward and the Coriolis force changes direction. For smooth channel, for both channel orientations, the heat transfer (Nu/Nu_s) on the leading surface is not impacted by an increase with Ro and a decrease up to 30% in Nu/Nu_s in observed on trailing surface at large Ro. Considering the ribbed channel, the effect of rotation is reduced in that heat transfer on trailing and leading surfaces has the same trend as the smooth channel but the difference between trailing and leading walls are reduced. Similar to ribs, the tilted channel orientation ($\beta=135^o$) further reduces the Nu/Nu_s difference between leading and trailing surfaces.

The outer wall heat transfer trends are similar for all cases studied. On the inner wall, the most notable effect of rotation on heat transfer occurs in the smooth channel with $\beta=135^{o}$. A decrease in heat transfer of about 40% is observed and then at the largest rotation number an increase is seen.

Correlations between regionally averaged Nu/Nu_s and Ro at region #4 and #9 are shown in **Figure 18**. Results for both smooth and different rib pitch-to-height ratios (P/e=5, 7.5, and 10) are provided at the orientation angle of 135^{o}.

For the smooth case, in the first passage, the Nu/Nu_s ratio increases substantially with higher Ro on the trailing and the outer surface, and decreases greatly on the inner wall. However, on the leading wall, Nu/Nu_s ratio experiences a minimum at low Ro and then increases to a value above 1. In the second passage, the Nu/Nu_s ratio's variation is limited around unit on the leading surface and a steep decrease of Nu/Nu_s is observed on the trailing wall. Besides, on outer and inner walls, the behavior of Nu/Nu_s is similar to that in the first passage, however, in a reduced range. For the current channel with 135^{o} orientation angle, in the first pass with radially outward flow, the Coriolis force skews the bulk flow towards the trailing and outer wall, which attributes to the Nu/Nu_s values above 1.0 on trailing and outer walls as well as the Nu/Nu_s values below 1.0 on leading and inner walls. In the second pass, the combined effects of the secondary flows induced by the 180^{o} turn and rotation determine the Nu/Nu_s ratio variation in the second passage.

For the ribbed cases, in the first passage, the Nu/Nu_s ratio experiences slight variations around 1.0 on the trailing wall and it decreases a lot and then increases slightly on the leading surface. On the outer wall, the Nu/Nu_s ratio increases

monotonously to a value smaller than smooth case. On the inner wall it starts to decrease at a higher Ro, comparing with the smooth case. In the second passage, on both leading and trailing surfaces, the Nu/Nu_s ratio elevates above 1.0 and the increase of heat transfer on the leading surface is about 10% higher than the trailing surface. On the outer wall, similar to the smooth case, the Nu/Nu_s ratio keeps increasing with Ro, however, on the inner wall, an increase of heat transfer is observed, which is opposite to the smooth data. In **Figures 10 and 11**, it is obvious that in the first passage, near the trailing surface, the secondary flow induced by ribs is in the opposite direction to that by rotation, thus the effect of rotation is reduced and the heat transfer enhancement is suppressed. For outer and inner walls, similar to stationary cases, the rib-induced vortex impinges directly on inner. Thus, ribs weaken the heat transfer on the outer wall and strengthen it on the inner wall, which is counteracting to the Coriolis effects by rotation. In the second passage, near the leading surface, the secondary flow induced by ribs is in the same direction as that by rotation, thus the effect of rotation is increased and the heat transfer enhancement is increased as much as 15%. However, near the trailing surface, the relatively thick boundary layer is largely reduced and as a result, the heat transfer on the trailing surface is slightly increasing. For outer and inner walls, the heat transfer is largely affected by the strong turn-induced secondary flows, Coriolis force and the ribs. The effect of different P/e ratios on Nu/Nu_s is not very obviously shown in **Figure 18**, in that the Nu_s in the denominator has already considered the heat transfer difference by P/e ratios.

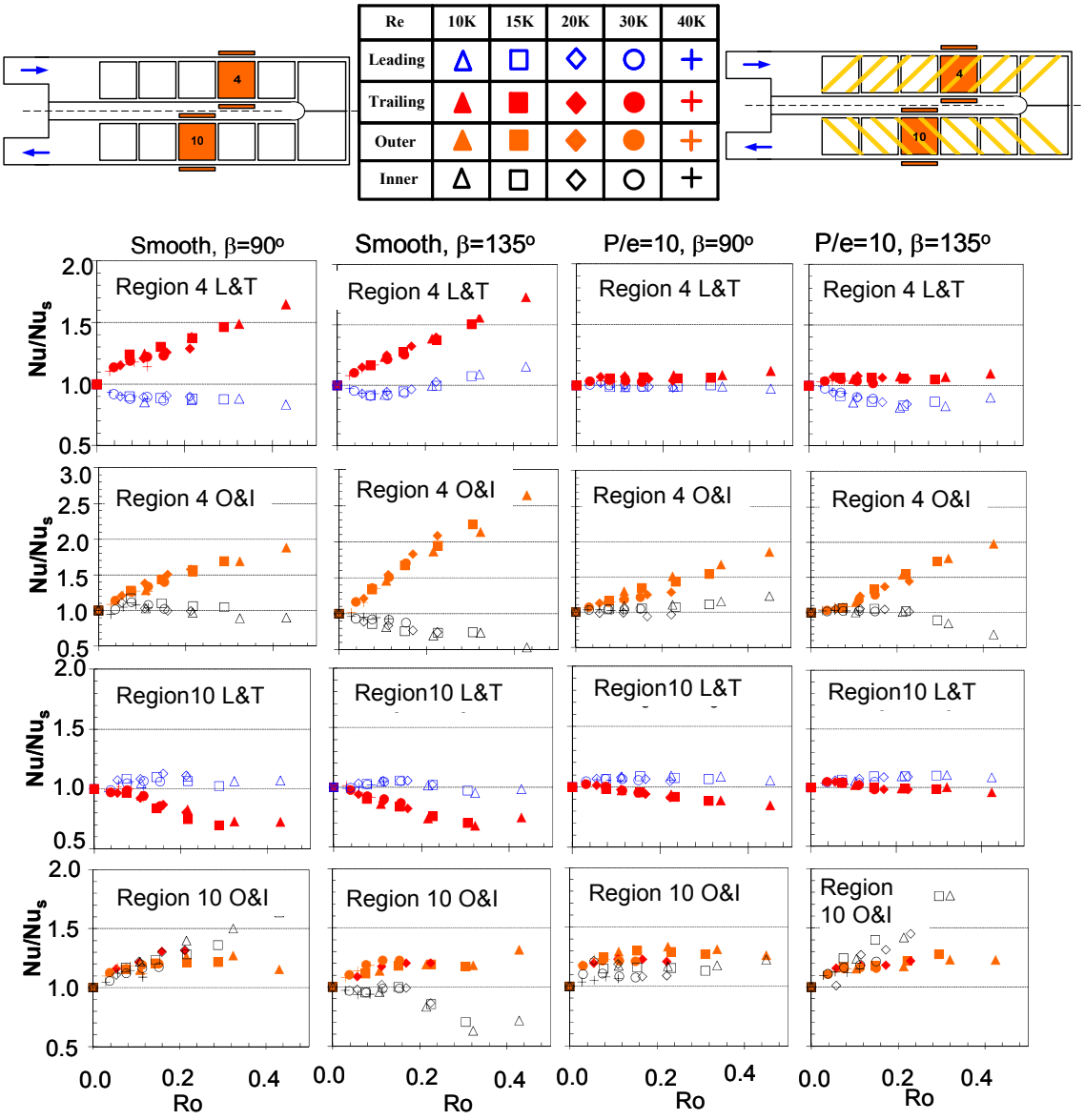

Fig. 17 Regionally-averaged Nu/Nu_s v.s. Ro at region #4 and #10 at β=90° and 135° for smooth and ribbed channels (P/e=10)

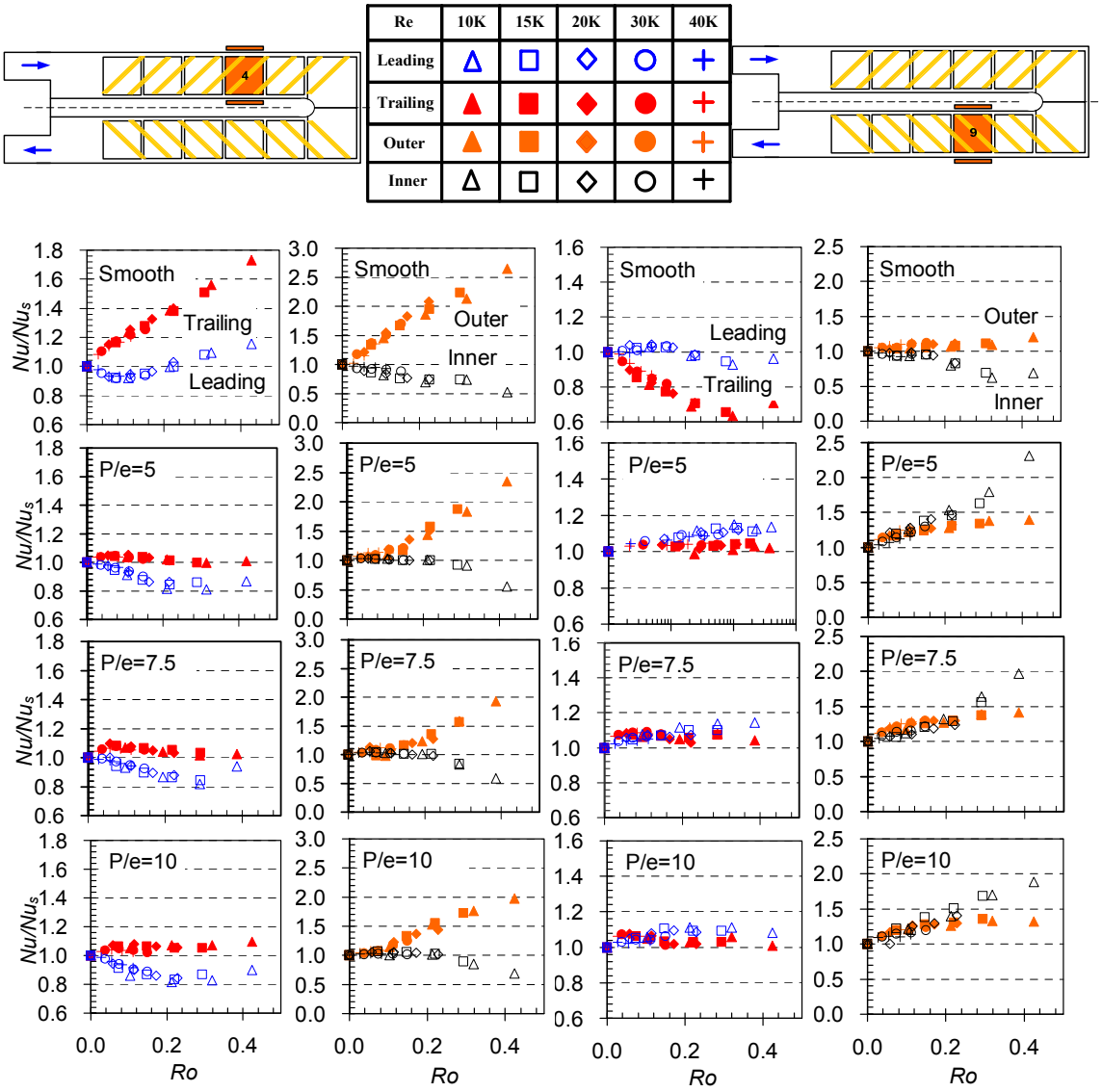

Fig. 18 Regionally-averaged Nu/Nu_s v.s. Ro at region #4 and region #9 at $\beta=135^o$ for smooth and different P/e cases (P/e=5, 7.5, and 10)

4.1.5 Buoyancy Parameter Effect

When the walls of the test section are heated, a temperature profile is developed in the fluid from mainstream core to wall surfaces. The temperature profile produces a variation of fluid density in the channel. The density variation and centrifugal force by rotation result in the rotation-induced buoyancy force that drives the hotter and lighter fluid near the heated surface toward the center of rotation. The combined effects of density difference and rotation on heater transfer are presented by studying the Nu/Nu_s ratios vary with the change of buoyancy parameter.

Correlations between regionally averaged Nu/Nu_s and Bo_x are shown in **Figures 19~21**. The data is focusing on leading and trailing surfaces for both smooth and ribbed (P/e=10) channels at $\beta=90^o$ and 135^o. The effect of the local buoyancy parameter on heat transfer in the first passage (region #1, #4, and #6) is presented in **Figure 19**. It is clear that the effect of rotation increases further from the entrance in the smooth channel for both angles studied. For perpendicularly rotating channel ($\beta=90^o$), at the entrance (region #1) the heat transfer (Nu/Nu_s) increase on the trailing surface is approximately 25-30%. At region #4, the increase in Nu/Nu_s at the largest Bo_x reaches 65-70%. At region #6, heat transfer is more than doubled on the trailing surface for the $\beta=90^o$ case. A similar observation is seen for the leading surface. At region #1 for the smooth $\beta=135^o$ case, the effect of rotation is minimal as Nu/Nu_s remains constant at unity. However, in region #4, an increase in heat transfer of about 15% is observed at the highest Bo. In region #6, the heat transfer on the leading surface now is approximately 60% higher than the stationary case. In the ribbed channel for both orientation angles, the variation trend

of Nu/Nu_s is similar to the smooth channel. However, rotation effect is largely reduced since the difference of Nu/Nu_s between leading and trailing surfaces is much smaller than that in the smooth channel. The effect of rotation is smallest for the ribbed channel in perpendicular rotating ($\beta=90^o$) case. The rotation effect slightly increases on the leading surface as the channel orientation is changed to $\beta=135^o$ as seen by reduction in heat transfer.

Figure 20 presents the effect of the local buoyancy parameter on heat transfer in the second passage (region #6, #10, and #12). For the smooth channel, the angle of rotation influences the heat transfer in the turn (region #7). For the $\beta=90^o$ case, the trailing surface heat transfer (Nu/Nu_s) is slightly enhanced with rotation. On the other hand, for the $\beta=135^o$ case, heat transfer is reduced on the trailing surface. At regions #10 and #12 of the smooth channel, both orientation angles ($\beta=90^o$, 135^o) show similar heat transfer trends for both the leading and trailing surfaces. Although, some data scatter occurs at region #12 for $\beta=90^o$ case on the leading surface. The reason for this maybe due to exist effects, but this is non-conclusive. For the ribbed channel, at the tilted orientation angle ($\beta=135^o$), trailing surface obtains heat transfer enhancement due to rotation, which is opposite to the phenomenon in the smooth channel. For both region #10 and region #12, the trend of heat transfer is similar to the smooth channel and the rotation effect is largely reduced.

Figure 21 shows the effect of the buoyancy parameter on the heat transfer on the tip cap (cap6 and cap7). To be clear, ribs are not placed on the tip cap, but on the adjacent leading and trailing walls. Both smooth cases ($\beta=90^o$, 135^o) and the ribbed

$\beta=90^o$ case show very similar trends in heat transfer as Bo_x is increased. For the ribbed $\beta=135^o$ case, a very large increase in heat transfer is observed. The heat transfer on tip cap7 nearly tripled with an increase in Bo_x. This increase is very beneficial since the tip portion of the blade is subjected to severe heat loads due to tip flow leakage between the rotating blade and the casing.

Correlations between regionally averaged Nu/Nu_s and Bo_x for smooth and different ribbed (P/e=5, 7.5, 10) cases are shown in **Figures 22 and 23**. Results are shown on all surfaces of region #4, #6, #7, and #9 at $\beta=135^o$.

The effects of the local buoyancy parameter (Bo_x) on Nu/Nu_s ratios in the first and second passages are shown in **Figure 22**. The trend of Nu/Nu_s with respect to Bo_x is very similar to that to Ro discussed in last section in that inlet density ratio keeps the value of 0.11 and effects of density ratio ($\Delta\rho/\rho_{b,x}$) on Nu/Nu_s can not be shown. At region #4 of the smooth channel, the most prominent phenomenon occurs at the leading surface where the Nu/Nu_s ratio experiences a slight drop and then an elevation. It can be explained as the flow stagnation and separation near the surface due to opposite directions of buoyancy force and bulk flow. For the ribbed cases, at region #4 & #9, the Nu/Nu_s ratios variations follow the trend of Nu/Nu_s to Ro in **Figure 22** respectively but in a different x-axis scale. Considering the three P/e ratios, on all surfaces, the Nu/Nu_s ratios are not very sensitive to P/e.

The effects of Bo_x on Nu/Nu_s ratios at region #6 and #7 in the turn portion are shown in **Figure 23**. For the smooth cases, at region #6, the Nu/Nu_s ratio experiences substantial increase on leading, trailing and outer walls but it elevates slightly at large

Bo_x on the cap surface. At region #7, the Nu/Nu_s ratio behaves differently where it increases little on leading, outer and cap walls and it decreases on the trailing surface. For the ribbed channels, at region #6, the Nu/Nu_s ratio elevates on all walls when Box increases and it is obvious that ribs weaken the effect of buoyancy on leading and trailing walls while they strengthen the buoyancy effect on the cap. At region #7, similar trend of Nu/Nu_s with Bo_x is observed on all surfaces as that at region #6. The effects of different P/e ratios on Nu/Nus are very similar to each other, except that on outer and cap walls Nu/Nus decreases slightly with higher P/e ratio at both region #6 and #7.

4.1.6 Passage Average Value with Correlation

In order to gain an overall perspective on the effect of rotation on heat transfer throughout the 2:1 aspect ratio channel with a tip turn, the average Nu/Nu_s ratios for the leading, trailing, outer, and inner walls have been plotted against the average buoyancy parameter as seen in **Figures 24 and 25**. The averaged Nu/Nu_s ratio and averaged Bo are obtained from the six copper plates on a given wall (leading, trailing, and outer) in a given pass (1st or 2nd). On the inner wall, the averaged Nu/Nu_s ratio and averaged Bo are based on five copper plates. Results from the 2:1 fully developed flow channel from Fu et al. [16] are used for comparison.

The effect of the channel orientation on the first pass averaged heat transfer for the leading and trailing surfaces in the smooth channel is clearly seen in **Figure 24 (a)**. The pass average heat transfer on the trailing surface in the smooth channel, for both orientation angles, increases by more than 50%, which agrees well with the results from

Fu et al. [16] even though the current study utilizes a developing flow entrance. The pass averaged heat transfer on the leading surface increases by approximately 15% when the angle of rotation is changed from $\beta=90^o$ to 135^o. This phenomenon of the reduced effect of rotation on heat transfer of the 135^o channel was also verified by Azad et al. [26]. It can be explained the Coriolis-induced vortices partially impinge on the trailing and as a result the effect of rotation is reduced compared with 90^o orientation channel used by Fu et al. [16]. In the second pass for the smooth channel, the effect of the angle of rotation is seen to have little effect on the leading and trailing pass averaged heat transfer. For the ribbed (P/e=10) channel, the effect of rotation and angle of rotation is minimal on the first and second pass average heat transfer. **Figure 24 (b)** shows the pass averaged heat transfer results for the outer and inner walls. The largest increase for the outer wall in the first pass averaged heat transfer occurs for the smooth channel with $\beta=135^o$ for which $Nu/Nu_s=2.4$. The other three cases show similar results to each other for the outer wall first pass average heat transfer. The most severe decrease in heat transfer for the inner wall first pass averaged heat transfer occurs in the smooth channel with $\beta=135^o$ in which a decrease of 50% is seen at the largest Bo value. In the second pass, all cases show an increase in heat transfer with rotation on the outer wall and inner wall. The only exception is the smooth channel with $\beta=135^o$ case in which the inner wall again shows a 40% decrease in heat transfer with rotation.

Figure 25 shows the average Nu/Nu_s ratios on leading, trailing, outer and inner surfaces in the first and second pass with respect to Bo_x for the smooth and ribbed (P/e=5, 7.5, and 10) cases. Similar to **Figure 24**, results from Fu et al. [16] are used for

comparison. On the trailing surface the Nu/Nu_s is almost coinciding and on the leading surface the Nu/Nu_s reduction with Bo_x is less than the fully-developed case. As shown in **Figures 9 and 10**, the Coriolis-induced vortices partially impinge on the trailing and as a result the effect of rotation is reduced compared with 90^o orientation channel used by Fu et al. [16]. This phenomenon of the reduced effect of rotation on heat transfer of the 135^o channel was also verified by Azad et al. [26]. However, it should be noticed that the absolute heat transfer level (Nu) of current study is higher than the fully-developed case. For those ribbed cases, it is shown in **Figures 9** and **10** that in the first pass near leading and trailing surfaces, secondary flows generated by 45^o parallel ribs and rotation are in the opposite direction. Consequently, the effect of rotation on heat transfer is diminished on trailing surface. Similarly, the heat transfer on the leading surface is further decreased because the velocity near leading is reduced by the rib-induced vortex and boundary layer becomes thicker. In the first pass, Coriolis-induced secondary flow transports relatively cool fluid from center portion of the passage and impinges it partially on the outer surface to increase heat transfer on the outer and decrease it on the inner wall, however, the rib-induced secondary flow guides the relatively hot fluid from leading and trailing surfaces to the outer wall, which is counter-acting to the rotation-induced vortex and explains the decreased effect of rotation on heat transfer on outer and inner surfaces after ribs are applied.

In the second pass, heat transfer will be increased on the leading surface and decreased on the trailing due to rotation, just opposite to the phenomena observed in the first pass. From **Figures 9 and 10**, the secondary flow induced by rotation and ribs are in

the same direction near leading and trailing surfaces. It is shown in **Figure 25** that the heat transfer is little increased on the leading surface because the effect of rotation is strengthened by ribs and it is largely increased on trailing since the vortices in the same direction increase the local velocity and boundary layer becomes thinner. In the second pass, very similar to what happens in first pass, secondary flows by Coriolis and ribs affects increase heat transfer on the outer and the inner wall. In spite of them, vortices by the 180o turn add their effect on the heat transfer on outer and inner surfaces, which is more complicated and need further study.

Correlations for predicting the effect of rotation on heat transfer in the smooth and ribbed channels (P/e=10) at two channel orientations angles ($\beta=90^o$ and 135^o) are developed. The correlations are shown as solid lines in **Figure 24 (a) and (b)**. A power law expression as shown in Eq. (8) was used to correlate the pass averaged Nu/Nu_s with Bo.

$$Nu/Nu_s=A\cdot Bo^a+B\cdot Bo^b \quad (8)$$

The coefficients A and B along with exponents a and b are listed in **Table 2** for the leading/trailing and outer/inner walls, respectively. On average the discrepancy between experimental data and the power law correlations is +/-10%.

Another set of correlations to predict the effect of rotation on heat transfer for the smooth and different P/e cases (P/e=5, 7.5 and 10) at $\beta=135^o$ is developed and shown as solid line in **Figure 25**. An expression of power law shown in Eq. (9) is used to correlate the passage-averaged Nu/Nu_s with Bo.

$$Nu/Nu_s=A\cdot Bo^a+B\cdot Bo^b+C\cdot Bo^c+D \quad (9)$$

Similarly to Table 2, the coefficients and exponents are listed in **Table 3** for all circumferential walls. The averaged discrepancy between experimental data and the power law correlation is lower than +/-7%.

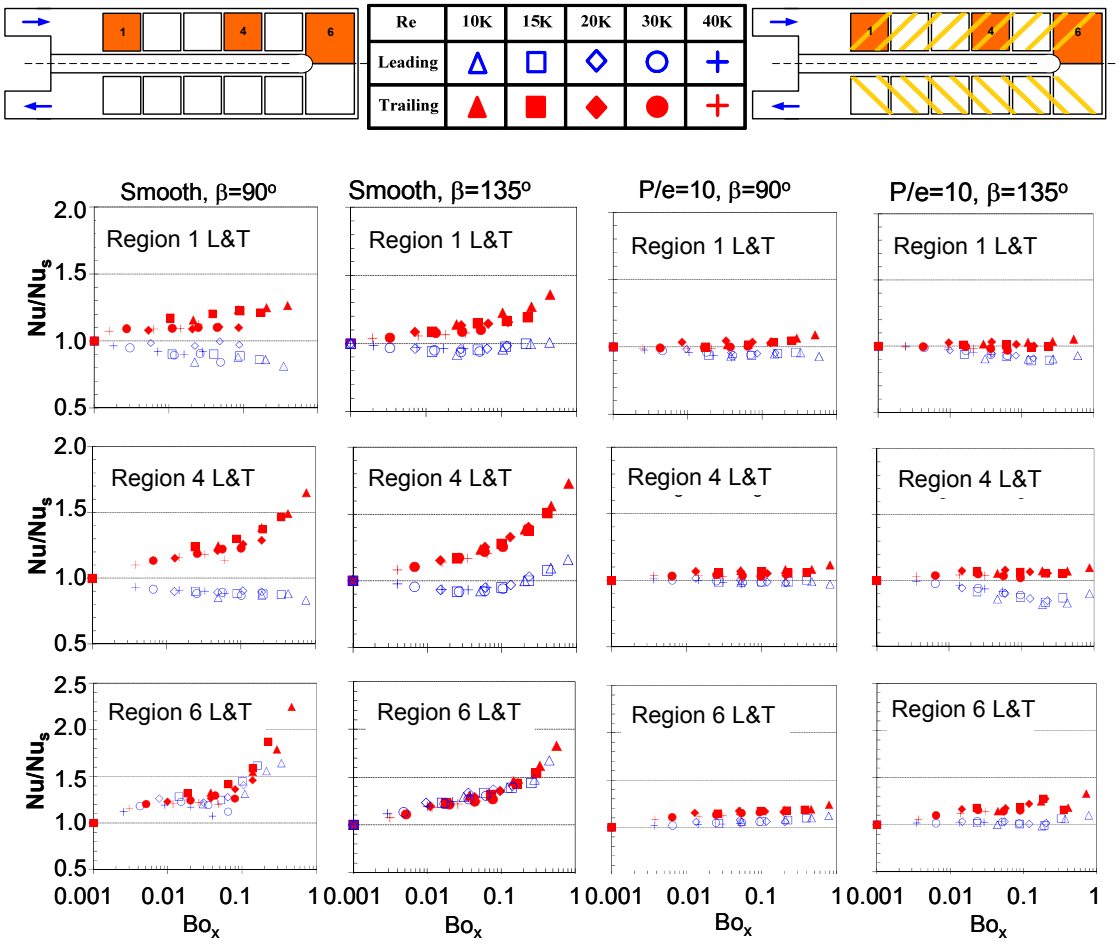

Fig. 19 Regionally-averaged Nu/Nu_s v.s. Bo_x on leading and trailing surfaces of region #1, #4, and #6 at β=90° and 135° for smooth and ribbed channels (P/e=10)

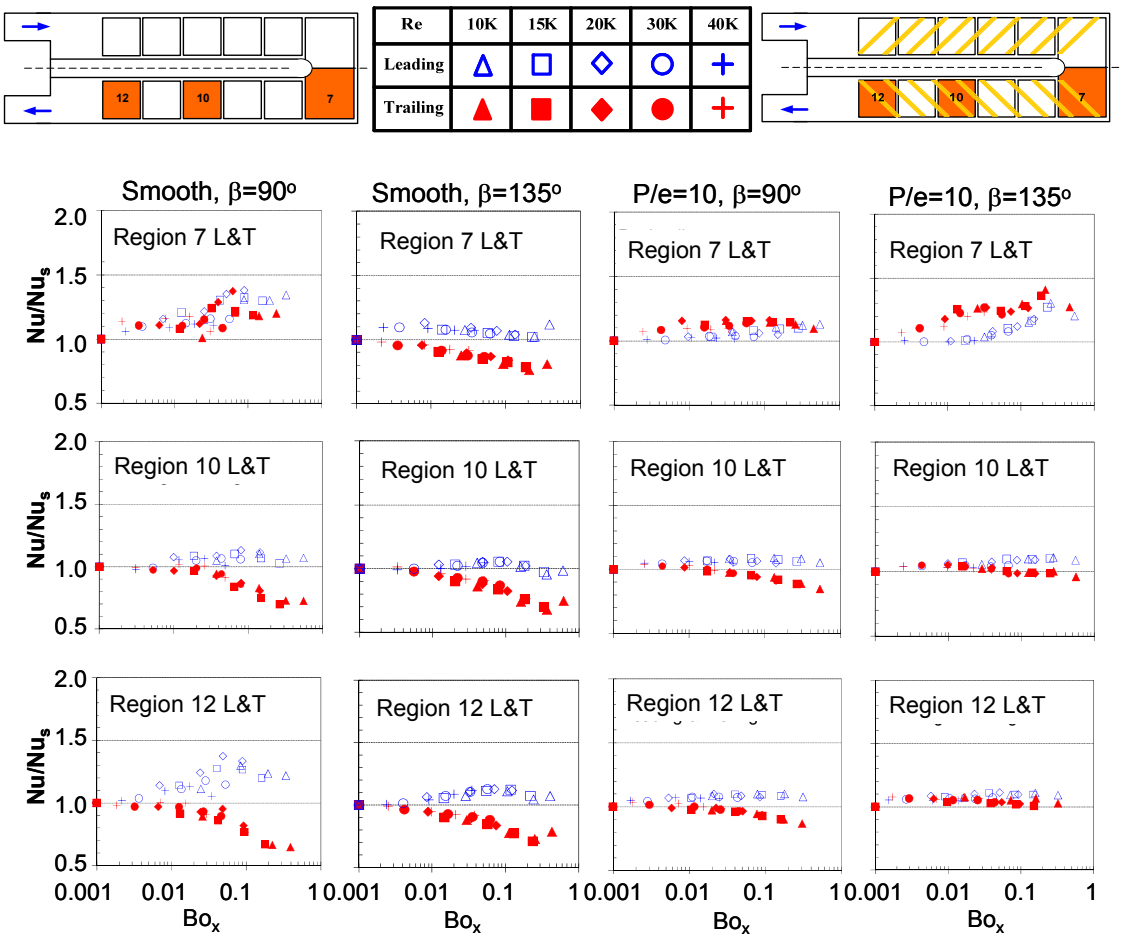

Fig. 20 Regionally-averaged Nu/Nu_s v.s. Bo_x on leading and trailing surfaces of region #7, #10, and #12 at β=90° and 135° for smooth and ribbed channels (P/e=10)

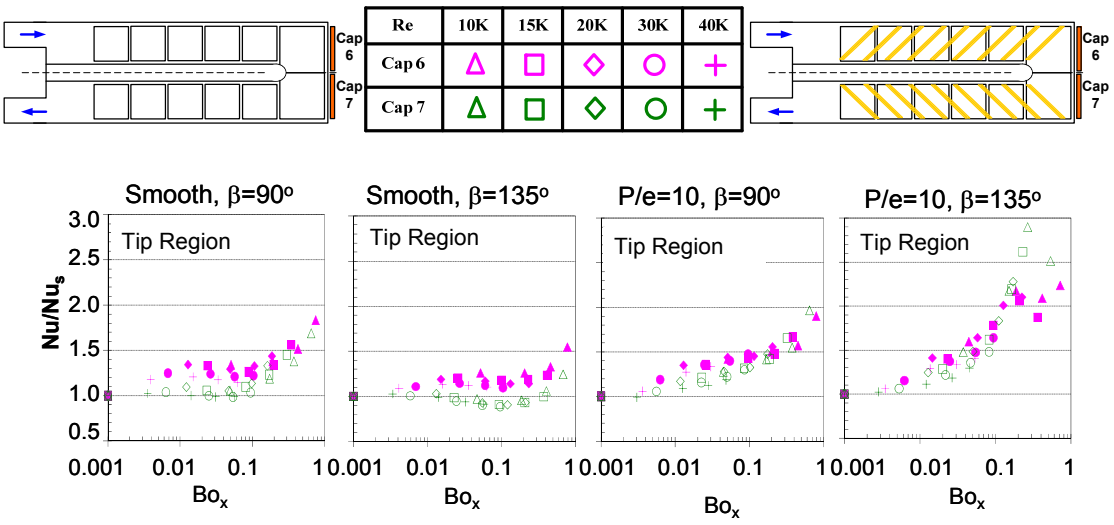

Fig. 21 Regionally-averaged Nu/Nu_s v.s. Bo_x on cap6 and cap7 at $\beta=90^o$ and 135^o for smooth and ribbed channels (P/e=10)

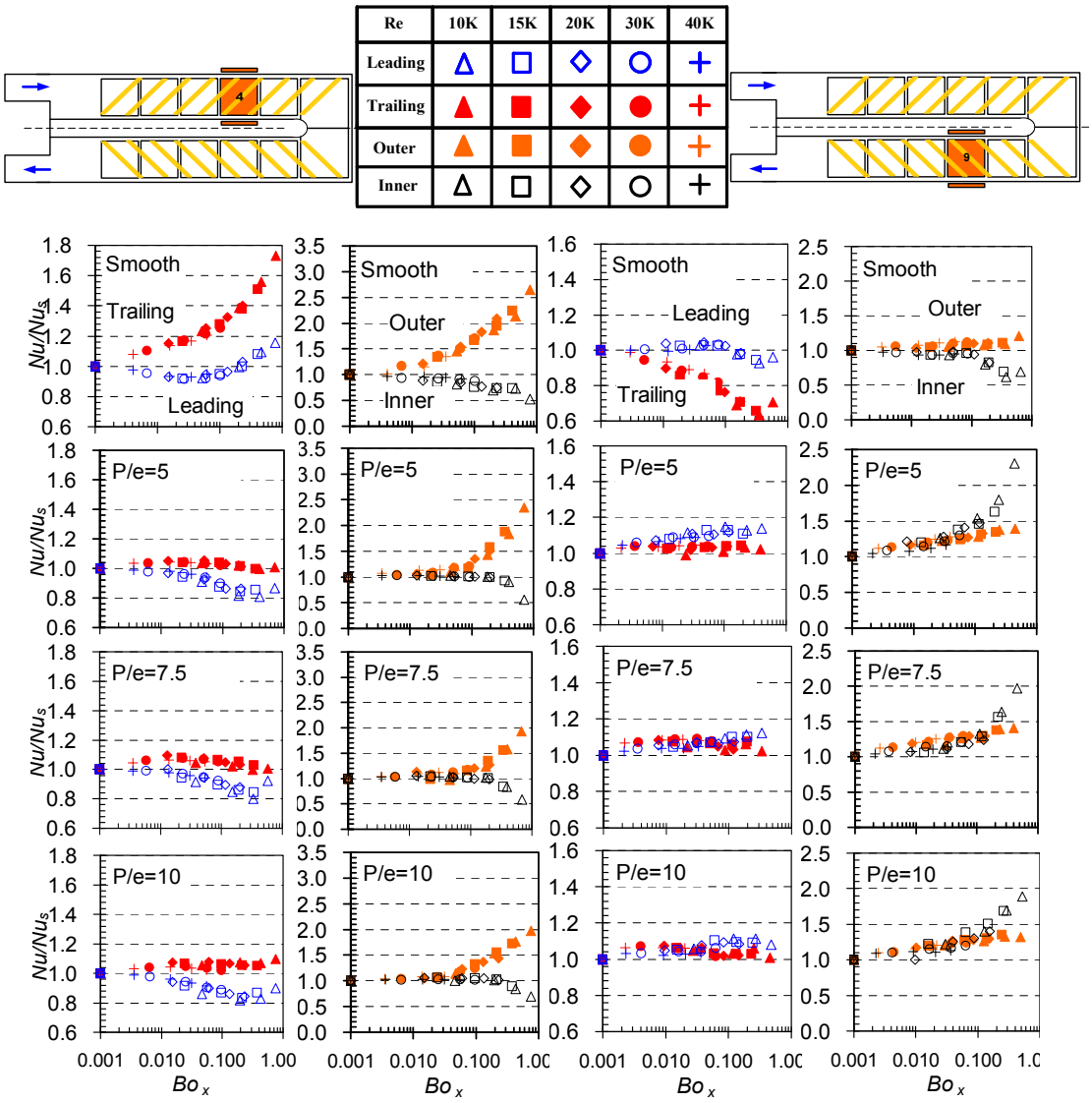

Fig. 22 Regionally-averaged Nu/Nu_s v.s. Bo_x at region #4 and #9 at $\beta=135^{o}$ for smooth and different P/e cases (P/e=5, 7.5, and 10)

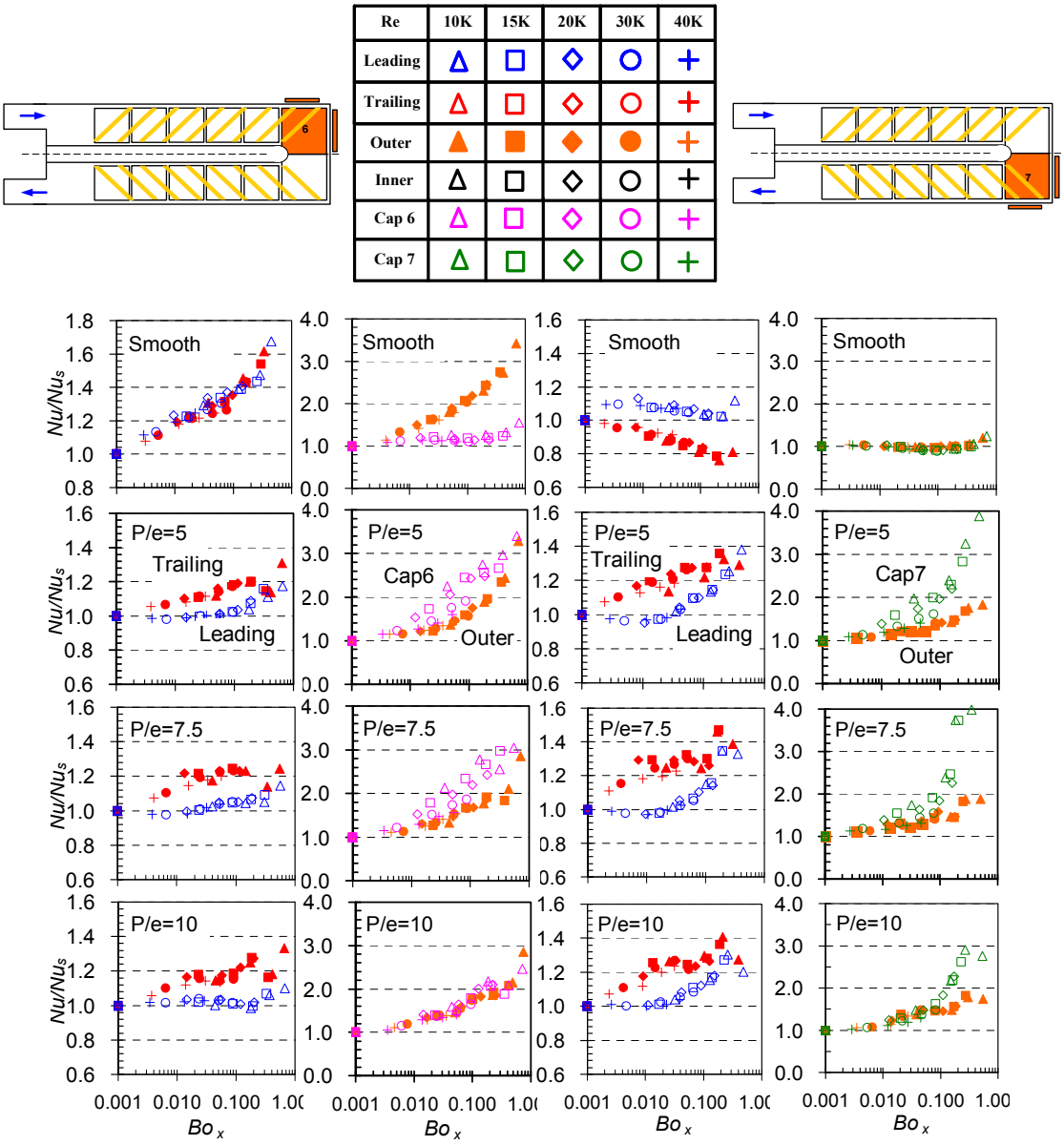

Fig. 23 Regionally-averaged Nu/Nu_s v.s. Bo_x at region #6 and #7 at $\beta=135^{o}$ for smooth and different P/e cases (P/e=5, 7.5, and 10)

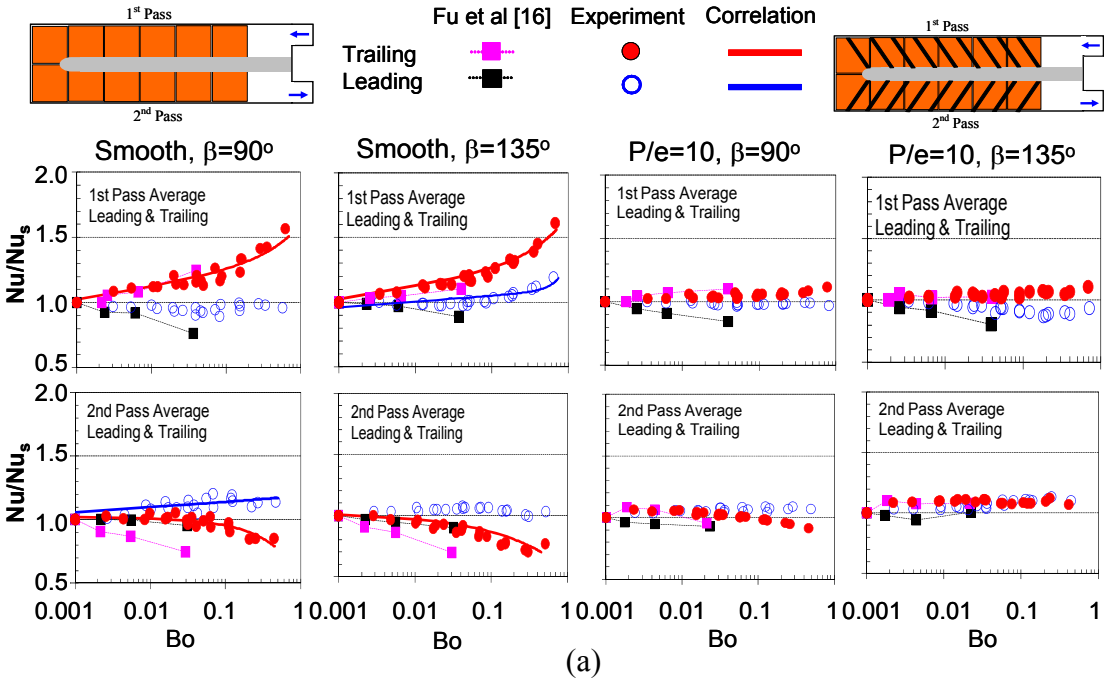

Fig. 24 Passage-averaged Nu/Nu_s ratios v.s. Bo at β=90° and 135° for smooth and ribbed channels on (*a*) leading & trailing surfaces (*b*) outer & inner walls

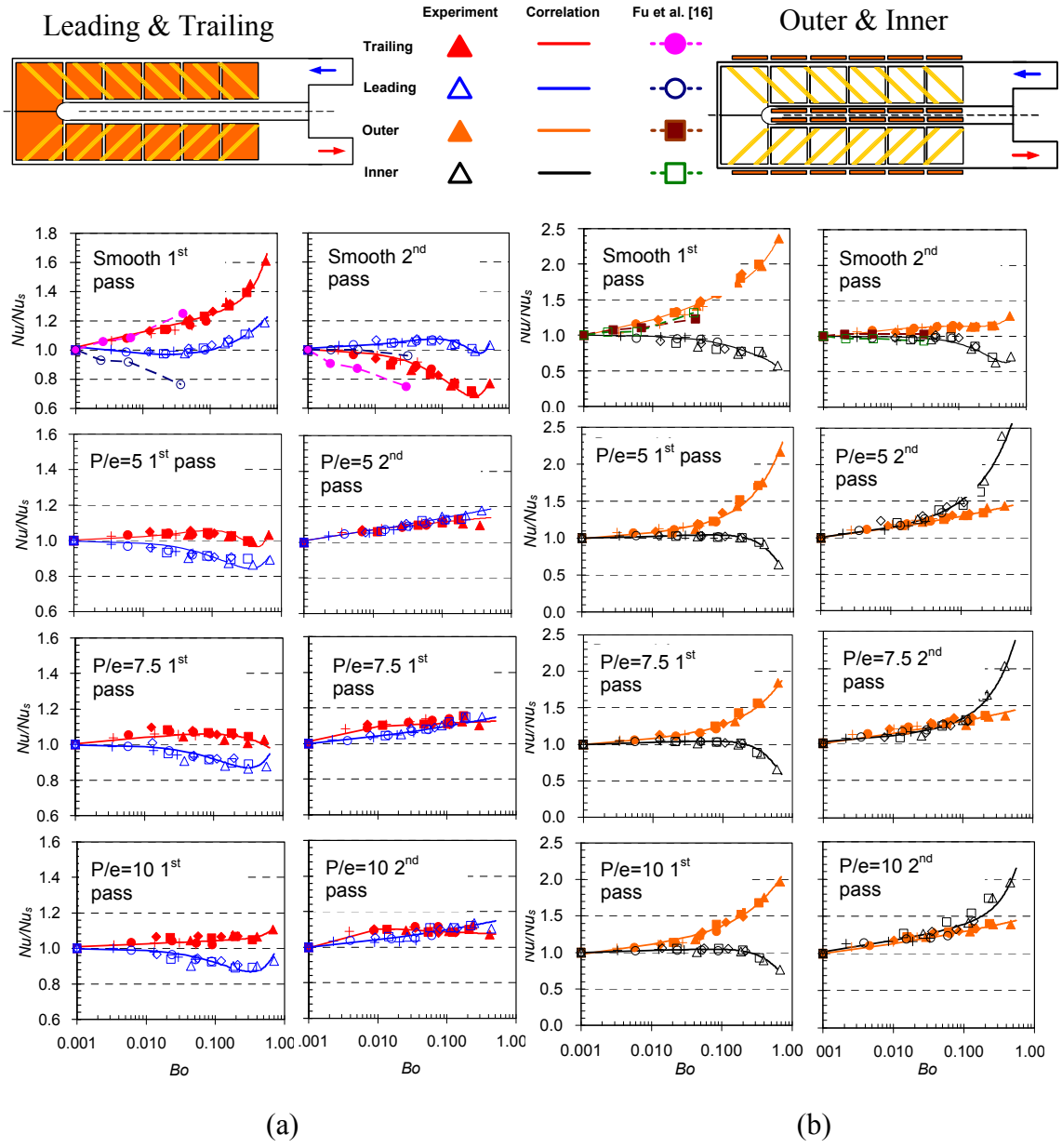

Fig. 25 Passage-averaged Nu/Nu_s ratios v.s. Bo at β=135° for smooth and different P/e cases on (*a*) leading & trailing surfaces (*b*) outer & inner walls

Table 2 Coefficients and exponents for Nu/Nu_s correlations at β=90° and 135° for smooth and ribbed channels on (*a*) leading and trailing surfaces (*b*) inner and outer walls

	L1	T1	L2	T2
		Smooth β=90°		
A	-----	1.350	1.150	1.000
B	-----	0.250	0.035	-0.450
a	-----	0.040	0.019	-0.003
b	-----	0.950	-0.050	0.940
Discrepancy	-----	8%	7%	6%
		Smooth β=135°		
A	1.100	1.35	-----	1.00
B	0.220	0.32	-----	-0.45
a	0.020	0.04	-----	-0.003
b	3.000	0.95	-----	0.500
Discrepancy	5%	6%	-----	9%

(a)

	I1	O1	I2	O2
		Smooth β=90°		
A	-----	1.350	1.260	1.400
B	-----	0.600	0.410	-0.600
a	-----	0.050	0.039	0.050
b	-----	0.400	0.500	1.500
Discrepancy	-----	7%	11%	9%
		Smooth β=135°		
A	1.390	1.350	1.300	1.050
B	-0.980	1.100	-0.850	0.500
a	0.040	0.060	0.039	0.005
b	0.400	0.400	0.500	1.000
b	0.400	0.400	0.500	1.000
Discrepancy	10%	8%	10%	7%
		P/e=10 β=135°		
A	1.050	1.350	1.100	1.550
B	0.300	0.700	0.200	0.000
a	0.005	0.040	0.010	0.065
b	1.000	0.900	1.000	0.000
Discrepancy	5%	9%	9%	11%
		P/e=10 β=135°		
A	1.050	1.350	1.250	1.450
B	-0.350	0.700	1.100	-----
a	0.005	0.050	0.040	0.050
b	1.000	0.600	0.550	-----
Discrepancy	5%	9%	12%	4%

(b)

Table 3 Coefficients and exponents for Nu/Nu_s correlations at $\beta=135^o$ for smooth and different P/e Ratio cases on all circumferential walls

	L1	T1	L2	T2	O1	I1	O2	I2
				Smooth				
A	1.39	1.41	4.5	-1.9	-1	1.4	-1.8	1.4
B	0.5	0.65	-2.95	2.5	1.45	0.8	1.8	-0.6
C	0	0	0.5	-1.25	-1.3	0.6	-1.4	1
D	-0.58	-0.05	1	1.01	1	0	1	0
a	-0.02	0.04	2.75	6	3.25	0.06	9	0.05
b	0.6	2	1.6	2.2	1.8	0.35	2.65	0.7
c	0	0	0.56	0.75	0.95	1.8	1.1	2
				P/e=5				
A	1.8	2.9	1.17	1.09	1.4	1.22	1.08	1
B	-1.69	-2.7	0.04	0.035	1.2	1.55	2.17	0
C	0	0.6	0	-0.018	-2	0	0	0
D	1	1	0	0.042	-0.12	0	0.29	0.5
a	1.34	2.55	0.03	0.01	3.2	0.03	0.06	0.1
b	0.99	1.6	-0.05	-0.05	0.01	1	0.9	0.3
c	0	0.71	0	-0.25	2.15	0	0	0
				P/e=7.5				
A	1.8	1.34	1.16	1.09	1.4	1.2	1.05	1
B	-1.63	-0.2	0.15	0.035	1.2	0.9	2.2	0
C	0	0	0	0.000	-2	0	0	0
D	1	-0.22	-0.14	0.006	-0.12	0.02	0.22	0.5
a	1.34	0.013	0.04	0.01	3.2	0.03	0.04	0.1
b	1	0.95	-0.08	-0.1	0.01	0.85	1.15	0.3
c	0	0	0	-1	2.15	0	0	0
				P/e=10				
A	1.79	1.36	1.16	1.05	1.5	1.29	1.2	1
B	-1.635	0.16	0.15	0.04	1.2	0.9	1.8	0
C	0	0	0	0.000	-2	0	0	0
D	1	-0.3	-0.14	-0.02	-0.12	0.11	0.4	0.5
a	1.34	0.0055	0.04	0.002	2.7	0.059	0.095	0.1
b	1.005	2.8	-0.08	-0.2	0.01	0.85	1.8	0.3
c	0	0	0	-1	2.15	0	0	0

4.2 Two Pass Rectangular Channel (AR=2:1) with a Hub Turn

4.2.1 Flow Behavior

The flow behaviors in the stationary two pass 2:1 channel with a hub turn is very similar to that in the stationary two pass 2:1 channel with a tip turn. The prominent mainstream flow behaviors include: entrance-induced separation, turn-induced separation and mainstream flow deflected by ribs as shown in **Figure 26**. When the mainstream air enters the test section through the hose fitting with circular cross-section, it expands rapidly into the short passage with square cross-section. Because of short distance in the passage, the flow enters the sharp turn when it is still in developing. At the same time, the turbulence level increases much based on previous research by Son et al. [31]. After the sharp turn, air goes into the heated first passage and thermal boundary layer starts to develop. Then, in the hub turn region without turning vane, the mainstream velocity is higher near the arc-shaped inner divider and flow starts to separate after its mid-point. At the same time, the secondary Dean vortex is generated in the cross-section planes perpendicular to mainstream and the Dean vortex pushes the mainstream core toward the hub wall. After the 180^o U-bend in the second passage, the flow is squeezed toward side wall by the recirculation bubble near inner wall. After approximately 4.5Dh distance in mainstream direction, the velocity restores to a more uniform distribution by Cheah et al. [33]. Then, bended by the 180^o sharp turn, flow enters the square unheated passage and exits through the hose fitting and hose.

After installing the turning vane, the flow in the upstream portion of the hub turn is not much affected by it. However, the flow behavior in the turn region and the after-

turn passage is significantly different from the case without turning vane. First, in the turn region, the passage is divided to two parts: the inner passage and the outer passage by the turning vane. In either of them, the Dean vortex is generated but in smaller size as discussed by Luo and Razinsky [37]. As a result, the secondary flow strength is weakened and the pressure gradient between the divider and the hub wall is reduced. Second, because of the turning vane, near the divider, flow separation is suppressed and the size of the recirculation zone in the second passage is largely reduced. Consequently, the velocity distribution is more uniform and the impingement on side wall of the second passage is weaker compared to the case without turning vane.

The influence of ribs on local flow behavior in this two passage 2:1 channel with a hub turn is exactly the same as that in two pass 2:1 aspect ratio channel with a tip turn discussed in last section and shown in **Figure 27**. In the hub turn portion, the pair of rib-induced secondary vortex still exists and pushes the mainstream core toward the inner divider, which is in the opposite direction of the Dean vortex. The combination of these two pair of vortices results in a secondary flow structure similar to the results by Schabacker et al. [30] shown in **Figure 28**. The Dean vortex is pushed toward the hub wall and the rib-induced vortex is near the inner divider. Consequently, the strength and scale of the Dean vortex is largely reduced and heat transfer is expected to drop on hub wall.

The flow behavior and consequent heat transfer level is also influenced by rotation and rotation induced buoyancy forces. **Figure 29** shows the secondary flow vortices induced by rotation and ribs in all passes, including the heated and unheated

passages. Attributing to the Coriolis force, mainstream favors the leading surface in the first passage with radial inward flow and favors the trailing surface in the second passage with radial outward flow. Due to the reversed directions of mainstream and buoyancy force in the passage with radial outward flow, to some point, flow starts to reverse and separation is formed. This mechanism is the same for the two pass 2:1 aspect ratio channel with a tip turn in its first passage (radially outward flow). Simultaneously, the Coriolis force induces a pair of vortices, impinging on the leading surface in passages with radial inward flow and trailing surface in passages with radial outward flow for the orientation angle (β) of 90^o. In the tilted channel ($\beta=135^o$), as in **Figure 29 (b)**, the pair of vortices impinges on the leading surface and the side wall in the passages with radial inward flow. They impinge on the trailing surface and the side wall in the passages with radial outward flow. Thus, compared to the $\beta=90^o$ case, the effect of rotation is expected to reduce on leading and trailing surfaces and to enhance on side and inner walls. The combination of these complex flow behaviors due to turn, ribs and rotation `may result in enhancement of the heat transfer, or they may have a negative impact on the heat transfer trend.

Rotation number (Ro) defined in Eq. (4) is used to describe the effect of rotation on heat transfer, same as the 2:1 channel with a tip turn. Similarly, the combined effect of rotation and coolant temperature gradient is evaluated by the local buoyancy parameter (Bo_x), which is defined in Eq. (10).

$$Bo_x=[(T_{w,x}-T_{b,x})/T_{b,x}](Ro)^2(R_x/D_h) \quad (10)$$

Here, in calculating the density ratio, $T_{f,x}$ in denominator of Eq. (4) is replaced by $T_{b,x.}$

The corresponding rotation number Ro and channel-averaged buoyancy parameter Bo at each tested Reynolds number and rotational speed are shown in **Figure 29**. In this two pass 2:1 channel with a hub turn, the highest rotation number of 0.45 is achieved at Reynolds numbers of 10,000 and rotation speed 400 rpm. Accordingly, the maximum local buoyancy parameter of 0.8 is obtained based on the highest Ro of 0.45 and an inlet density ratio of 0.12.

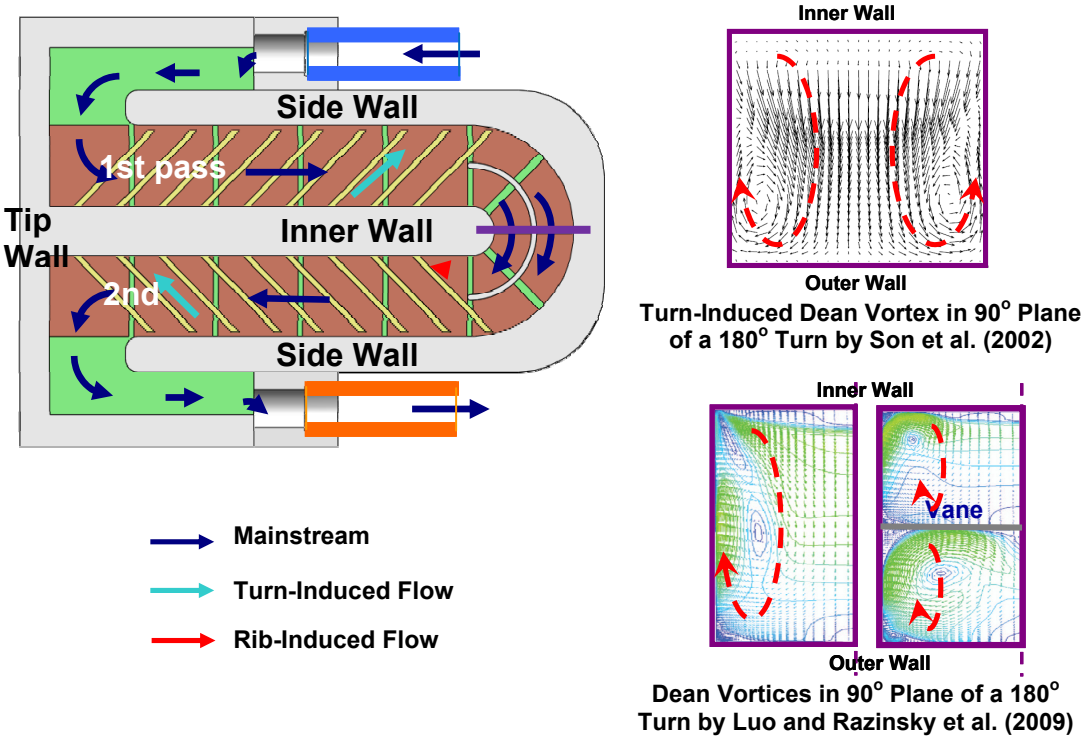

Fig. 26 Conceptual view of mainstream flow behaviors in the 2:1 test section with a hub turn

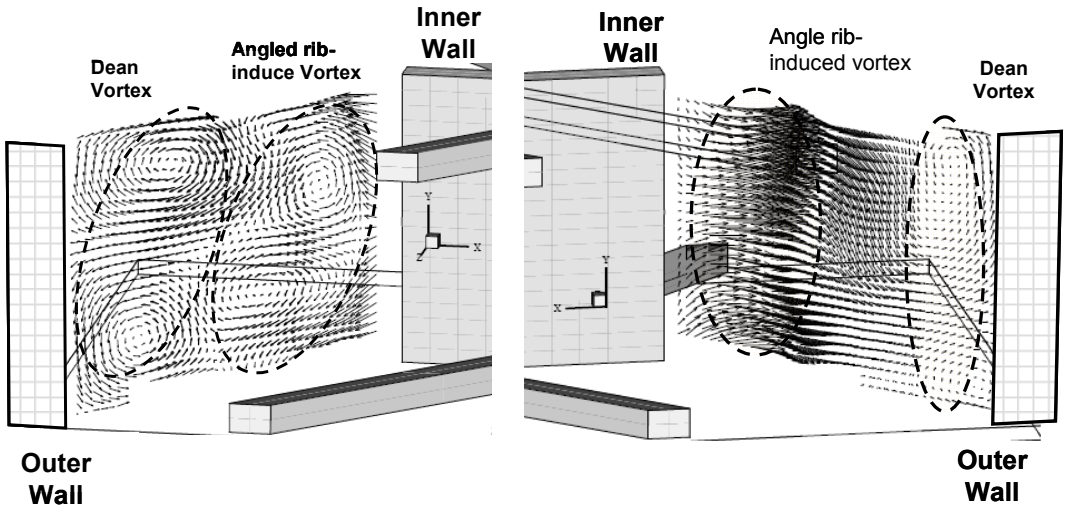

Fig. 27 Secondary flow field at 45° and 135° cross-section plane of the 180° sharp turn by Schabacker et al. (1999)

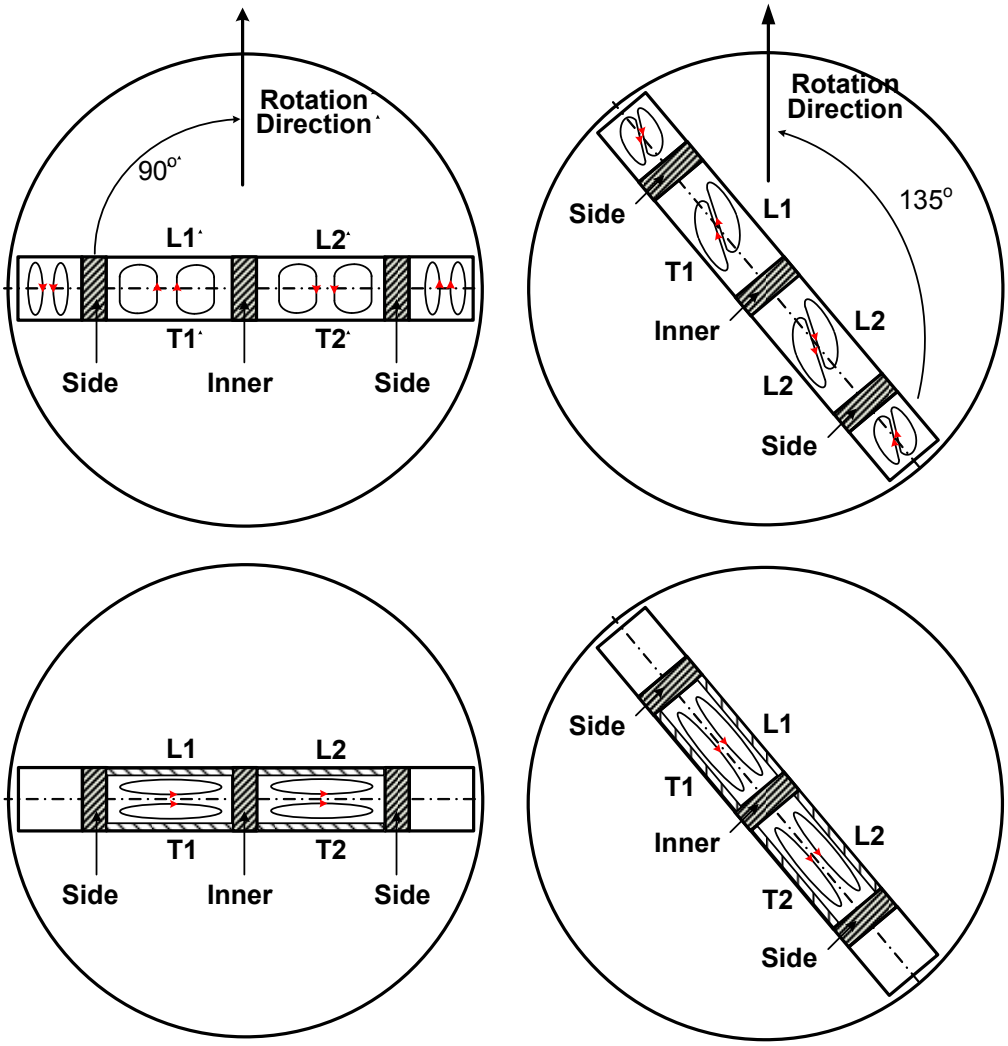

(a) (b)

Fig. 28 Conceptual view of the secondary vortices induced by rotation and angled ribs at β of (*a*) 90° and (*b*) 135°

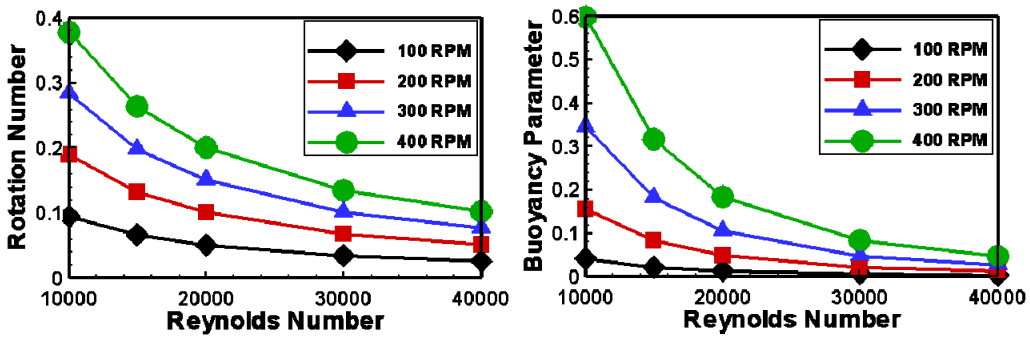

Fig. 29 Rotation number and buoyancy parameter at different Re and rotation speeds

4.2.2 Vane Conduction Effect Correction

The turning vane is made of SLS Nylon PA and the thermal conductivity is 0.7 W/(m K). When it is applied in the hub turn region, heat is conducted from the leading and trailing surfaces to the vane and convected away by air. To calculate the actual heat transfer coefficient on leading and trailing surfaces, heat conducted from them to the vane must be deducted. The turning vane in the shape of half circle is considered as two constant cross-section fins extending from leading and trailing surfaces to the mid-plane of the vane. On the mid-plane, insulation boundary condition is assumed and temperature obtained on the leading and trailing walls is considered as the base temperature of the fin.

Heat conduction is calculated in the turn portion region by region on both leading and trailing walls via Eq. (11).

$$Q_f=(kA_chP)^{1/2}(T_{w,x}-T_{b,x})\tanh(1/2\,L(h\,P/k\,A_c)^{-1/2}) \qquad (11)$$

Here, k is the thermal conductivity of the SLS Nylon PA. L, P, A_c are height, perimeter and cross-section area of the vane respectively. The heat transfer coefficient h on the vane surface is assumed to be the same level as that on hub wall in each region. Temperature difference refers to that between copper plates surface and the bulk flow. The actual convection heat transfer Q_a on leading or trailing walls after installing the vane is shown as in Eq. (12) and Q_a is used to replace Q_n to calculate the heat transfer coefficient in Eq. (1) and the corresponding part of the vane cross-section area A_c must be deducted from projection areas of each copper plates on lading and trailing walls.

$$Q_a=Q_n-Q_f \tag{12}$$

This correction procedure is applied to cases of all Reynolds numbers and rotation speeds. It is observed that the case of Re=10,000 and rpm=400 gives the highest conduction effect by vane and the largest disparity of Nu/Nu_o is 15% for both smooth and ribbed channels at $\beta=90^o$. The streamwise distribution of Nu/Nu_o before and after correction at Re=10,000 and 40,000 in stationary and rotating conditions (rpm=0 and 400) is shown at $\beta=90^o$ in **Figure 30**.

4.2.3 Heat Transfer in Stationary Channel

Smooth Channel

The streamwise Nu_s/Nu_o ratio distributions in the stationary channel at Re=20,000 and 40,000 are presented in **Figure 31**. Comparisons made on each heated surface (leading, trailing, side, and inner walls) between cases with and without turning vane. Twelve regions are shown and region #1 and region #14 are excluded because of higher uncertainty.

In the first passage after the sharp turn, on leading and trailing surfaces, Nu ratio (Nu_s/Nu_o) is decreasing due to entrance effect for both cases with or without vane. On side wall, Nu_s/Nu_o keeps decreasing until region #5, where a small increase occurs for both cases. On inner wall, Nu ratio experiences a decrease due to the entrance, and then increases at region #5 to different levels for both cases. After installing the turning vane, the 20% heat transfer increase on inner wall at region #5 attributes to the local flow acceleration due to the vane.

In the hub turn portion, on leading and trailing surfaces, Nu ratio (Nu_s/Nu_o) keeps increasing because of the secondary flow and turn-induced turbulent mixing. The case with turning vane shows a lower level of heat transfer than the case with vane because the turning vane reduces the secondary flow strength as well as the turbulent mixing. On side wall (hub wall), for the case without turning vane, Nu_s/Nu_o shows an increasing trend to highest value of 3.2 which is similar to leading and trailing walls, however, after applying the vane, Nu_s/Nu_o is substantially decreased to 2.0 and it is due to the shrinkage

of the strength and scale of the Dean vortex, which directly transport the relatively cold air from the mainstream core to hub wall.

In the second passage, on leading and trailing walls, the decreasing trend of Nu ratio (Nu_s/Nu_o) is similar to that in the first passage and the case with vane presents a 10%~15% lower level than the case without vane because of the reduced secondary flow and turbulent mixing introduced by the turning vane. On side wall, except for the decreasing trend, the level of Nu_s/Nu_o is reduced by 40% after applying the vane because the flow impingement on the side wall due to recirculation zone near inner is largely reduced. On inner wall, for both cases, region #10 shows the lowest heat transfer coefficient in whole field due to the recirculation zone. Nu_s/Nu_o recovers at region #11 and keeps a constant value after it in streamwise direction. Due to the lower turbulent intensity in the second passage after installing the vane, the Nu ratio decreases approximately 5%~10% on inner wall.

The effect of Reynolds number on Nu ratio is observed between (a) and (b) of **Figure 31**. The Nu_s/Nu_o ratio on all surfaces in the channel decreases slightly with increasing Reynolds number. This can be explained as that the increase of Nu_s is not as much as the increase of Nu_o, which is calculated by the Dittus-Boelter/McAdams correlation.

Ribbed Channel

The streamwise Nu_s/Nu_o ratio distributions in the in the stationary channel at Re=20,000 and 40,000 are presented in **Figure 32**. Comparisons to smooth channel are

made on each heated surface for cases with and without turning vane. Similar to smooth channel, region #1 and region #14 are excluded because of higher uncertainty.

In the first passage after the sharp turn, on leading, trailing, and side walls, heat transfer is decreasing due to entrance effect and increasing again because of the elevated secondary flow and turbulent mixing by ribs. On inner wall, the relatively higher level of heat transfer compared to side wall is by rib-induced vortex, which impinges the mainstream cold fluid to inner wall. In the hub turn portion, heat transfer drops dramatically attributing to the absence of ribs. The difference between leading and trailing is due to the staggered configuration of ribs and its effect still exists in turn portion. In the second passage, on leading and trailing surfaces Nu_s/Nu_o restores to the level before the U-bend and on side wall, it is even higher than that in the first passage because of the mainstream favoring toward side wall right after the turn as well as the rib-induced secondary vortex impinging on side wall in the second passage as discussed in flow behavior.

The effect of ribs is obviously seen by comparing to the smooth channel data. For the case without turning vane, on trailing and leading surfaces in the first or the second passage, after installing the ribs, Nu_s/Nu_o increases up to 1.5 times of the smooth data. On side wall, it is approximately 10% and 30% higher in the first and second passage respectively. On inner wall, the heat transfer elevates 10% in the first passage and keeps the same level in the second. It is very interesting that for this ribbed channel, on the hub wall, heat transfer is substantially decreased compared to the smooth channel. This can be explained by the opposite direction of rib-induced vortex and Dean vortex. In the PIV

result by Schabacker et al. [30] shown in **Figure 27**, two pairs of vortices exist simultaneously and Dean vortex is compressed toward hub wall by the rib-induced secondary flow. The reduced size and strength of Dean vortex result in the decreased heat transfer on hub wall for ribbed channel. For the case with turning vane, the heat transfer enhancement due to ribs is quite similar to that without turning vane on leading and trailing surfaces and is not repeated here. On hub wall, the low level of heat transfer due to ribs vanishes. Possibly, the turning vane isolates the Dean vortex and the rib-induced vortex in outer and inner channel respectively and the Dean vortex restores in the outer channel. The validity of this explanation needs further CFD and visualized experimental results.

The effect of the turning vane is obtained by comparing the plots between left and right columns, which represent the cases with and without turning vane. In the first passage, Nu_s/Nu_o ratios on all surfaces are close between these two cases which suggest that the vane does not affect the flow and heat transfer upstream. In the hub turn portion, heat transfer does not show much difference between the two cases on leading, trailing surfaces, however, on hub wall it increases around 30% after the vane is applied. In the second passage, on all surfaces, Nu_s/Nu_o ratios decrease about 20% after the application of turning vane. Concerning the effect of the Reynolds number, it can be obtained by comparison between **Figure 32 (a)** and **(b)**. It is very obvious that Nu_s/Nu_o ratio on all surfaces decreases slightly with increasing Reynolds number. This can be explained as that the increase of Nu_s is not as much as the increase of Nu_o, which is calculated by the Dittus-Boelter/McAdams correlation.

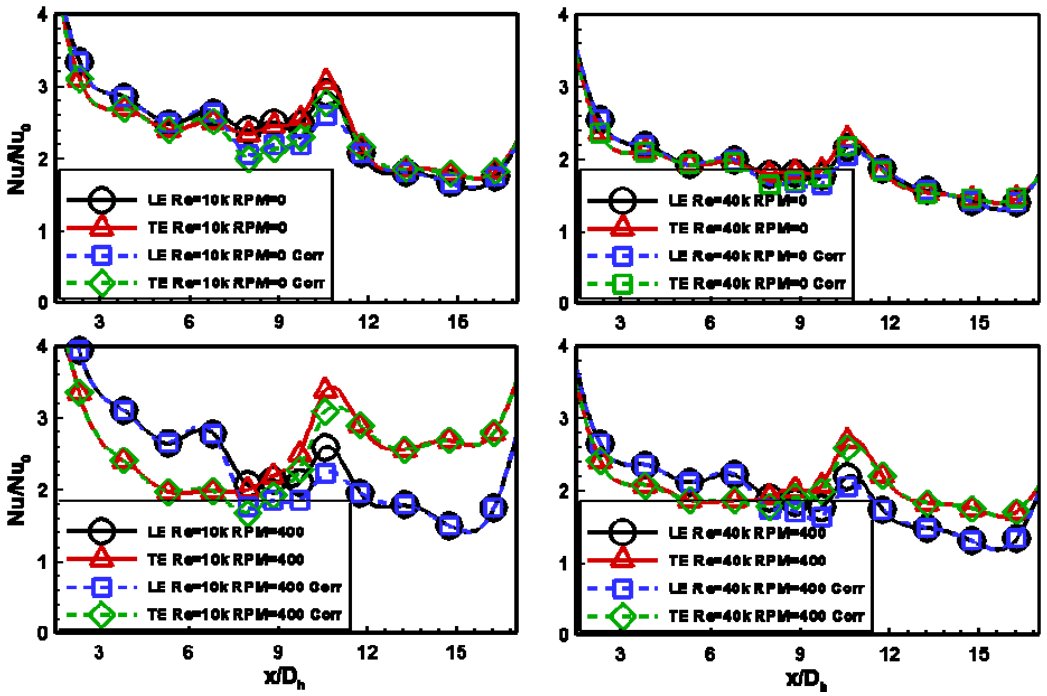

(a)

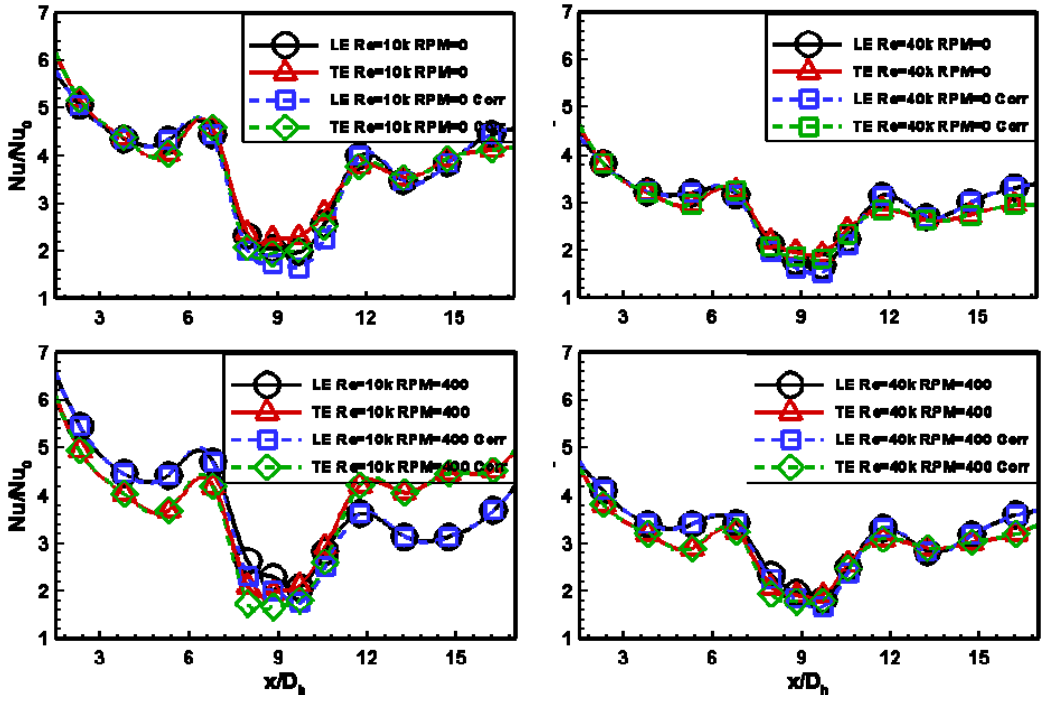

(b)

Fig. 30 Streamwise Nu/Nu$_o$ ratio after vane conduction correction at β=90^o for (*a*) smooth channel (*b*) ribbed channel

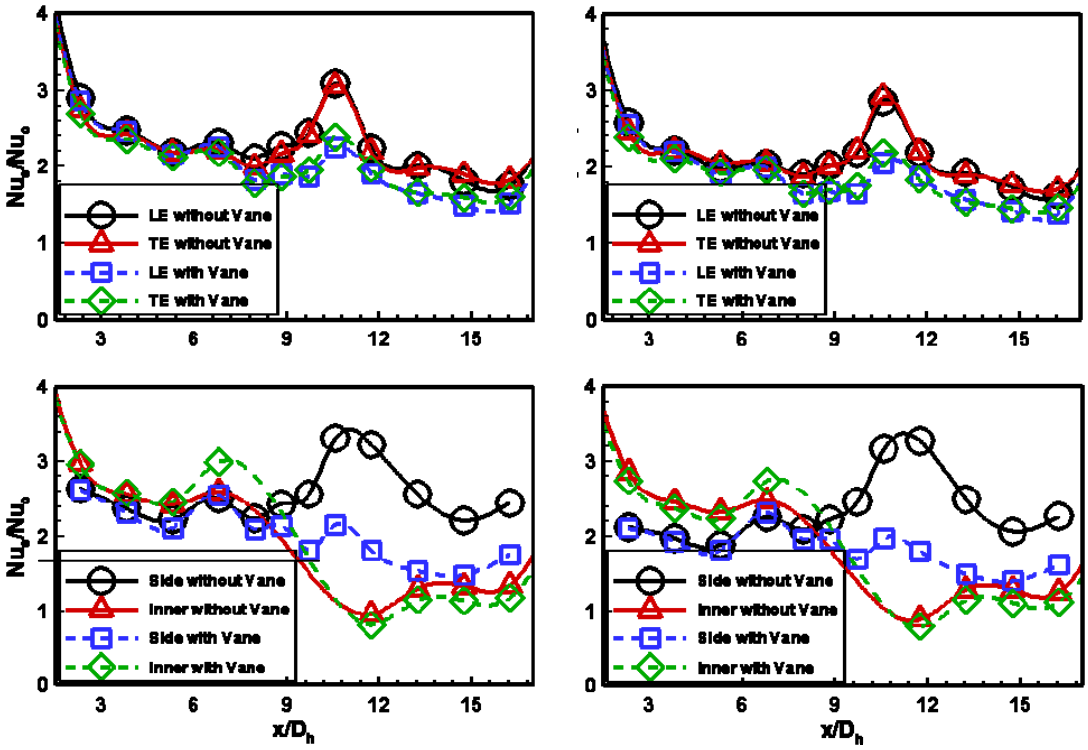

Fig. 31 Stationary streamwise Nu_s/Nu_o in smooth channel on all surfaces at (*a*) Re=20k and (*b*) Re=40k

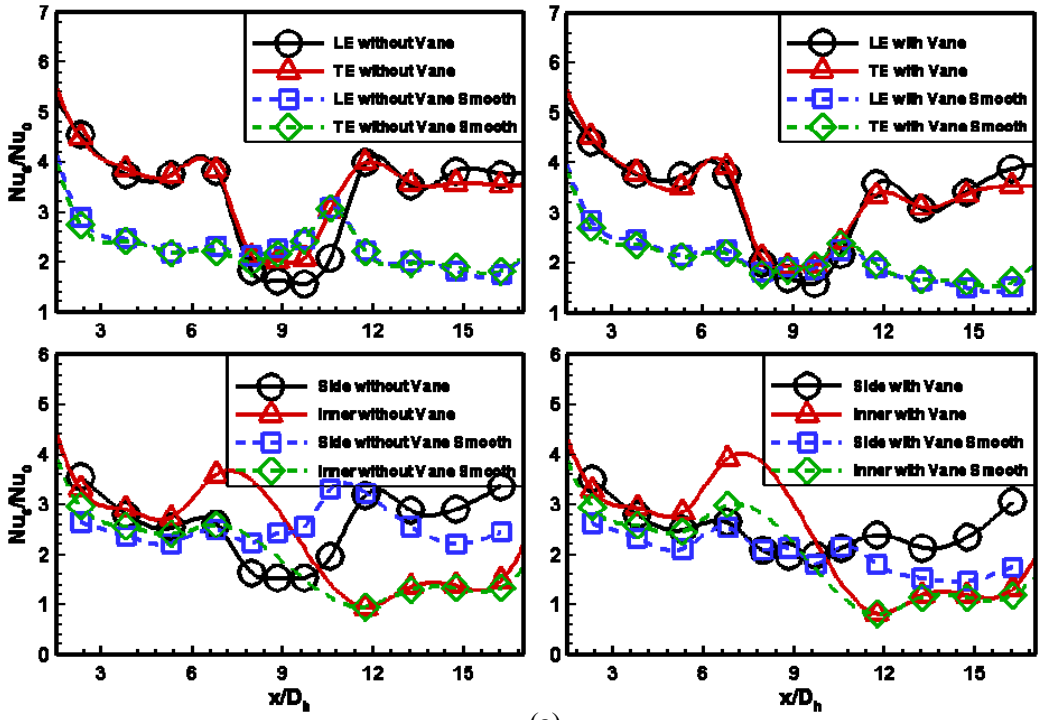

(a)

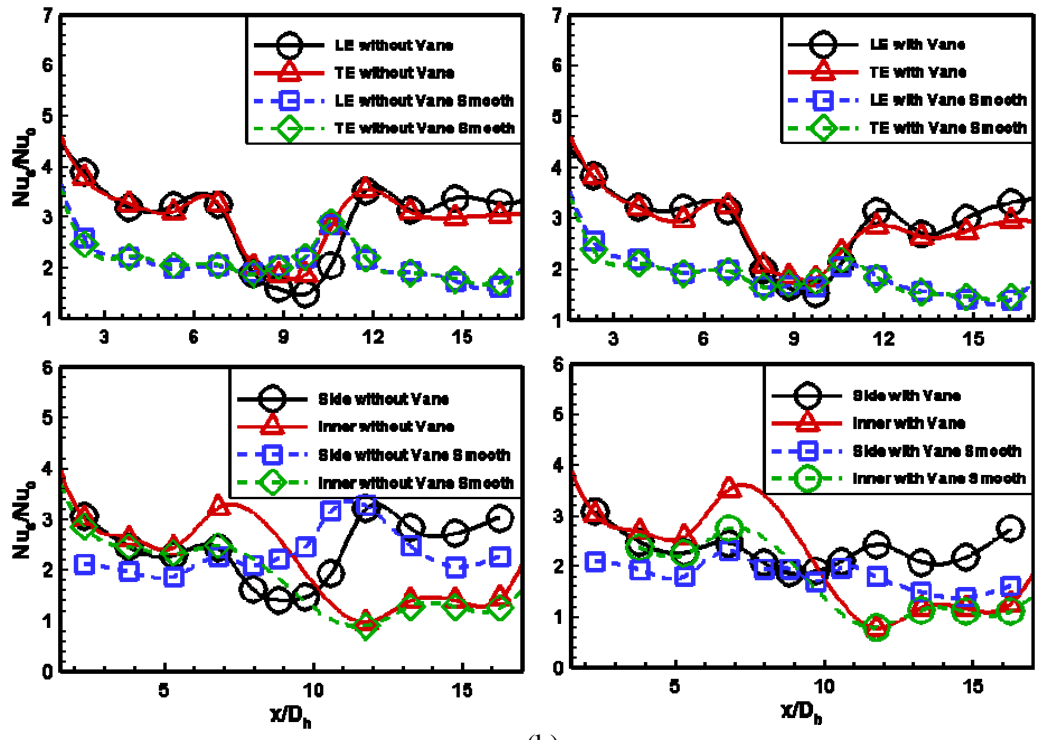

(b)

Fig. 32 Stationary streamwise Nu_s/Nu_o ratio in smooth and ribbed channels on all surfaces at (*a*) Re=20k and (*b*) Re=40k

4.2.4 Heat Transfer in Rotating Channel

Smooth Channel

The streamwise Nu/Nu_o ratio distribution in the rotating smooth channel at rpm=400 and Re=20,000 is shown in **Figure 33**. The corresponding rotation number at this Re and rpm is around 0.2. Comparisons made on each heated surface (leading, trailing, side and inner walls) between cases with and without turning vane at $\beta=90^o$. Similar to the stationary data, only 12 regions are shown.

In the first passage after the sharp turn, on leading surface, Nu ratio (Nu/Nu_o) is decreasing and values are very close between cases with and without turning vane. Similar phenomenon is observed on trailing surface also. However, due to rotation, in this passage with radially inward flow, the mainstream velocity favors the leading side. As a result, the heat transfer level (Nu/Nu_o) at current Ro increases up to 20% on the leading surface compared to the stationary result in **Figure 31**. Contrarily, the Nu/Nu_o ratio on trailing decreased about 10%. On side wall, streamwise Nu/Nu_o is decreasing and bouncing up at region #5 for both cases with or without turning vane.

In the hub turn portion at current rotation number, on leading surface, heat transfer level (Nu/Nu_o) drops 30% when flow enters the hub turn and then keeps a constant value and increases before it exits the turn. This heat transfer behavior is valid for both cases with and without turning vane and the initial heat transfer drop for the case with vane is little lower than the other. On trailing wall, for both cases, Nu/Nu_o experiences a continuous increase up to 40% before flow exits the hub turn. Only in region #9, there shows an obvious difference of Nu ratio between leading and trailing

surfaces. On side wall (hub wall), for both the cases, Nu/Nu_o keeps decreasing to region #8 and increases substantially before the flow exits at region #9.

In the second passage, on leading surface, both cases present a streamwise decreasing in trend, however, Nu/Nu_o value given by the case with vane is 10% lower than the other due to the lower turbulent mixing induced by turning vane. Similar streamwise trend is observed on trailing surface, except that the difference of Nu/Nu_o ratio between two cases is little higher than that on leading surface. Compared to **Figure 31**, due to rotation, in this passage with radially outward flow, the mainstream velocity favors the trailing side, and the heat transfer coefficient on leading is reduced and that on trailing is enhanced for both cases with and without turning vane. On side wall, for the case without turning vane, Nu ratio experiences an initial great increase at region #10 and then a steep drop at region #11. After applying the vane, a gradual decrease of heat transfer in streamwise direction is observed and the level of Nu ratio decreases substantially compared to the case without vane. The reason for this big difference is the same as that of the stationary channel stated before. On inner wall, a similar trend of Nu/Nu_o to the stationary channel is observed for both cases because of similar mainstream flow behaviors. However, the level of the Nu ratio is elevated due to rotation.

Ribbed Channel

The streamwise Nu/Nu_o ratio distribution in the in the ribbed rotating channel at Re=20,000 and rpm=400 ($Ro \cong 0.2$) is presented in **Figure 34**. Comparisons to smooth

channel are made on each heated surface for cases with and without turning vane at $\beta=90^{o}$. Similar to previous section, twelve regions are shown in streamwise direction.

For both cases with or without turning vane, in the rotating channel, on all surfaces, the trend of the streamwise Nu ratio profile is similar to that of the stationary channel at Re=20,000 as shown in **Figure 32 (a)** and the difference in level shows the effect of rotation at current rotation number. In the first passage, heat transfer on leading surface is elevated and that on trailing is reduced and it is reversed in the second pass. In the turn portion at rotation number of 0.2, streamwise Nu/Nu_o ratio on leading side is increased and the difference between leading and trailing is reduced compared to the stationary channel.

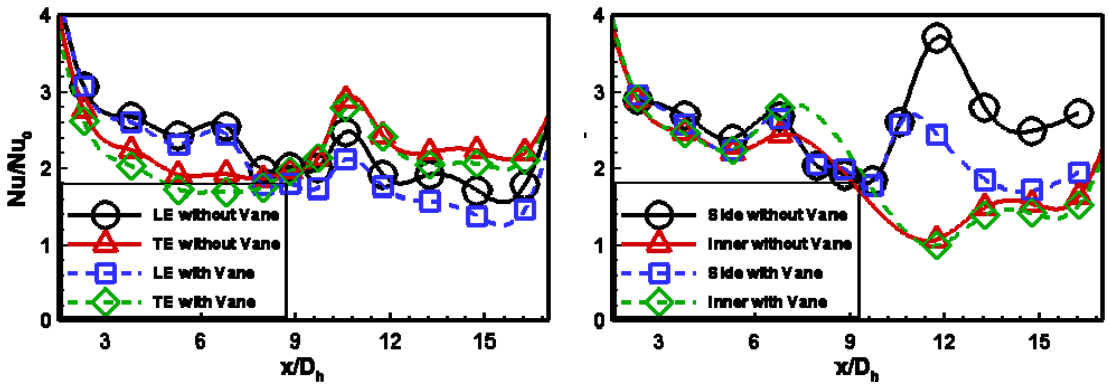

Fig. 33 Streamwise Nu/Nu_o ratio in smooth channel at Re=20k rpm=400 and $\beta=90^{o}$ on (*a*) leading & trailing surfaces (*b*) side & inner walls

The effect of ribs in the rotating condition as shown in **Figure 34** is to increase overall heat transfer coefficient on ribbed surfaces significantly, no matter it has turning vane or not. At the same time, the disparity between leading and trailing surfaces due to rotation is reduced by ribs in the first and the second passages, compared to the smooth channel. On side wall, at current Ro of 0.2, the streamwise Nu/Nu_o ratio is not obviously affected by application of ribs on leading and trailing surfaces along the channel. On inner wall of the first passage, especially at region #5, the heat transfer coefficient is increased compared to the smooth channel. However, effect of ribs on inner is not obvious in the second passage.

The effect of the turning vane in the rotating condition (Ro=0.2) is observed by comparing the plots between left and right columns in **Figure 34**. Similar to the stationary channel shown in **Figure 32**, the vane does not affect the upstream flow and heat transfer behavior much. In the hub turn portion, heat transfer on leading and trailing surfaces is slightly reduced while that on hub wall is increased after the application of turning vane. In the second pass, Nu ratio is decreased on all surfaces when the vane is applied. Especially, at region #10, heat transfer coefficient drops by 30% because the recirculation zone on inner wall is reduced and consequently mainstream flow squeezed on side wall is weakened.

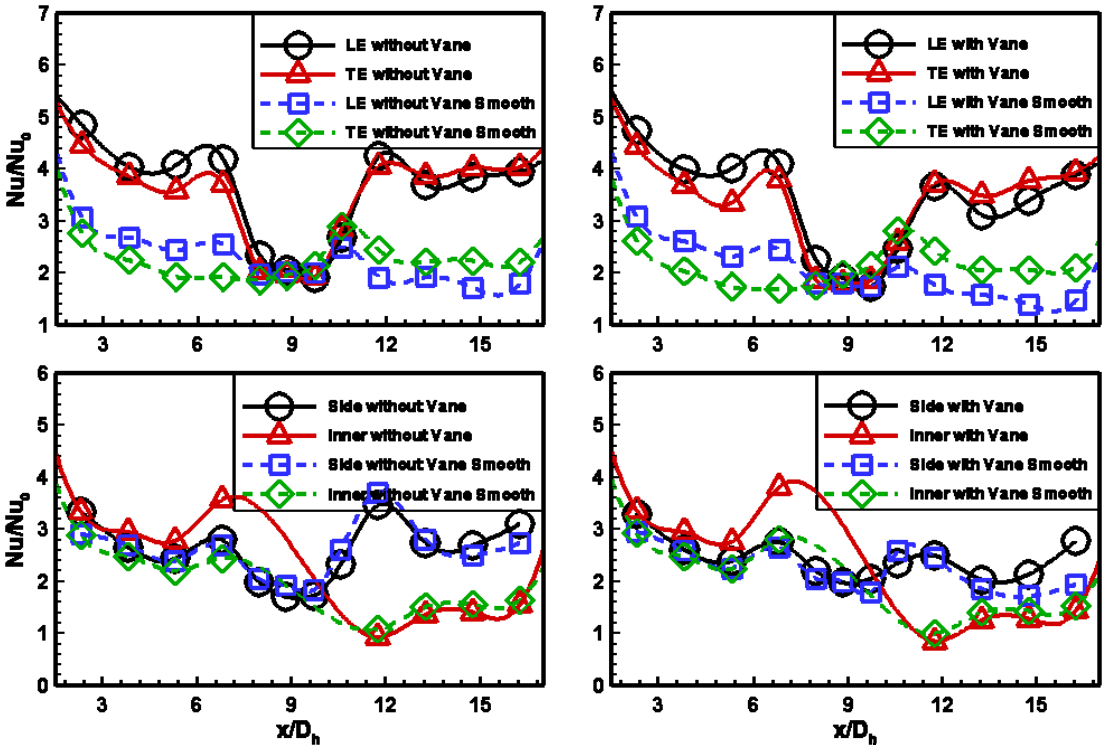

Fig. 34 Streamwise Nu/Nu$_o$ ratio in smooth and ribbed channels on all surfaces at Re=20k rpm=400 and β=90^o (*a*) w/o vane (*b*) w/- vane

4.2.5 Heat Transfer in Rotating Channel – Orientation Angle

Smooth Channel

The effect of the channel orientation angle on streamwise Nu/Nu_o distribution in the smooth channel is shown in **Figure 35**. Two orientation angles of $\beta=90^o$ and 135^o are studied for both cases with and without turning vane at Re=20,000 and rpm=400. The corresponding rotation number at this Re and rpm is around 0.2. As stated before, only 12 regions are shown.

Figure 35 (a) shows the effect of β on streamwise Nu/Nu_o distribution without turning vane. On all surfaces of the first passage, heat transfer behavior of $\beta=135^o$ follows the same trend as that of $\beta=90^o$, however, the Nu/Nu_o difference between leading and trailing surfaces is reduced and that between side and inner walls is increased. As shown in **Figure 28**, in the first passage with radially inward flow, at orientation angle of $\beta=90^o$, the rotation-induced secondary flow impinges the cold mainstream core directly on leading surface and circulates the heated fluid back to trailing surface. In stead, at $\beta=135^o$, the vortex transports the cold air to the leading and side wall and moves the heated fluid back to trailing and inner wall. The partial effect of Coriolis on leading and trailing surfaces and extra effect on side and inner walls at $\beta=135^o$ explains the phenomenon.

In the hub turn portion under the rotating condition ($Ro\cong0.2$), on leading and trailing surfaces, streamwise Nu/Nu_o ratio reveals a low level at region #6, #7, and #8 and increases at region #9 for both orientation angles. The Nu/Nu_o value of $\beta=135^o$ shows 15% lower at maximum compared to $\beta=90^o$. On side wall (hub wall), similar

trend to leading and trailing faces is observed for both orientation angles and their data points are almost on top of each other at region #6, #7, and #8. At region #9, heat transfer coefficient is 10% lower at $\beta=135^{o}$.

In the second passage under the rotating condition ($Ro\cong0.2$), on leading and trailing surfaces, Nu/Nu_o is little lower for $\beta=135^{o}$, however, the difference between leading and trailing is the same for the two orientation angles. Thus, the effect of β is not very obvious on leading and trailing. On side wall, the trend of Nu/Nu_o of $\beta=135^{o}$ is very similar to that of $\beta=90^{o}$, but in a lower value, especially at region #10, which means the mainstream flow squeezed on side wall at region #10 is weakened for the 135^{o} channel orientation. On inner wall, the Nu/Nu_o at $\beta=135^{o}$ shares the same trend with $\beta=90^{o}$, but the level is approximately 15% lower. Detailed flow structure resolution requires flow visualization experiments or CFD simulation.

Figure 35 (b) presents the effect of β on streamwise Nu/Nu_o distribution with turning vane. On all surfaces of the first passage, heat transfer behaviors for both orientation angles are close to the case without turning vane in trend and level as shown in **Figure 35 (a)**. On all surfaces of the turn portion, no obvious difference of Nu/Nu_o is observed between two orientation angles. In the second passage, on leading and trailing, similar to turn portion, the effect of orientation angle is not clearly seen. However, on side and inner walls, the difference between those two surfaces is increased and the effect of orientation angle is large enough. This phenomenon can be explained as the secondary flow behavior at $\beta=135^{o}$ as stated and it becomes obvious because the vane helps to reduce the secondary flow and the recirculation zone. As the result, the

complexity of the mainstream in the second passage is largely reduced and the orientation angle's effect on secondary flow becomes more important.

Ribbed Channel

The effect of the channel orientation angle on streamwise Nu/Nu_o distribution in the ribbed channel is shown in **Figure 36**. Two orientation angles of $\beta=90^o$ and 135^o are studied for both cases with and without turning vane at Re=20,000 and rpm=400. The corresponding rotation number at this Re and rpm is around 0.2. It is obvious that, for both cases, the streamwise Nu/Nu_o does not show a big variation between $\beta=90^o$ and 135^o on all surfaces.

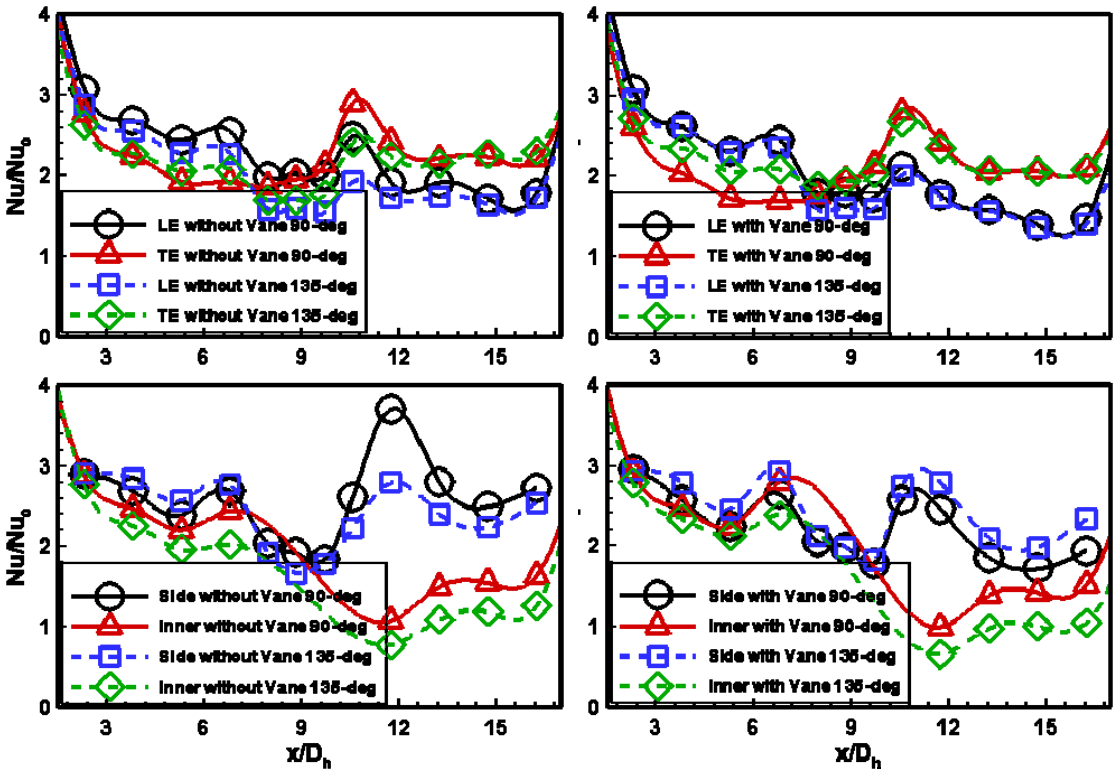

(a) (b)

Fig. 35 Streamwise Nu/Nu_o ratio in smooth channel on all surfaces at Re=20k rpm=400 (*a*) w/o vane (*b*) w/- vane

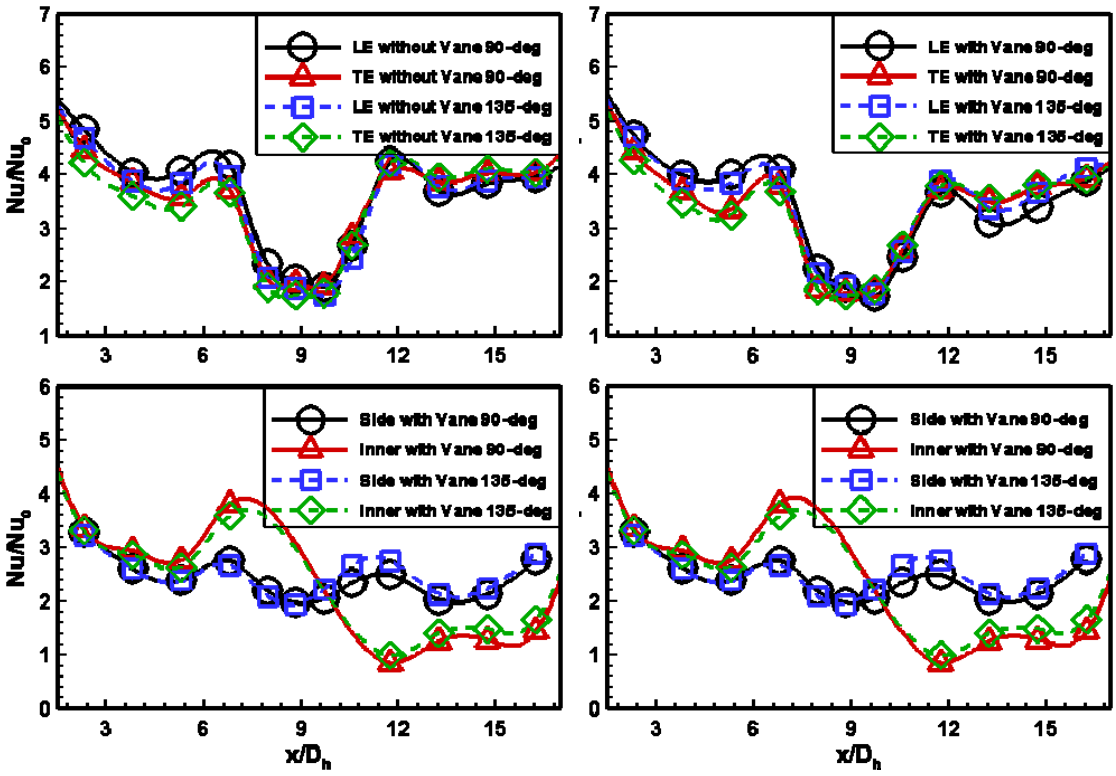

(a) (b)

Fig. 36 Streamwise Nu/Nu$_o$ ratio in ribbed channel on all surfaces at Re=20k rpm=400 (*a*) w/o vane (*b*) w/- vane

4.2.6 Rotation Number Effect

Smooth Channel

The rotation number (Ro) as defined in Eq. (4) is used to describe the ratio of the Coriolis force to the bulk inertial force and can be reached by various combinations of rotational speed and mainstream flow velocity. The rotation number in this study varies from 0 to 0.45. In **Figures 37~40**, the effect of rotation on heat transfer (Nu/Nu_s) is presented as a function of the rotation number at region #4, #5, #6, #7, #8, #9, and #10. These six regions are positioned before, in or after the hub turn portion. The stationary Nusselt number (Nu_s) is chosen as the denominator so that the effects of rotation can be compared.

In **Figure 37**, correlation between regionally averaged Nu/Nu_s and Ro at region #4 and #5 is shown. Result of the two cases without and with vane at two channel orientation angles ($\beta=90^o$ and 135^o) at region #4 is shown in **Figure 37 (a)**. For the case without vane, on leading surface, Nu ratio (Nu/Nu_s) increases to 1.15 and keeps at that value approximately with increasing rotation number. The difference of Nu/Nu_s ratio between $\beta=90^o$ and 135^o is very limited. On trailing surface, Nu/Nu_s ratio experiences a decrease to 0.8 and then a slight increase for $\beta=90^o$. Comparatively, for $\beta=135^o$, the trend of Nu/Nu_s is the same, however, the level of variation is smaller. On side wall, Nu/Nu_s ratios increase to 1.25 and 1.1 for $\beta=135^o$ and 90^o respectively and holds these values with increasing Ro. On inner wall, both Nu/Nu_s ratios for $\beta=90^o$ and 135^o experience a slight increase and a gradual decrease in trend. At large Ro, data of $\beta=135^o$ is little lower than the $\beta=90^o$. The effect of channel orientation is obvious because the difference of

Nu/Nu_s between leading and trailing surfaces is reduced and that between side and inner walls are increased for orientation angle of $\beta=135^o$ compared to $\beta=90^o$. In this first passage with radially inward flow, the mainstream velocity is favoring the leading side (when $\beta=90^o$) or leading and side wall (when $\beta=135^o$) due to Coriolis as known, thus, the Nu/Nu_s increase on leading (when $\beta=90^o$) or that on both leading and side walls (when $\beta=135^o$) can be expected. However, comparing these two orientation angles, as shown in **Figure 28**, the strength of the partial impingement from rotation-induced vortex on leading for the tilted channel ($\beta=135^o$) is not as strong as the perpendicular impingement ($\beta=90^o$). Simultaneously, extra impingement on side wall for the tilted channel ($\beta=135^o$) induces a larger difference between side and inner walls comparing to perpendicular channel ($\beta=90^o$). For the case with turning vane shown in the right column of **Figure 37 (a)**, on all surfaces and for both orientation angles, the trend and level of Nu/Nu_s are very similar to the case without vane which suggests that the vane does not affect the upstream portion obviously.

In **Figure 37 (b)**, similar content but at region #5 is presented. The effects of rotation, orientation angle and vane are very close to these at region #4 on leading, trailing and side walls. For both the cases without and with vane, the difference of Nu/Nu_s between two orientation angles is more obvious on inner wall and the case without vane experiences a larger Nu/Nu_s variation.

In **Figure 38**, correlation between Nu/Nu_s and Ro in the first half of the U-bend (region #6 and #7) is shown. At region #6, as shown in **Figure 38 (a)**, for the case without turning vane, on leading surface, after a slight increase at small Ro, Nu/Nu_s

drops continuously to 0.8 (when $\beta=90^o$) and 0.7 (when $\beta=135^o$) respectively. On trailing surface, the Nu/Nu_s ratio is elevated to 1.12 before it goes down to 0.7 at highest Ro and the difference of Nu/Nu_s between two orientation angles is not much. On side wall (hub wall), Nu/Nu_s experiences a similar trend to trailing and reaches its lowest value of 0.7 for both $\beta=90^o$ and 135^o. Thus, rotation reduces heat transfer rate dramatically on all surfaces in the hub turn portion of a smooth channel at high Ro. For the case with turning vane, on leading surface, Nu/Nu_s drops continuously to 0.85 (when $\beta=90^o$) and 0.8 (when $\beta=135^o$) respectively after an initial slight elevation. On trailing surface and side wall, the initial increase and afterward decrease of Nu/Nu_s is mild and the lowest value of Nu/Nu_s reaches 0.85 for both orientation angles. Very small difference of Nu/Nu_s for different orientation angles is observed on side wall. To compare between cases with and without turning vane, on all surfaces, the vane helps to reduce the effect of rotation in that the substantial reduction in heat transfer due to rotation is compensated.

In **Figure 38 (b)**, Nu/Nu_s and Ro correlation at region #7 is shown. The effects of rotation, orientation angle and vane are very close to these at region #6 on leading and trailing surfaces. On side wall (hub wall) of the case without vane, Nu/Nu_s decreases monotonously to 0.55 for both $\beta=90^o$ and 135^o. However, after installing the vane, the Nu/Nu_s ratio experiences an initial increase and decrease similar to the trend at region #6 though the level of reduction of Nu/Nu_s is lower.

Figure 39 presents the correlation between Nu/Nu_s and Ro in the second half of the U-bend (region #8 and #9). At region #8, as shown in **Figure 39 (a)**, for the case

without vane, on leading and trailing surfaces, the huge drop of Nu/Nu_s is steeper for both orientation angles compared to region #6 and #7, especially for $\beta=135^o$. At the same time, the level of Nu/Nu_s differentiates a lot between $\beta=90^o$ and 135^o at large Ro. On side wall (hub wall), Nu/Nu_s is reduced to 0.5 for both $\beta=90^o$ and 135^o, lower than that at region #6 and #7. For the case with vane, on all surfaces, despite the same trend of Nu/Nu_s compared to region #6 and #7, the drop of Nu/Nu_s due to rotation is reduced. The difference of Nu/Nu_s between two orientation angles is very small on hub, similar to region #6, and #7. At region #9, as shown in **Figure 39 (b)**, for the case without vane, on all surfaces, Nu/Nu_s shows a very similar trend and value as region #8 for both $\beta=90^o$ and 135^o. In addition, channel orientation obviously affects Nu/Nu_s on trailing and leading surfaces. For the case with vane, on all surfaces, the Nu/Nu_s ratios are higher than those at region #8. Especially, on trailing and side wall (hub wall), at large Ro, Nu/Nu_s levels are higher than 1. Concerning the effect of channel orientation, only on side wall (hub wall), $\beta=135^o$ shows an approximately 10% higher heat transfer than $\beta=90^o$.

Figure 40 shows the correlation between Nu/Nu_s and Ro in the second passage at region #10 and #11. At region #10, as shown in **Figure 40 (a)**, for the case without vane, on leading surface, Nu/Nu_s experiences a decrease to 0.8 at Ro=0.2 and rebounds back to 0.9 at Ro=0.42 when $\beta=90^o$. It reduces continuously to 0.7 at Ro=0.4 when $\beta=135^o$. On trailing surface, Nu/Nu_s ratio increases to 1.15 at highest Ro when $\beta=90^o$ and it varies around unit when $\beta=135^o$. On side wall, Nu/Nu_s decreases and recovers to 1 for both orientation angles. On inner wall, trends of Nu/Nu_s diverge for $\beta=90^o$ and 135^o and

maximum difference between them is up to 0.9 at highest Ro. For the case with vane, on leading surface, Nu/Nu_s decreases to 0.85 at Ro=0.1 and increases slightly for both $\beta=90^o$ and 135^o. On trailing surfaces, Nu/Nu_s is growing to 1.35 monotonously for both orientation angles. On side wall, the trend of heat transfer in rotation is changed significantly by turning vane and Nu/Nu_s increases to 1.45 and 1.8 respectively for both $\beta=90^o$ and 135^o. On inner wall, the diverging tendency still exists between $\beta=90^o$ and 135^o and the vane decreases the difference of Nu/Nu_s between two orientation angles. It is shown in **Figure 40 (b)**, the heat transfer behaviors in rotation at region #11 are not much different from that at region #10 including the effects of rotation, vane and orientation angle. In this second passage with radially outward flow, secondary vortex due to rotation moves the cold mainstream core to trailing surface (when $\beta=90^o$) or trailing and side wall ($\beta=135^o$). Thus the heat transfer in rotation increases on trailing and decreases on leading at both $\beta=90^o$ and $\beta=135^o$. The rebounds of Nu/Nu_s at large Ro on leading surface is due to the flow reversal, which is induced by the different direction of buoyancy force and mainstream velocity.

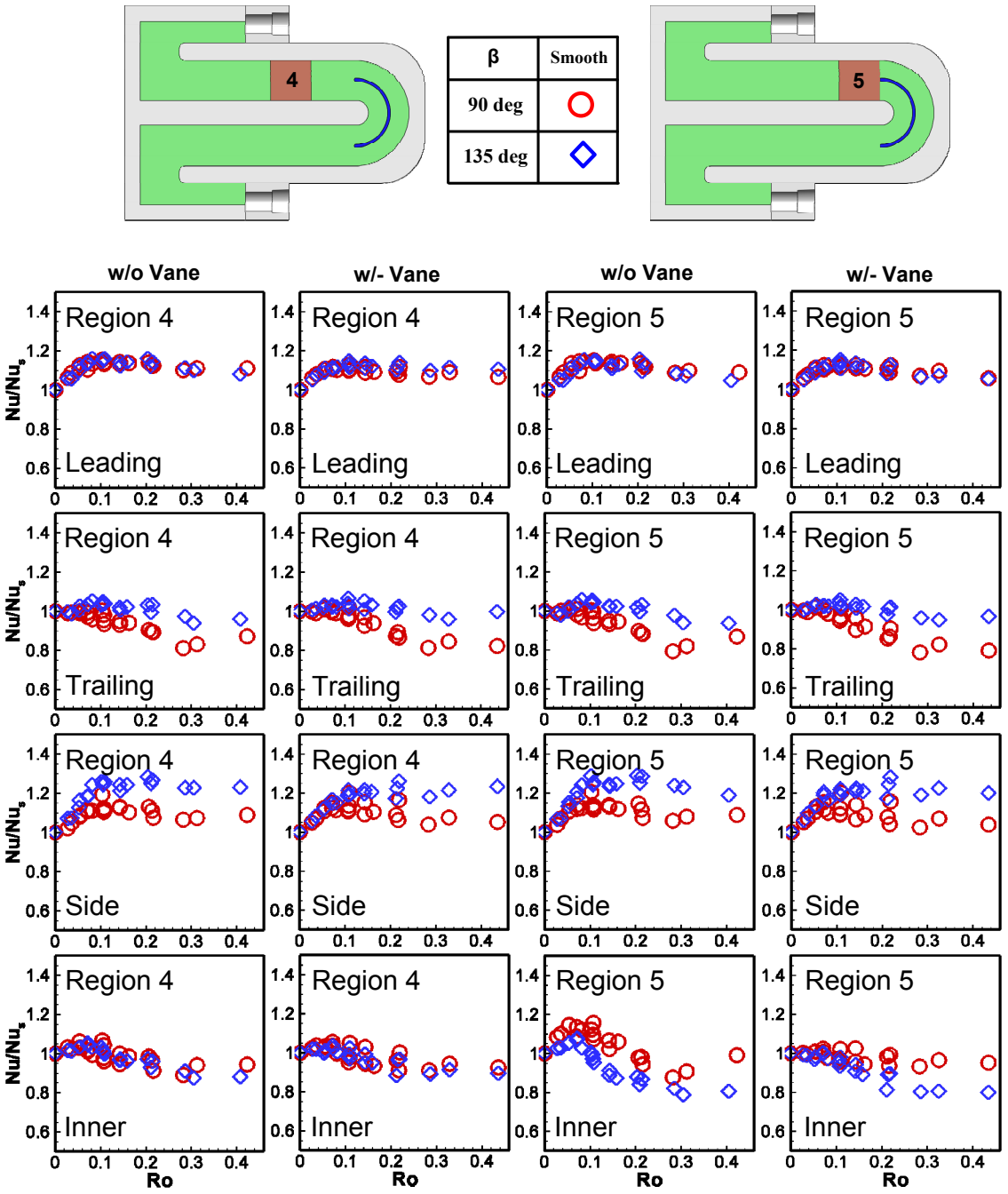

Fig. 37 Regionally-averaged Nu/Nu_s v.s. Ro in smooth channel for both cases w/o and w/- vane at β=90° and 135° for (*a*) region #4 and (*b*) region #5

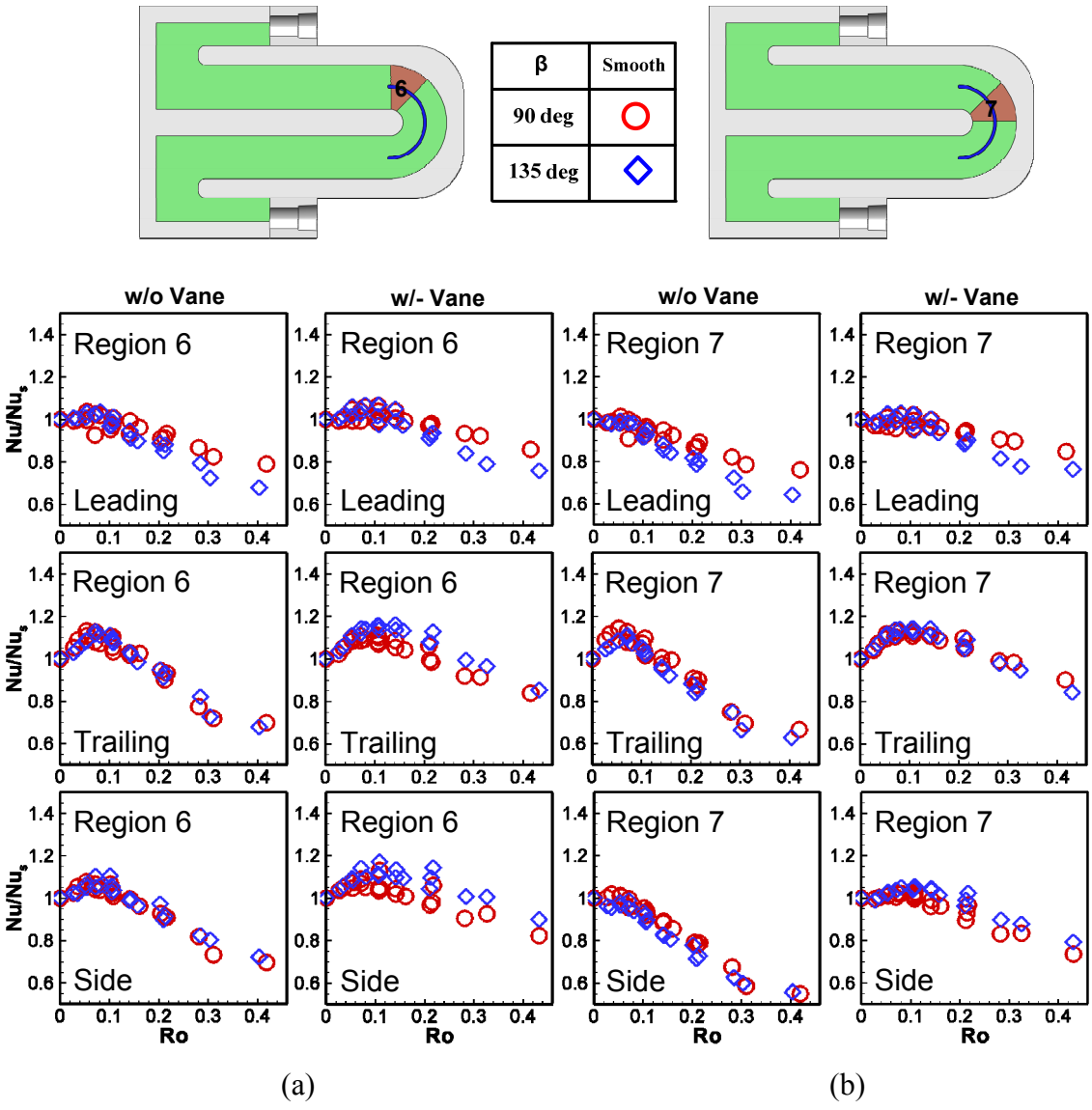

Fig. 38 Regionally-averaged Nu/Nu_s v.s. Ro in smooth channel for both cases w/o and w/- vane at β=90° and 135° for (*a*) region #6 and (*b*) region #7

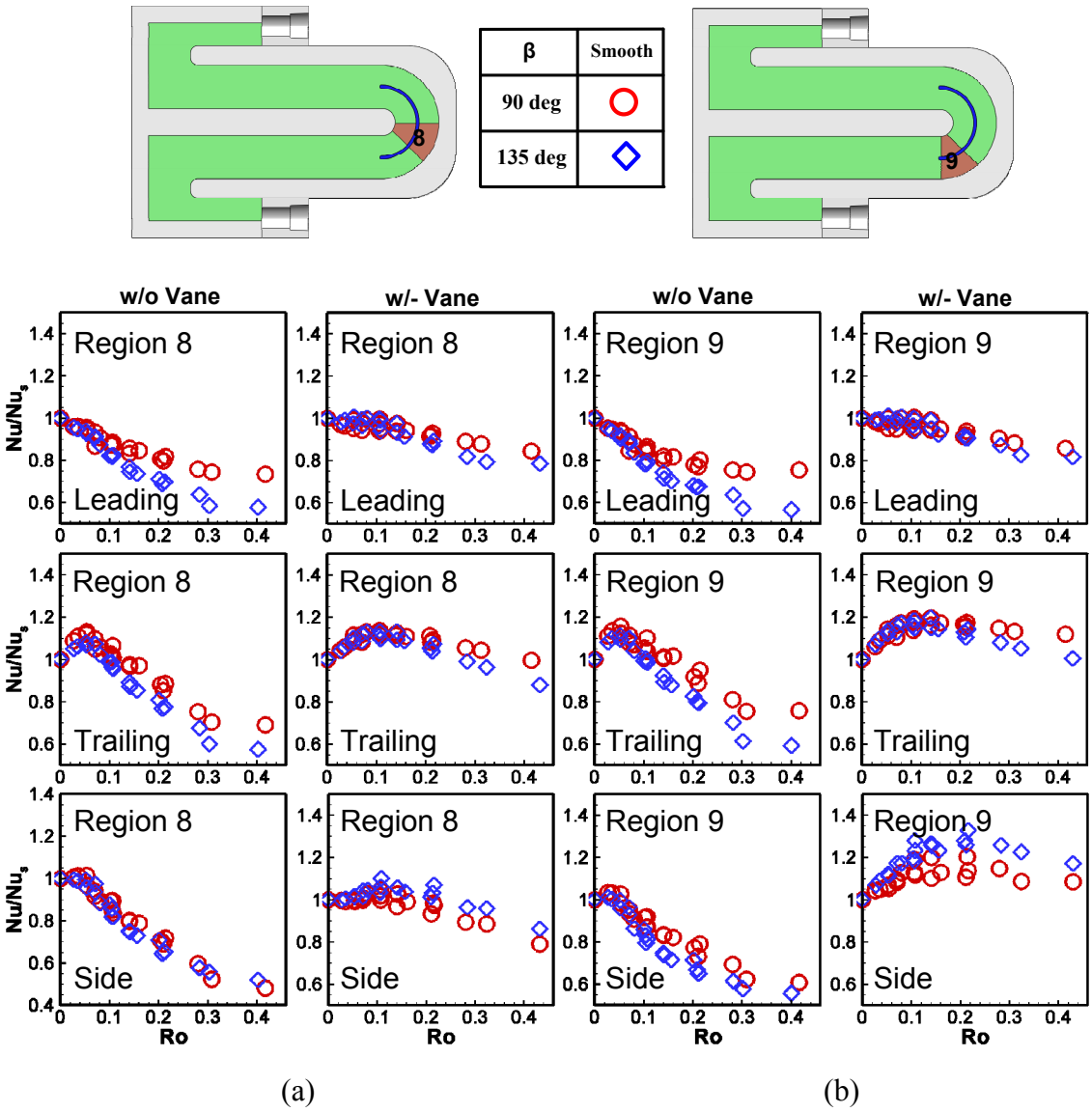

Fig. 39 Regionally-averaged Nu/Nu$_s$ v.s. Ro in smooth channel for both cases w/o and w/- vane at β=90^o and 135^o for (*a*) region #8 and (*b*) region #9

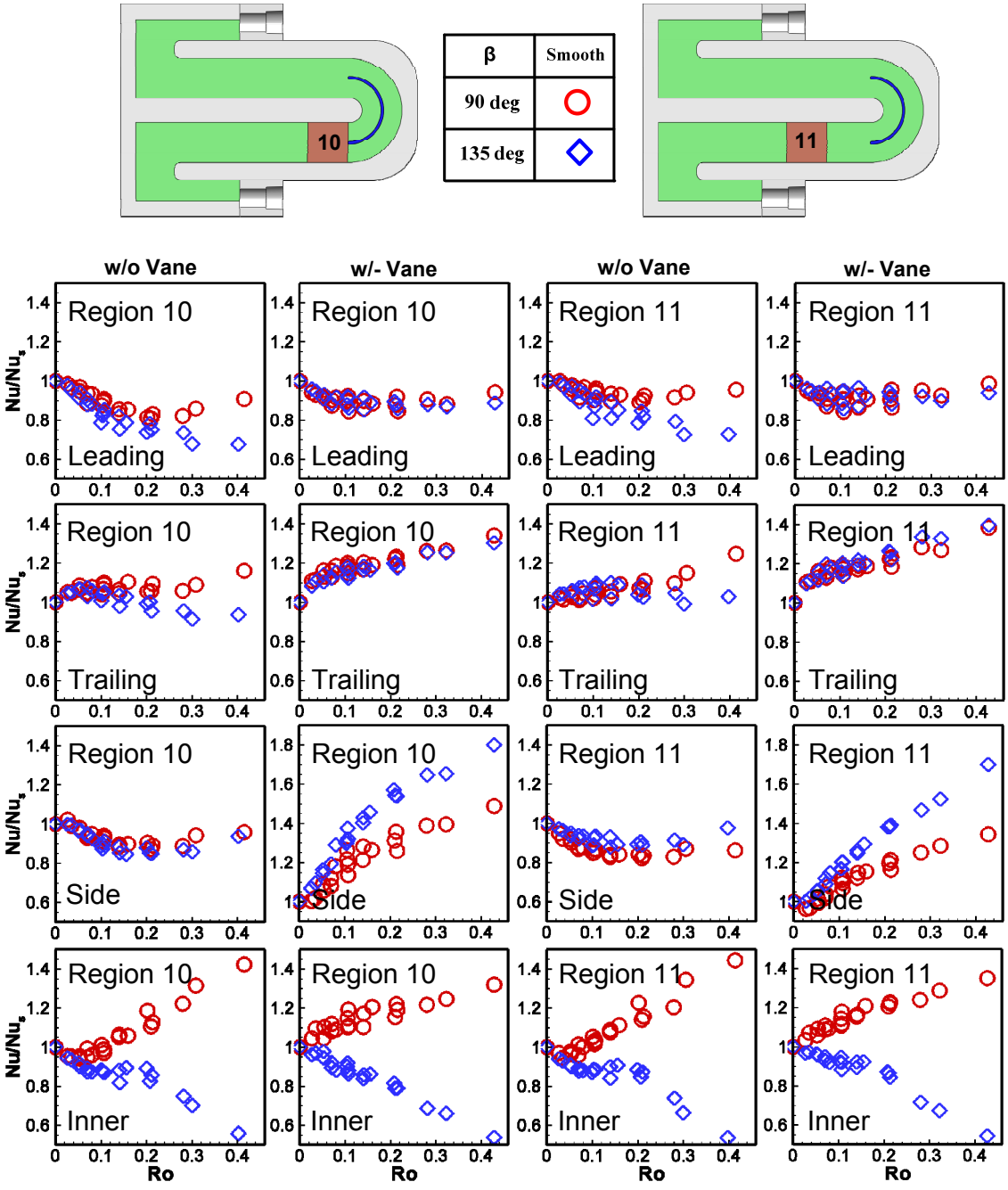

(a) (b)

Fig. 40 Regionally-averaged Nu/Nu_s v.s. Ro in smooth channel for both cases w/o and w/- vane at β=90° and 135° for (*a*) region #10 and (*b*) region #11

Ribbed Channel

In **Figures 41~44**, the effect of rotation on heat transfer (Nu/Nu_s) in the ribbed channel is presented as a function of the rotation number at region #4, #5, #6, #7, #8, #9, and #10. Data in the smooth channel are also presented for comparison at the same regions. These six regions are positioned near the hub turn portion. The stationary Nusselt number (Nu_s) in the ribbed and the smooth channel is chosen as the denominator respectively so that the effects of rotation can be compared.

In **Figure 41**, correlation between regionally averaged Nu/Nu_s and Ro at region #4 and #5 is shown. Comparisons with smooth data are made on all surfaces. Results of the two cases without and with vane at two channel orientation angles ($\beta=90^o$ and 135^o) at region #4 are presented in **Figure 41 (a)**. For the case without turning vane, Nu/Nu_s ratio increases gradually to 1.05 on leading surface and decreases gradually to 0.95 on trailing surface. On side wall, it experiences a slight decrease and then recovers to unit. On inner wall, the Nu ratio is elevated slightly and reduced gradually to 0.95. The trend and level of Nu/Nu_s at $\beta=135^o$ is very similar to that of perpendicular rotating ($\beta=90^o$). Comparing to the smooth data, in whole scale, the variations of the heat transfer coefficient due to rotation on all surfaces are smaller though their trend keeps the same. Especially on side wall, the initial increase of Nu/Nu_s from the smooth data is not observed for the ribbed channel. Besides, compared with the smooth data, effect of orientation angle is reduced because the difference between leading and trailing surfaces for $\beta=135^o$ is smaller than that for $\beta=90^o$. For the case with turning vane, on all surfaces and for both orientation angles, the trend and level of Nu/Nu_s are very similar to the case

without vane. This is also valid for data in the smooth channel. This proves again that the vane does not affect the flow and heat transfer upstream in both ribbed and smooth channels. In **Figure 41 (b)**, similar content but at region #5 is presented. The effects of rotation, ribs, orientation angle and vane are very close to these at region #4 on leading, trailing, side and inner surfaces of the ribbed channel. Little difference of heat transfer behavior is observed on side wall of the ribbed channel in that the initial slight decrease of Nu ratio at region #4 disappears and Nu/Nu_s at region #5 increases monotonously to 1.1.

In **Figure 42**, correlation between Nu/Nu_s and Ro in the first half of the U-bend (region #6 and #7) is shown. Comparisons with smooth data are made on all surfaces. Results of the two cases without and with vane at two channel orientation angles ($\beta=90^o$ and 135^o) are presented. At region #6, as shown in **Figure 42 (a)**, for the case without turning vane, on leading surface, Nu/Nu_s increases to 1.3 (for $\beta=90^o$) and 1.15 (for $\beta=135^o$). On trailing surface, Nu/Nus gets an initial drop and gradually recovers to unit at Ro=0.2. Then, Nu/Nus shows a decrease for $\beta=90^o$ and a slight increase for $\beta=135^o$. Similarly, on side wall (hub wall), Nu/Nu_s is elevated gradually to 1.15 for both orientation angles ($\beta=90^o$ and 135^o). The effect of channel orientation is obvious in that the difference of Nu ratio between leading and trailing surfaces is larger for $\beta=90^o$ than that for $\beta=135^o$. Comparing to smooth data, ribs hugely influence the heat transfer in rotating channel because the steep drop of Nu/Nu_s for the smooth data disappears. For the case with turning vane, the Nu/Nu_s presents a similar trend of heat transfer variation due to rotation at both orientation angles, however, the variation on all surfaces is

reduced compared to the case without vane. Thus, the effects of rotation on Nu/Nu_s are the same for both cases with and without vane; however, the rotation effect is weakened by the turning vane. In **Figure 42 (b)**, Nu/Nu_s and Ro correlation at region #7 is shown. In the ribbed channel, effects of rotation, ribs, orientation angle and vane are very close to these at region #6 on leading, trailing surfaces. and side (hub) walls.

Figure 43 presents the correlation between Nu/Nu_s and Ro in the second half of the U-bend (region #8 and #9). Results of the two cases without and with vane at two channel orientation angles ($\beta=90^o$ and 135^o) are presented. At region #8, as shown in **Figure 43 (a)**, the heat transfer behavior is close to that at region #6 and #7 as discussed. Larger difference between leading and trailing surfaces is observed for $\beta=90^o$ than that for $\beta=135^o$. Ribs stop the steep drop of Nu/Nu_s and attributes to a higher value of Nu/Nu_s at large Ro. The effect of rotation on Nu/Nu_s is the same for both cases with and without vane and it is weakened by application of the turning vane. However, compared to region #6 (or region #7), large disparity between $\beta=90^o$ and $\beta=135^o$ on leading and trailing surfaces is reduced and bigger gap is observed between these two orientation angles on side (hub) wall. In **Figure 43 (b)**, Nu/Nu_s and Ro correlation at region #9 is shown for both cases without and with cases at two channel orientations ($\beta=90^o$ and 135^o). In the ribbed channel, effects of rotation, ribs, orientation angle and turning vane are close to these at region #8 on all walls in trend, however, the Nu/Nu_s level is increased on all surfaces.

In **Figure 44**, correlation between regionally averaged Nu/Nu_s and Ro at region #10 and #11 is shown. Comparisons with smooth data are made on all surfaces. Result of

the two cases without and with vane at two channel orientation angles ($\beta=90^o$ and 135^o) at region #10 is presented in **Figure 44 (a)**. For the case without turning vane, on leading surface, Nu/Nu_s experiences slight variation and reaches 0.98 (for $\beta=90^o$) and 1.13 (for $\beta=135^o$) respectively. On trailing surface, it remains around unit (for $\beta=90^o$) or elevates gradually to 1.15 (for $\beta=135^o$). On side wall, at both orientation angles, Nu/Nu_s gradually increases to 1.2 and on inner wall, at both orientation angles, Nu/Nu_s is increasing. On all surfaces, tilted-rotating channel has higher Nu/Nu_s ratio at large Ro. Comparing to the smooth channel, the effect of rotation is largely reduced by ribs since the difference between leading and trailing are minimal for both orientation angles. Besides, on side wall, the Nu/Nu_s level is largely increased while on inner wall, the diverging trend of Nu/Nu_s in smooth channel between $\beta=90^o$ and $\beta=135^o$ disappears. For the case with turning vane, on leading surface, Nu/Nu_s reduces to 0.9 (for $\beta=90^o$) or increases slightly to 1.05 (for $\beta=135^o$) respectively. On trailing surface, Nu/Nu_s increases to 1.1 (for $\beta=90^o$) and 1.2 (for $\beta=135^o$) respectively. On side wall, it is elevated to 1.1 (for $\beta=90^o$) and 1.4 (for $\beta=135^o$) monotonously. On inner wall, it increases to 1.4 (for $\beta=90^o$) and 1.25 (for $\beta=135^o$) at largest Ro respectively. On all surfaces (in a wide Ro range), tilted-rotating channel has higher heat transfer coefficient (Nu/Nu_s). Comparing to the smooth channel, the effect of rotation is declined by ribs for the same reason as the case without vane. Simultaneously, the huge increase of Nu/Nu_s on side wall is suppressed by ribs for both orientation angles. On inner wall, the bifurcating trend of Nu/Nu_s between $\beta=90^o$ and $\beta=135^o$ is not observed in ribbed channel. The turning vane in the ribbed channel is to increase the effect of rotation since difference of Nu/Nu_s

between leading and trailing surfaces for both orientation angles are increased after installation of the turning vane. In addition, difference of Nu/Nu_s ratio between $\beta=90^o$ and $\beta=135^o$ is increased on side wall and inner wall. In **Figure 44 (b)**, Nu/Nu_s and Ro correlation at region #11 is shown. In the ribbed channel, effects of rotation, ribs, orientation angle and vane are very close to these at region #10 on leading, trailing, and side wall and inner wall.

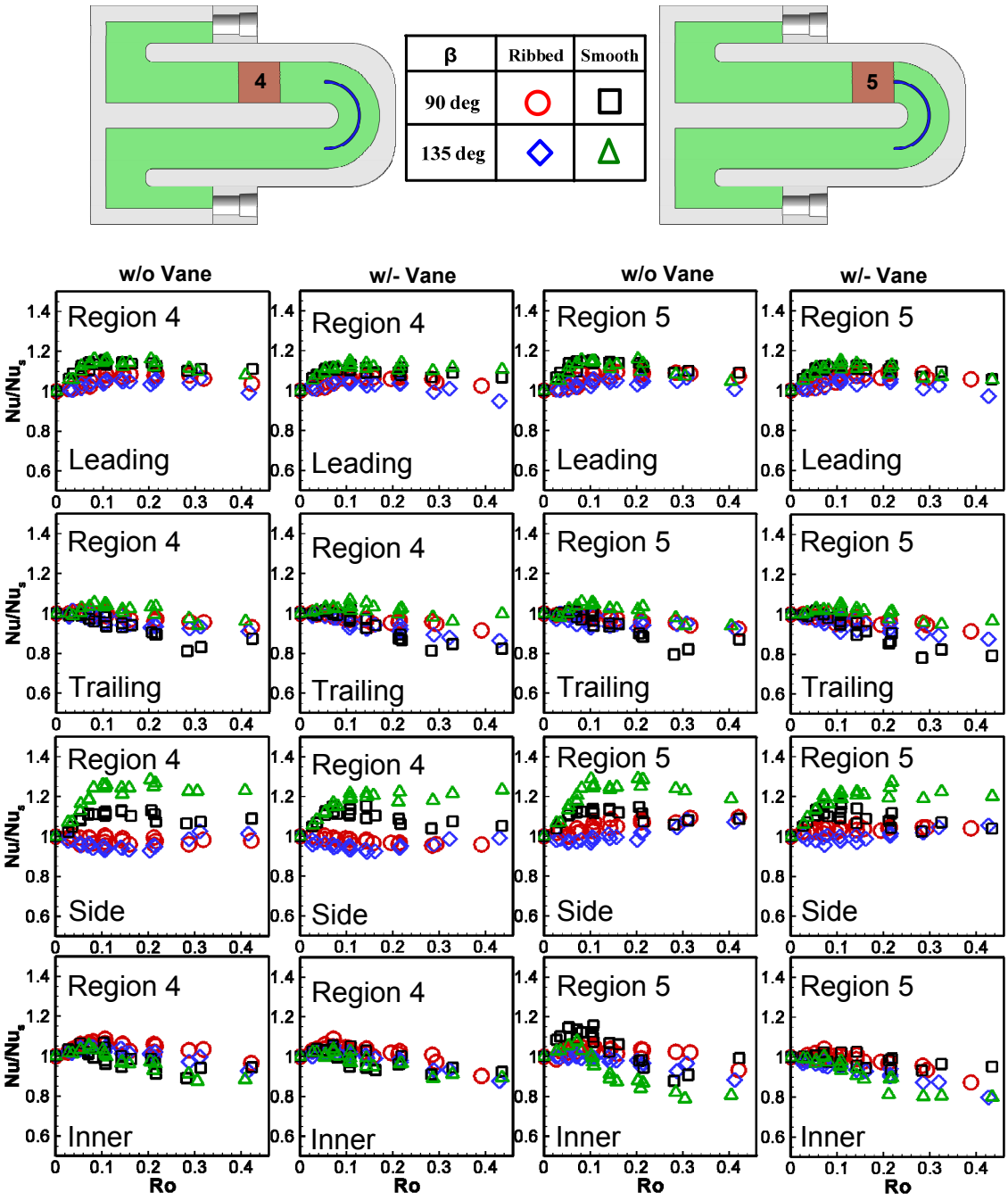

Fig. 41 Regionally-averaged Nu/Nu_s v.s. Ro in smooth and ribbed channels for both cases w/o and w/- vane at β=90° and 135° for (*a*) region #4 and (*b*) region #5

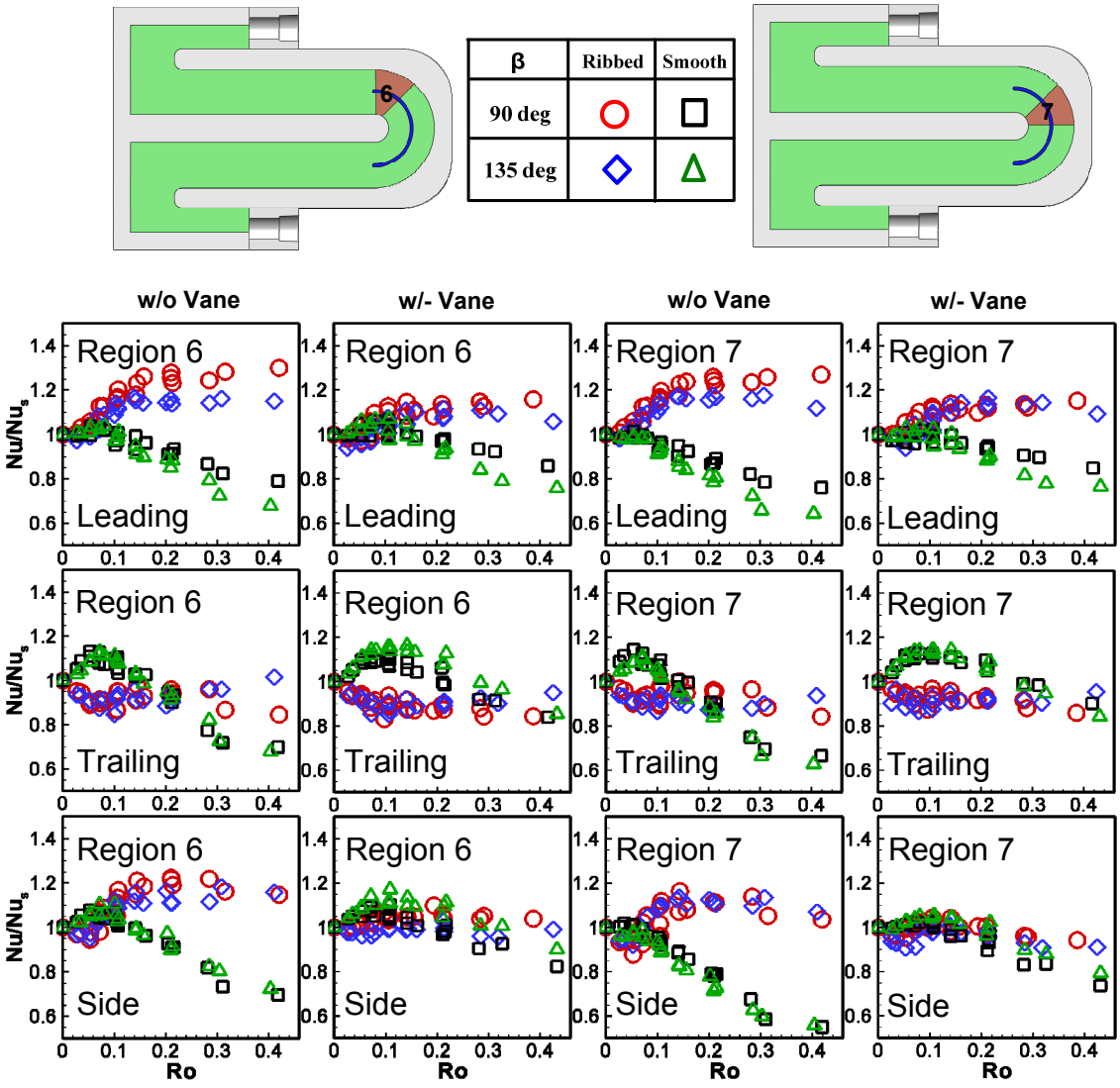

Fig. 42 Regionally-averaged Nu/Nu_s v.s. Ro in smooth and ribbed channels for both cases w/o and w/- vane at β=90° and 135° for (*a*) region #6 and (*b*) region #7

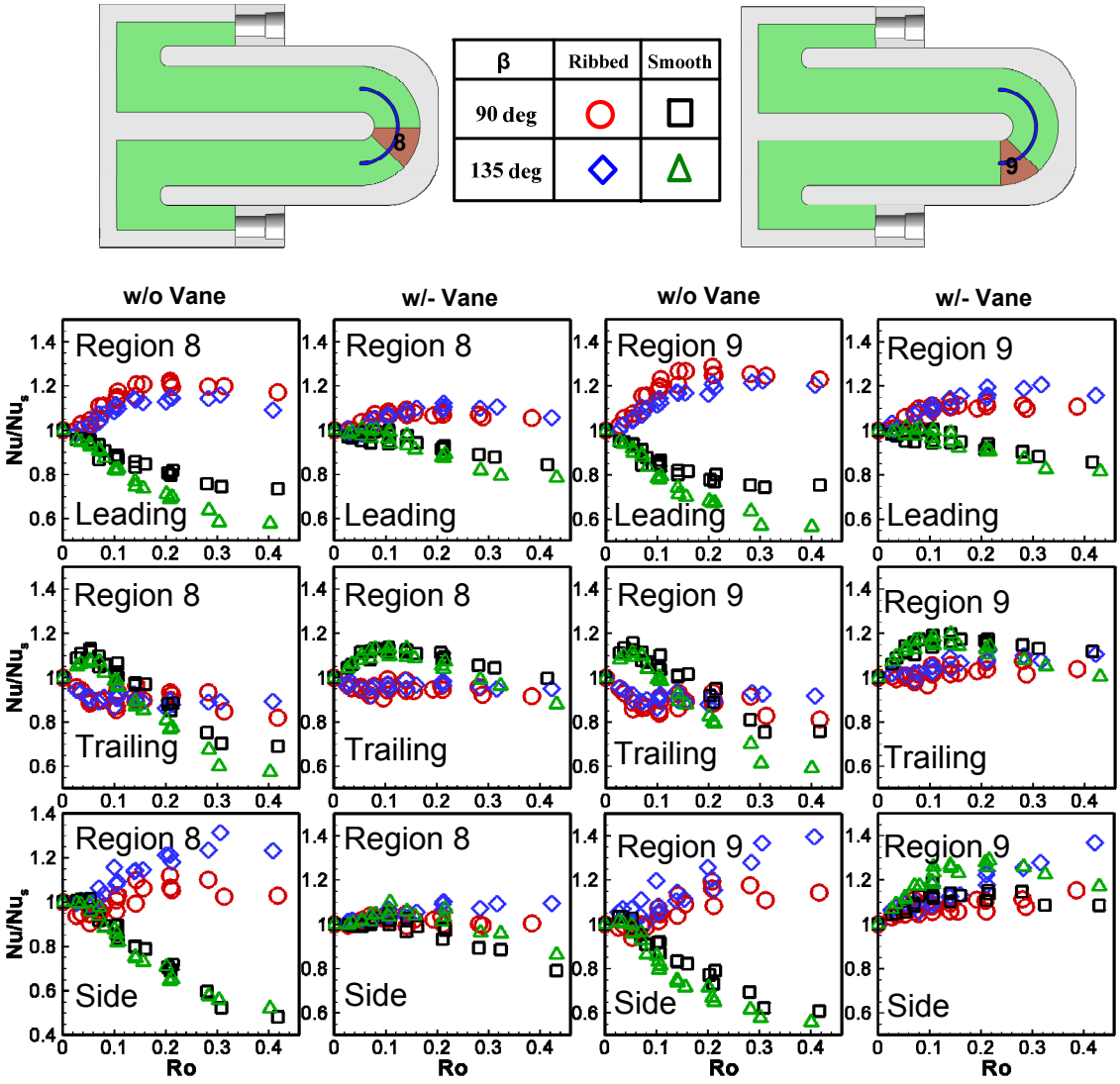

Figure 43 Regionally-averaged Nu/Nu_s v.s. Ro in smooth and ribbed channels for both cases w/o and w/- vane at β=90° and 135° for (*a*) region #8 and (*b*) region #9

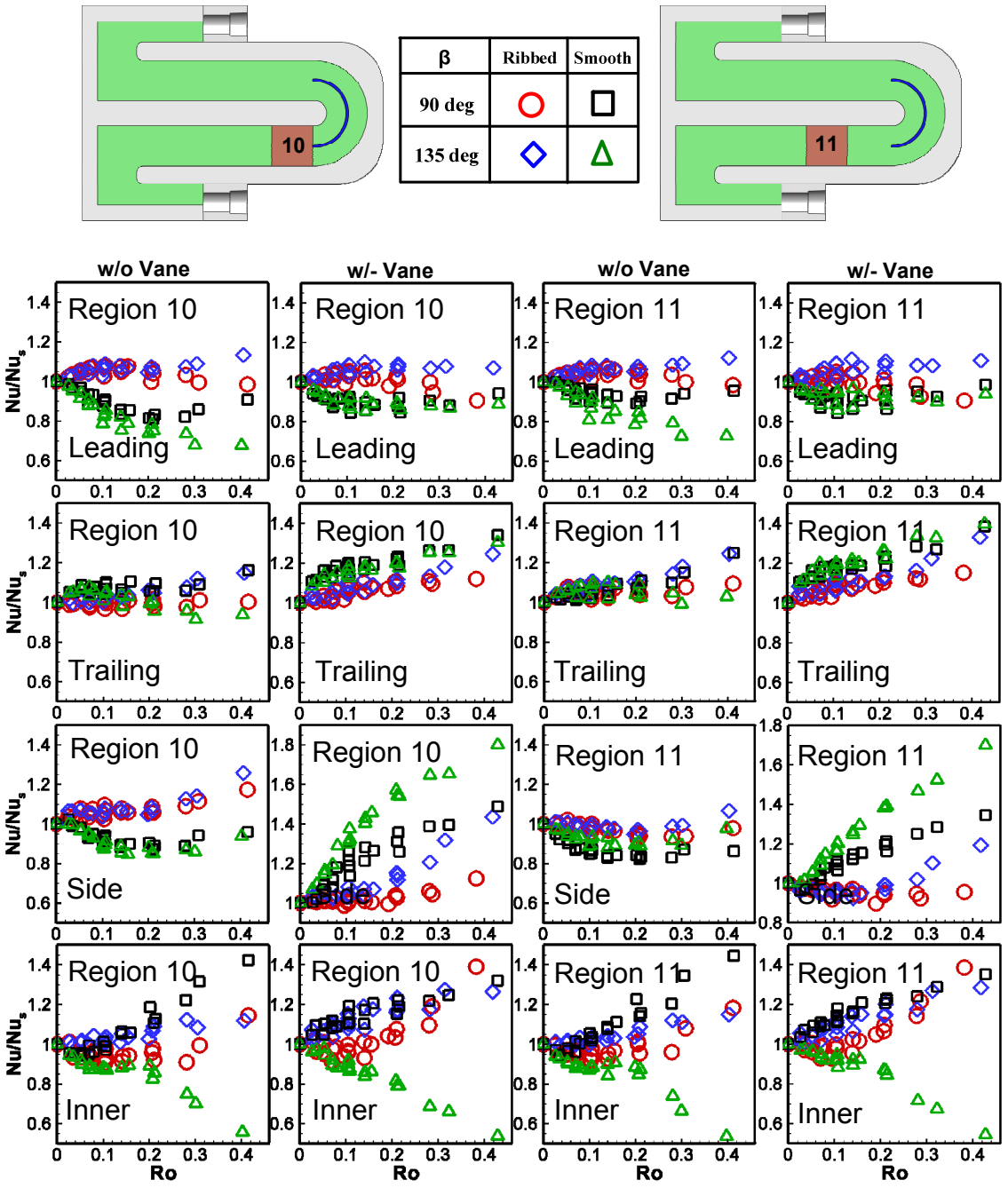

Fig. 44 Regionally-averaged Nu/Nu_s v.s. Ro in smooth and ribbed channels for both cases w/o and w/- vane at β=90° and 135° for (*a*) region #10 and (*b*) region #11

5. CONCLUSIONS

5.1 Two Pass Rectangular Channel (AR=2:1) with a Tip Turn

This research studied the heat transfer behavior in two-pass rotating smooth and ribbed channels (AR=2:1) with a tip turn at two channel orientation angles (β=90^o and 135^o). The effect of rib pitch-to-height ratios is also discussed. Based on the result, the following conclusions are made for the smooth channel:

1. For the stationary case (Re=10,000 to 40,000), the streamwise Nu_s/Nu_o ratios increase with decreasing rib pitch-to-height ratios (P/e=10, 7.5 and 5) on trailing, leading, inner (first pass) and outer (second pass) surfaces and larger Re produces smaller Nu_s/Nu_o ratio on all surfaces.
2. For the rotating case, at large rotation number or buoyancy parameter, the streamwise Nu/Nu_o ratios are greatly affected for both smooth and ribbed cases.
3. The effect of rotation on heat transfer is to increase Nu/Nu_s on trailing surface and decrease it on leading in the first passage with radially outward flow. On the contrary, Nu/Nu_s is decreased on trailing and enhanced on leading surface in the second passage with radially outward flow. In both first and second passages, the Nu ratio (Nu/Nu_s) is increased on outer wall due to rotation.
4. Nu/Nu_s~Ro correlation exists on all surfaces in the first passage, tip turn portion, and the second passage. The effect of rotation on Nu/Nu_s is largely decreased by applying ribs on leading and trailing surfaces for this 2:1 aspect ratio channel. The substantial variations of Nu/Nu_s on the leading or trailing surface due to rotation are

reduced. The effect of rotation on heat transfer on outer and inner surfaces is slightly decreased by ribs in the first pass. In the second pass, the heat transfer due to rotation is tremendously increased on the inner surface due to the combined effects of ribs, rotation and 180^o turn induced secondary flows. The heat transfer in rotating condition is largely enhanced on the tip wall (Cap6 and Cap7) as much as 4 times in ribbed channel, compared to stationary case.

5. The smooth channel oriented at an angle of 135^o, shows a smaller difference in heat transfer levels (Nu/Nu_s) between leading and trailing surfaces compared to the 90^o smooth channel. A beneficial increase in Nu/Nu_s is observed on the leading surface in the first pass for the smooth $\beta=135^o$ case. The ribbed 2:1 channel shows little dependence on channel orientation, for the two rotation angles studied. For the tip cap, in the smooth channel the effect of the channel orientation on heat transfer (Nu/Nu_s) is mild. In the ribbed channel, changing the channel orientation from 90^o to 135^o caused Nu/Nu_s on tip cap to increase. The Nu/Nu_s on the outer wall (1st and 2nd pass) shows little dependence on channel orientation. Conversely, the inner wall heat transfer shows dependence on channel orientation and ribs.
6. The effect of rib pitch-to-height ratios (P/e=5, 7.5 and 10) on the Nu/Nu_s ratio is small under rotation conditions.
7. Regardless of channel orientation the smooth channel pass-averaged heat transfer (Nu/Nu_s) increases by more than 50% on the trailing surface in the first pass with rotation. In the second pass, Nu/Nu_s is reduced by 30% on the trailing surface with rotation. The ribbed channel shows little change in pass averaged heat transfer on the

leading and trailing surfaces under rotating conditions for all rib pitch-to-height ratios (P/e=5, 7.5, and 10).

5.2 Two Pass Rectangular Channel (AR=2:1) with a Hub Turn

5.2.1 Smooth Channel

This research studied the heat transfer behavior in a two-pass rotating ribbed channels (AR=2:1) focusing on the hub turn portion at two channel orientation angles (β=90^o and 135^o). The effect of the turning vane is also discussed. Based on the result, the following conclusions are made for the smooth channel:

1. For the stationary smooth channel (Re=20,000 and Re=40,000), after applying the turning vane, Nu_s/Nu_o ratio decreases on leading and trailing surfaces to 25% and on side wall to 40% in the turn portion and after-turn passage. The overall Nu_s/Nu_o distribution is decreased when Reynolds number increases.
2. For the rotating smooth channel (Re=20,000, rpm=400, and β=90^o), corresponding Nu/Nu_o ratio decreases on all surfaces in after-turn passage when installing the vane.
3. For the rotating smooth channel (Re=20,000 and rpm=400), tilted channel orientation angle (β=135^o) reduces the difference of Nu/Nu_o between leading and trailing surfaces in the first passage.
4. Nu/Nu_s~Ro correlation exists on all surfaces in the first passage, hub turn portion, and the second passage. In the first passage with radially inward flow, heat transfer (Nu/Nu_s) is increased on leading and decreased on trailing surface. In the second passage with radially outward flow, on the contrary, Nu/Nu_s is decreasing on leading

and increasing on trailing. In the hub turn region, Nu/Nu_s decreases dramatically on all surfaces at large Ro number.

5. After installing the turning vane, Nu/Nu_s~Ro correlation in the first passage is not affected. In the hub turn portion, the substantial decrease of Nu/Nu_s is compensated by the turning vane. In the second passage, Nu/Nu_s on leading, trailing and side walls is increased by the vane.

5.2.2 Ribbed Channel

This research studied the heat transfer behavior in a ribbed two-pass rotating channel (AR=2:1) focusing on the hub turn portion at two channel orientation angles ($\beta=90^o$ and 135^o). The effects of ribs and the turning vane are also discussed. Based on the result, the following conclusions are made:

1. For the stationary channel (Re=20,000 and Re=40,000), after the installation of square ribs (P/e=8, $e/D_h=0.1$, $\alpha=45^o$), Nu_s/Nu_o ratio increases on all surfaces in the first and the second passage as much to 170% compared to the smooth channel. In the turn portion, it decreases as much to 60% on side wall compared to the smooth channel. The overall Nu_s/Nu_o distribution is decreased when Reynolds number increases for the ribbed channel.
2. For the stationary ribbed channel (Re=20,000 and Re=40,000), after the installation of the turning vane, in the hub turn portion, Nu_s/Nu_o ratio is not much affected on leading and trailing surfaces and is elevated by 30% on side (hub) wall. In the second passage, Nu_s/Nu_o ratio is decreased as 10% on leading and trailing surfaces and it

drops 30% on side wall. The overall Nu_s/Nu_o distribution is decreased when Reynolds number increases for the ribbed channel with turning vane.

3. For the rotating ribbed channel (Re=20,000, rpm=400, and $\beta=90^o$), in the first passage with radially inward flow, Nu/Nu_o ratio is higher on leading than that on trailing and it is reversed in the second passage with radially outward flow. In the hub turn portion, difference between leading and trailing wall is small.
4. For the rotating channel (Re=20,000, rpm=400, and $\beta=90^o$), after the application of the rib, Nu/Nu_o increases up to 25% in the first passage and it grows up to 40% in the second passage on leading and trailing surfaces. However, the effect of rotation is weakened by the ribs in that the difference between leading and trailing surfaces in both passages is reduced compared to the smooth channel. The Nu/Nu_o on all surfaces of the hub turn portion is not much affected by upstream and downstream ribs.
5. For the rotating ribbed channel (Re=20,000, rpm=400, and $\beta=90^o$), after the installation of the turning vane, Nu/Nu_o level is reduced by around 10% on leading and trailing surfaces and it decreases to 40% on side wall in the turn portion and after-turn passage.
6. For the rotating ribbed channel (Re=20,000, rpm=400), effect channel orientation angles ($\beta=90^o$ and 135^o) on streamwise Nu/Nu_o is not clearly observed.
7. Nu/Nu_s~Ro correlation exists on all surfaces in the first passage, hub turn, and the second passage of the ribbed channel. In the first passage with radially inward flow, heat transfer (Nu/Nu_s) is increased on leading and decreased on trailing surface. In

the second passage with radially outward flow, Nu/Nu_s is varying slightly above unit on leading and trailing surfaces and it is increasing with Ro on side and inner walls. In the hub turn portion, Nu/Nu_s is above 1 on leading surface and hub wall and it is varying around 0.9 on trailing surface.

8. Comparing with the smooth channel, the effect of rotation is reduced in the first /second passages and the hub turn portion by ribs.
9. Effect of channel orientation angles ($\beta=90^o$ and 135^o) is very obvious in the first-half of the turn portion at region #6 and #7.
10. After application of the turning vane, Nu/Nu_s~Ro correlation in the first passage is not affected. In the hub turn portion, the rotation effect is weakened by the vane. In the second passage, Nu/Nu_s on all surfaces is increased by the vane.

REFERENCES

[1] Han, J.C., Dutta, S., and Ekkad, S.V., 2000, Gas Turbine Heat Transfer and Cooling Technology, Taylor and Francis, New York.

[2] Wagner, J.H., Johnson, B.V., and Hajek, T.J., 1991a, "Heat Transfer in Rotating Passages with Smooth Walls and Radial Outward Flow," ASME J. Turbomachinery, **113**, pp. 42-51.

[3] Wagner, J.H., Johnson, B.V., and Kooper, F.C., 1991b, "Heat Transfer in Rotating Passage with Smooth Walls," ASME J. Turbomachinery, **113**, pp. 321-330.

[4] Han, J.C., Zhang, Y.M., and Kalkuehler, K., 1993, "Uneven Wall Temperature Effect on Local Heat Transfer in a Rotating Two-Pass Square Channel with Smooth Walls," ASME J. Heat Transfer, **115**, pp. 912-920.

[5] Huh, M., Lei, J., Liu, Y.H., and Han, J.C., 2009, "High Rotation Number Effects on Heat Transfer in a Rectangular (AR=2:1) Two-Pass Channel," ASME Paper No. GT2009-5942.

[6] Dutta, S., Andrews, M.J., and Han, J.C., 1996, "Prediction of Turbulent Heat Transfer in Rotating Smooth Square Ducts," Int. J. Heat Mass Transfer, **39**, pp. 2505-2514.

[7] Liu, Y.H., Huh, M., Han, J.C., and Chopra, S., 2008, "Heat Transfer in a Two-Pass Rectangular Channel (AR=1:4) under High Rotation Numbers," ASME J. Heat Transfer, **130**, pp. 081701-1 – 081701-9.

[8] Zhou, F., Lagrone, J., and Acharya, S., 2007, "Internal Cooling in 4:1 AR Passages at High Rotation Numbers," ASME J. Heat Transfer, **129**, pp. 1666-1675.

[9] Taslim, M.E., Bondi, L.A., and Kercher, D.M., 1991, "An Experimental Investigation of Heat Transfer in an Orthogonally Rotating Channel Roughened with 45 deg Criss-Cross Ribs on Two Opposite Walls," ASME J. Turbomachinery, **113**, pp. 346-353.

[10] Wagner, J.H., Johnson, B.V., Graziana, R.A., and Yeh, F.C., 1992, "Heat Transfer in Rotating Serpentine Passages with Trips Normal to the Flow," ASME J. Turbomachinery, **114**, pp. 847-857.

[11] Zhou, F. and Acharya, S., 2008, "Heat Transfer at High Rotation Numbers in a Two-Pass 4:1 Aspect Ratio Rectangular Channel with 45 deg Skewed Ribs," ASME J. Turbomachinery, **130**, pp. 021019-1-021019-12.

[12] Han, J.C., 1988, "Heat Transfer and Friction Characteristics in Rectangular Channels with Rib Turbulators," ASME J. Heat Transfer, **110**, pp. 321-328.

[13] Han, J.C. and Park, J.S., 1988, "Developing Heat Transfer in Rectangular Channels with Rib Turbulators," Int. J. Heat Mass Transfer, **31**, pp. 183-195.

[14] Park, J.S., Han, J.C., Huang, Y., and Ou, S., 1992, "Heat Transfer Performance Comparisons of Five Different Rectangular Channels with Parallel Angled Ribs," Int. J. Heat Mass Transfer, **35**, pp. 2891-2903.

[15] Fu, W.L., Wright, L.M., and Han, J.C., 2004, "Heat Transfer in Two-Pass Rotating Rectangular Channels (AR=1:2 and AR=1:4) with 45o Angled Rib Turbulators," ASME Paper No. GT 2004-53261.

[16] Fu, W.L., Wright, L.M., and Han, J.C., 2005, "Buoyancy Effects on Heat Transfer in Five Different Aspect-Ratio Rectangular Channels with Smooth Walls and 45-Degree Ribbed Walls," ASME Paper No. GT 2005-68493.

[17] Su, G., Chen, H.C., Han, J.C., and Heidmann, D., 2004, "Computation of Flow and Heat Transfer in Two-Pass Rotating Rectangular Channels (AR=1:1, AR=1:2, AR=1:4) with 45-Deg Angled Ribs by a Reynolds Stress Turbulence Model," ASME Paper No. GT2004-53662.

[18] Han, J.C., Glicksman L.R., and Rohsenow, W.M., 1978, "An Investigation of Heat Transfer and Friction for Rib-Roughened Surfaces," Int. J. Heat Mass Transfer, **21**, pp. 1143-1156.

[19] Taslim, M.E. and Spring, S.D., 1994, "Effects of Turbulator Profile and Spacing on Heat Transfer and Friction in a Channel," AIAA J. Thermophysics Heat Transfer, **8**, pp.555-562.

[20] Liu, Y.H., Wright, L.M., Fu, W.L., and Han, J.C., 2006, "Rib Spacing Effect on Heat Transfer and Pressure Loss in a Rotating Two-Pass Rectangular Channel (AR=1:2) with 45-Degree Angled Ribs," ASME Paper No. GT2006-90368.

[21] Huh, M., Liu, Y.H., and Han, J.C., 2009, "Rib-Spacing Effect on Heat Transfer in Rectangular Channels at High Rotation Numbers," AIAA J. Thermophysics Heat Transfer, **23**, pp. 294-304.

[22] Park, C.,W. and Lau, S.C., 1998, "Effect of Channel Orientation of Local Heat (Mass) Transfer Distributions in a Rotating Two-Pass Square Channel with Smooth Walls," ASME J. Heat Transfer, **120**, pp. 624-632.

[23] Parsons, J.A., Han, J.C., and Zhang, Y., 1995, "Effect of Model Orientation and Wall Heating Condition on Local Heat Transfer in a Rotating Two-Pass Square Channel with Rib Turbulators," Int. J. Heat Mass Transfer, **38**, pp. 1151-1159.

[24] Johnson, B.V., Wagner, J.H., Steuber, G.D., and Yeh, F.C., 1994, "Heat Transfer in Rotating Serpentine Passages with Selected Model Orientations for Smooth or Skewed Trip Walls," ASME J. Turbomachinery, **116**, pp. 738-744.

[25] Dutta, S. and Han, J.C., 1996, "Local Heat Transfer in Rotating Smooth and Ribbed Two-Pass Square Channels with Three Channel Orientations," ASME J. Heat Transfer, **118**, pp. 578-584.

[26] Azad, G.S., Uddin, M.J., Han, J.C., Moon, H.K., and Glezer, B., 2002, "Heat Transfer in a Two-Pass Rectangular Rotating Channel with 45-deg Angled Rib Turbulators," ASME J. Turbomachinery, **124**, pp. 251-259.

[27] Al-Hadhrami, L.M., Griffith, T.S., and Han, J.C., 2002, "Heat Transfer in Two-Pass Rotating Rectangular Channels (AR=2) with Parallel and Crossed 45^{o} V-shaped Rib Turbulators," AIAA Paper No. A02-13915.

[28] Metzger, D.E. and Sahm, M.K., 1986, "Heat Transfer around Sharp 180-deg Turns in Smooth Rectangular Channels," ASME J. Heat Transfer, **108**, pp. 500-506.

[29] Han, J.C., Chandra, P.R., and Lau, S.C., 1988, "Local Heat/Mass Transfer Distributions around Sharp180-deg Turns in Two-Pass Smooth and Rib-Roughed Channels," ASEM J. Heat Transfer, **110**, pp. 91-98.

[30] Schabacker, J., Bolcs, A., and Johnson, B.V., 1998, "PIV Investigation of the Flow Characteristics in an Internal Coolant Passage with Two Ducts Connected by a Sharp 180 Deg Bend," ASME Paper No. 98-GT-544.

[31] Son., S.Y., Kihm, K.D., and Han, J.C., 2002, "PIV Flow Measurements for Heat Transfer Characterization in Two-Pass Square Channels with Smooth and 90^{o} Ribbed Walls," Int. J. Heat Mass Transfer, **45**, pp. 4809-4822.

[32] Lucci, J. M., Amano, R. S., and Guntur, K., 2007, "Turbulent Flow and Heat Transfer in Variable Geometry U-Bend Blade Cooling Passage," ASME Paper No. GT2007-27120.

[33] Cheah, S.C., Iacovides, H., Jackson, D.C., Ji, H., and Lauder, B.E., 1996, "LDA Investigation of the Flow Development through Rotating U-Ducts," ASME J. Turbomachinery, **118**, pp. 590-596.

[34] Hwang, J.J. and Lai, D.Y., 1998, "Three-Dimensional Mixed Convection in a Rotating Multi-Pass Square Channel," Int. J. Heat Mass Transfer, **41**, pp. 979-991.

[35] Liou, T.M. and Chen, C.C., 1999, "Heat Transfer in a Rotating Two-Pass Smooth Passage with a 180º Turn," Int. J. Heat Mass Transfer, **42**, pp. 231-247.

[36] Liou, T.M., Chen, C.C., and Chen, M.Y., 2003, "Rotating Effect on Fluid Flow in Two Smooth Ducts Connected by a 180-degree Bend," ASME J. of Fluid Engineering, **125**, pp. 138-148.

[37] Luo, J., and Razinsky, E.H., 2007, "Analysis of Turbulent Flow in 180° Turning Ducts with and without Guide Vanes," ASME Paper No. GT2007-28173.

[38] Zehnder, F., Schüler, M., and Weigand, B., 2009, "The Effect of Turning Vanes on Pressure Loss and Heat Transfer of a Ribbed Rectangular Two-Pass Internal Cooling Channel," ASME Paper No. GT2009-59482.

[39] Chen, W., Ren, J., and Jiang, H.D., 2010, "Effect of Turning Vane Configurations on Heat Transfer and Pressure Drop in a Ribbed Internal Cooling System," ASME Paper No. GT2010-22273.

[40] Kline, S.J. and McClintock, F.A., 1953, "Describing Uncertainty in Single-Sample Experiments," Mech. Eng., **75**, pp. 3-8.

[41] al-Qahtani, M., Jang, Y.J., Chen, H.C., and Han, J.C., 2002, "Flow and Heat Transfer in Rotating Two-Pass Rectangular Channels (AR=2) by Reynolds Stress Turbulenc Model," Int. J. Heat Mass, **45**, pp. 1823-1838.

VITA

Name:	Jiang Lei
Address:	3123 TAMU, Department of Mechanical Engineering, Texas A&M University, College Station, Texas, 77843
Email Address:	lei.jiang1980@hotmail.com
Education:	B.S., Mechanical Engineering, Xi'an Jiaotong University, 2002 M.S., Mechanical Engineering, Xi'an Jiaotong University, 2006 Ph.D., Mechanical Engineering, Texas A&M University, 2011